MODELING, DESIGN AND FABRICATION OF SUBSTRATE-EMBEDDED INDUCTORS WITH HIGH INDUCTANCE DENSITY AND LOW DC RESISTANCE FOR INTEGRATED VOLTAGE REGULATORS

A Dissertation
Presented to
The Academic Faculty

by

Srinidhi Suresh

In Partial Fulfillment
of the Requirements for the Degree
Master of Science in the
School of Materials Science and Engineering

Georgia Institute of Technology
May 2020

MODELING, DESIGN AND FABRICATION OF SUBSTRATE-EMBEDDED INDUCTORS WITH HIGH INDUCTANCE DENSITY AND LOW DC RESISTANCE FOR INTEGRATED VOLTAGE REGULATORS

Approved by:

Prof. Rao Tummala, Advisor
School of Materials Science and Engineering
Georgia Institute of Technology

Prof. Madhavan Swaminathan, Co-Advisor
School of Electrical and Computer Engineering
Georgia Institute of Technology

Dr. Hamid Garmestani
School of Materials Science and Engineering
Georgia Institute of Technology

Date Approved: April 13, 2020

Dedicated to my Amma and Appa

ACKNOWLEDGEMENTS

By submitting this thesis, my beautiful journey at Georgia Institute of Technology comes to an end. This would not have been possible without the support, guidance and help of many people to whom I will always be grateful. First and foremost, I would like to thank my advisor, Prof. Rao Tummala, for giving me the opportunity to join his group (as his last student before retirement) and work under his supervision. His enthusiasm for research and guidance with respect to an overall development by working on industry and academic projects have inspired me throughout my studies as a Masters student. I want to thank my co-advisor, Prof. Madhavan Swaminathan for his immense insight into my work, and exposing me to new opportunities in the field. I would like to thank Prof. Hamid Garmestani for being on my thesis defense committee and for providing insightful comments about my work.

Next, I would like to thank my mentor, Dr. Himani Sharma. She has stood by me through both my professional and personal difficulties, and I could not have asked for a better mentor.

Being part of a research group full of motivated and knowledgeable members is key to the success of a graduate student. I feel very fortunate to have been part of such a group at the 3D Systems Packaging Research Center, who have made this feel like home. I would especially like to mention Claudio Alvarez for his expertise, patience and relentless help on electrical modeling as well as fabrication - without which my progress would have been impossible. His insight to electrical characterization and general working of IVRs has helped broaden my knowledge from an electrical perspective. This thesis could not have been completed without support from Panasonic during our collaboration.

Many thanks to Chandrasekharan Nair for introducing the concepts of packaging, ANSYS modeling, warpage and structural stability analysis. A shout out to Pratik Nimbalkar, Gaurav Khurana, Jenefa Joana and Emanuel Torres for making these two years memorable. I will miss our breaks, impromptu plans and trips. I also appreciate the support of Prahalad Murali in the fabrication process towards the end of my work. I am grateful to Atom Watanabe, Shreya Dwarakanath, Siddharth Ravichandran, Bartlet DeProspo, Nithin Nedumthakady, Rui Zhang, Omkar Gupte, Mohan Kashyap, Ramon Sosa, Haksun Lee and all other fellow GRAs for their invaluable insight. I want to thank the research and lab staff at PRC, who have imparted their knowledge and shown support, including Dr. Vanessa Smet, Dr. Fuhan Liu, Dr. Mohan Kathaperumal, Chris White, Lila Dahal and Carol Mills, Brian McGlade and Chelsea Heath for taking care of my administrative needs. I also want to thank Dracy Blackwell, Teresa Nelson and Dr. Preet Singh from the School of Materials Science and Engineering for their guidance during my time at Tech.

I would like to specially mention Nilesh Varadan, Shubham Rampalliwar, Shashank Dhar and all my friends from ICT and Georgia Tech, who have stood by me over the past two years.

I am indebted to my parents for their unconditional love and support throughout my life. They taught me to never give up and have continuously provided me not only hope and motivation, but everything I need to build myself a better future.

TABLE OF CONTENTS

LIST OF TABLES

LIST OF FIGURES

LIST OF SYMBOLS AND ABBREVIATIONS

ABF	Ajinomoto Buildup Film
AC	Alternating Current
CMC	Copper-Magnetic-Copper
CTE	Coefficient of Thermal Expansion
DC	Direct Current
EM	Electromagnetic
FEM	Finite-Element Method
FIVR	Fully Integrated Voltage Regulator
FMR	Ferromagnetic Resonance
FOM	Figure of Merit
I/O	Input-Output
IVR	Integrated Voltage Regulator
LLG	Landau-Lifshitz-Gilbert
LTCC	Low-Temperature Co-Fired Ceramic Technology
MCM	Magnetic-Copper-Magnetic
MEMS	Micro-Electro-Mechanical Systems
MPC	Metal Polymer Composite
Ms	Saturation Magnetization
PCB	Printed Circuit Board
PMIC	Power Management Integration Circuits
PVD	Physical Vapor Deposition
RDL	Redistribution Layer
RF	Radio Frequency
SAP	Semi-Additive Patterning
SEM	Scanning Electron Microscopy
SIP	Supply in Package
SOC	System on Chip
UV	Ultraviolet
VNA	Vector Network Analyzer

SUMMARY

Increased functionality demands in today's electronic devices drive the need to make power modules as small as possible. Power needs vary on the board depending on the applications, varying from high-performance computing, artificial intelligence, data servers and centers. Since there is an integration of components with different voltage requirements on the same board, power modules are assembled on the package to deliver differential voltage. When the power module is integrated with the processor, it is known as Integrated Voltage Regulator (IVR). Miniaturization and integration of the module closer to the load not only increases the power delivery network, but also reduces the associated interconnection lengths and parasitics. Package integration so far has focused majorly on the embedding of active components. Inductors, one of the key components of the power module responsible for energy storage are also the bulkiest. Therefore, embedding of inductors must be the focus, allowing proximity to ICs thereby increasing the power module efficiency.

Modules containing IVRs with integrated magnetic cores have shown higher efficiencies as compared to the traditional surface mount inductors. This is because of the low power density and large sizes of the on-chip inductors. Embedded magnetic core-based inductors can lower the losses by integrating closer to the processors. However, most of the magnetic materials available for inductor technologies suffer from high losses (due to low permeability, eddy currents, proximity effects) and cannot deliver the required high-power densities and current handling.

This work starts with discussing the role of inductors in IVRs. It reviews the state-of-the-art inductor fabrication technologies, properties of materials that affect inductor performance and the different topologies that can be explored for embedding inductors in the substrate. The required inductor performance for achieving a 95% IVR efficiency for high voltage single-step conversions of 48V to 1V and 12V to 1V, and low voltage conversions of 3.3V to 1V and 1.7V to 1V.

The objective of this research is to model, design and fabricate substrate-embedded inductors with high inductance density and low DC resistance for low (1-10 MHz) and high frequency (100-140 MHz) applications. Materials with high permeability at low frequency are designed for high power handling capabilities, and low permeability materials with high frequency stability are designed for high frequency applications. Toroid-based composite inductors were designed to achieve high-inductance densities and low DC resistance for low and high frequency ranges. These structures were fabricated by a modified Semi-Additive Patterning (SAP) process. These structures are shown to have ultra-thin form factors (< 200 microns), capable of achieving high inductance densities of up to 20 nH/mm^2 and DC resistance less than 20 mΩ for single inductors. Combination of the designed materials and toroidal design for coupled and tapped inductors can provide and inductance density of up to 100 nH/mm^2.

CHAPTER 1. INTRODUCTION

1.1 Evolution of integrated power modules

Smart, wearable and flexible electronics are the upcoming electronic devices which are pushing for higher functionalization, with miniaturization at low cost. This requires the integration of multiple technologies such as Radio Frequency (RF), Micro-Electro-Mechanical Systems (MEMS), analog, digital and sensors into one package. With higher functionality, there is a need for higher power storage and conversion circuits. This leads to a decrease in the available system area and requires the integration of devices with differential voltage levels in the same package [1, 2]. To achieve this, various power converters are incorporated in the system. A converter system consists of active components such as switches and diodes on power management integrated circuits (PMIC), that are integrated with passive components namely, capacitors and inductors, together known as a power module. When the power module is integrated with the processor, it is known as Integrated Voltage Regulator (IVR).

The first conventional power converter was a discrete power module which was manufactured by Texas Instruments with 10 discrete components mounted side by side on a FR4 substrate as shown in Figure 1.1. The system is limited due to large passive components and interconnect parasitics.

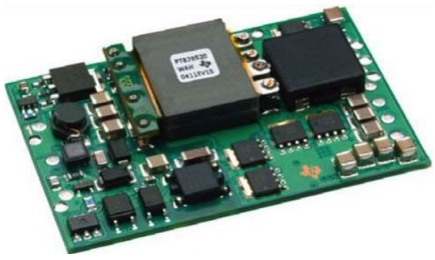

Figure 1.1: Discrete DC-DC converter module [3]

Today, there is a need for multiple power converters, to power different functional blocks of the system, each requiring several passive components used to create a stable power supply. This leads to many challenges in miniaturizing the system while maintaining efficient power management [4, 5]. This was initially tackled by embedding of active components in the package, first shown by TDK who demonstrated a 60% reduction in the PCB real estate [1].

In recent times, there has been a gradual shift from discrete power modules to power supply in package (SIP). This architecture integrates one or more passives into the same package as that of the PMIC, either in a 2D or 3D stacking structure [3]. Another architecture developed is a chip-scale package, with passives assembled on a chip-scale PCB with embedded PMICs. It uses a thin Si-die embedded in an organic core with power components mounted on the top. Figure 1.2 shows the schematic of TI's package.

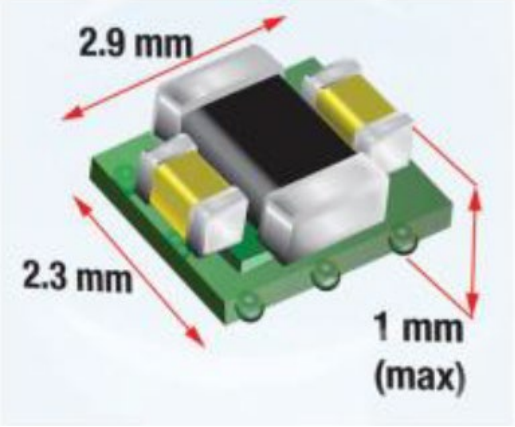

Figure 1.2: TI's module with embedded die and power components [6]

But despite these developments, there remains a limitation in the degree of miniaturization that can be achieved because of limited integration of components in a side-by-side 2D package. Inductors, the largest components in the module [3] are designed to have a large surface footprint and thickness to accommodate the required currents and

offset lower efficiency. This leads to long interconnections and high associated parasitics. In order to further the miniaturization and thereby improve efficiency, these inductors must be embedded. This leads to lower losses, more efficient power delivery network supplemented by shorter interconnections and lower parasitics. Therefore, a transition to 3D stacking package with embedded inductors in completely integrated voltage regulators can overcome the limitations. This evolution of embedding of components in a power converter is shown in Figure 1.3.

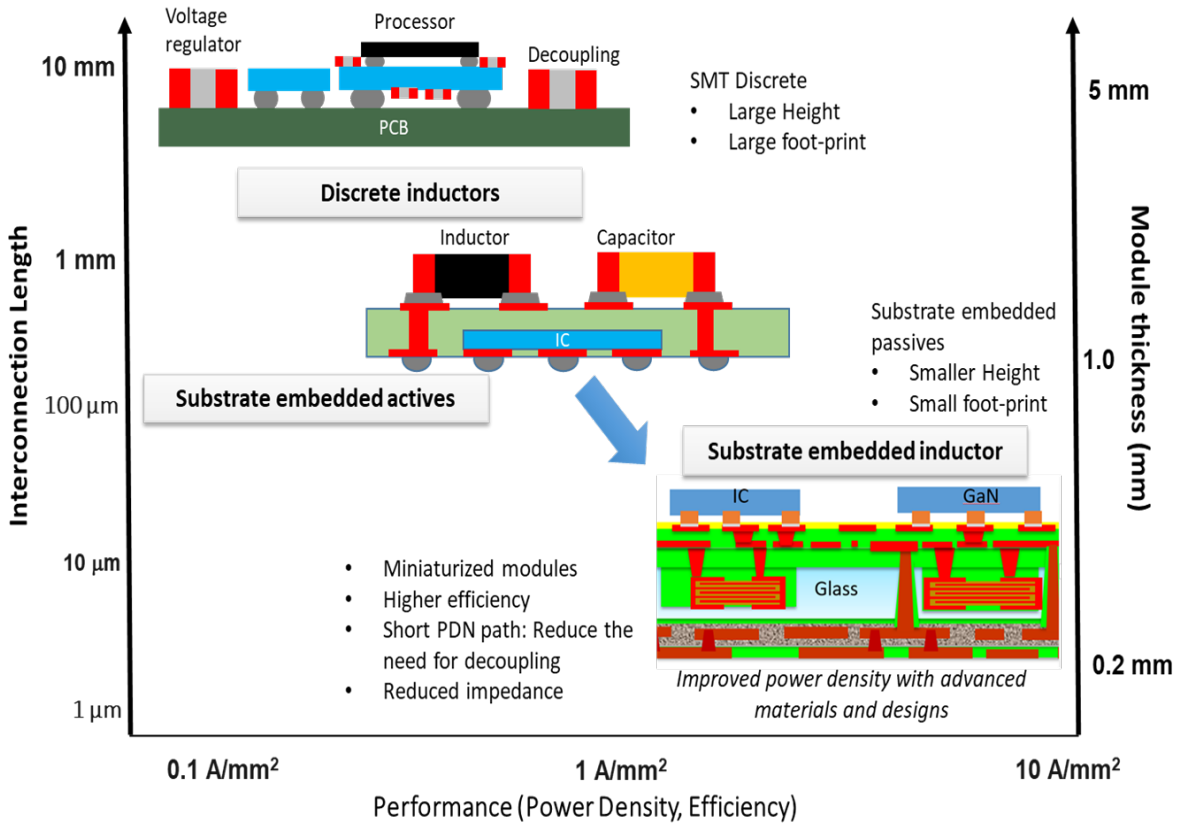

Figure 1.3: Evolution in miniaturization of integrated power modules

The focus of current research is towards the development of embedded inductors from magnetic materials and improving their power-handling and efficiency.

1.2 Emergence of inductor embedding

In power modules with switching regulators or hybrid converter topologies, capacitors and inductors are the primary passive components in the modules. While several advances were reported in capacitor technologies [7–9] to reduce the thickness profile for easier substrate integration, inductors have been lagging. There are currently four approaches to inductor fabrication: (i) discrete inductors (ii) inductors in package (iii) inductors in substrate and (iv) air core inductors. The inductors with the thinnest profile thus far when packaged separately has been demonstrated by Murata with a thickness of 400 μm. These inductors also lack copper terminations which creates additional problems with respect to assembly and reliability due to solder cracking resulting from coefficient of thermal expansion (CTE) mismatch. On-chip inductors were demonstrated by Tyndall as shown in Figure 1.4 (a) which mimics power supply on chip structure with a high inductance density, but low current handling due to inductors being in the form of thin films [10].

Inductors in package was first demonstrated by Sumida's power structure in inductor which consists of an embedded coil inductor structure occupying one half of the magnetic core, with the active components embedded in a cavity under the inductor in the other half of the core. Since the inductor volume in such a structure can be as large as the package itself, it shows a high current handling, low DC resistance and a 2.8% increase in efficiency with 3-5 A of current [11]. This structure is seen in Figure 1.4 (b). Inductors embedded in a substrate showed a shielding effect induced by FR4 epoxy layers surrounding metal-flake

composites that acted as the substrate. The 4-layer structure as seen in Figure 1.4 (c), was demonstrated by Virginia Tech showed an efficiency of 85% [12].

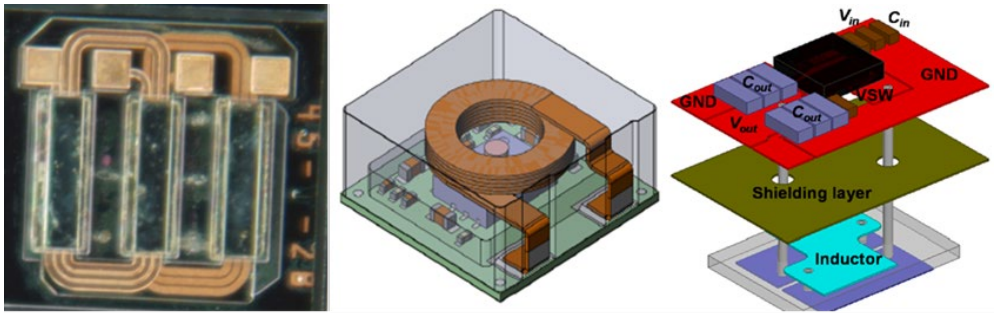

Figure 1.4: Inductor fabrication approach (a) Tyndall's on-chip inductors [10] (b) Sumida's inductor in package architecture [11] (c) Inductors in PCB substrate [12]

Instead of integrating inductors into the substrate, a more common approach is to form the inductor directly into the substrate to further reduce the module size. These are called formed inductors. The foremost formed inductor is Intel's air-core inductor in the Fully Integrated Voltage Regulator (FIVR). However, since the magnetic loop is enclosed in air, the inductance density is low, degrading the efficiency [13]. To offset the loss, higher number of windings and coil length is required which in turn increases the DC resistance. Figure 1.5 shows integrated air-core inductors by Intel.

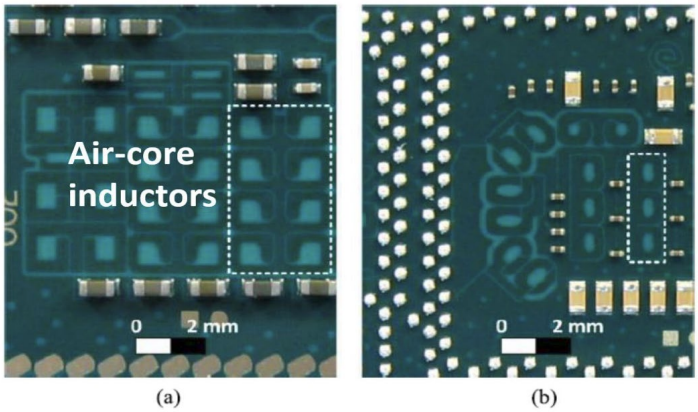

Figure 1.5: Integrated air-core inductors in process packages [13]

Incorporating magnetic materials as cores in formed inductors can improve the inductance while reducing the DC resistance. The magnetic flux is enhanced by the magnetic particles without the need for a greater number of windings. However, there are two main barriers to the embedding of inductors in magnetic core substrates. The first being, magnetic materials are usually unstable at higher frequencies. Magnetic materials are characterized by permeability which has two parts to it:

$$\mu = \mu' + i\mu'' \tag{1}$$

where, μ' is the real permeability and μ'' is the imaginary permeability. As the frequency increases, the eddy current and ferromagnetic resonance loses increase, due to which the real permeability starts to decrease and the imaginary permeability increases. This creates a situation like the air-core inductors. With increased needs for higher operation frequency and higher switching needs like 48V-1V, inductors with high inductance at high frequency are needed.

The second barrier is the saturation current of the magnetic materials, which directly impacts the current handling. Under external applied magnetic field (H), magnetic materials are magnetized resulting in an induced flux density (B), where increasing H field would lead to increase in B field. When the external field reaches the anisotropy (H_k), any further increase in H field would not lead to any increase in B field. Then, the material is said to reach the saturation state. The flux at saturation is known as M_s (saturation magnetization). Since the permeability of magnetic materials is defined as:

$$\mu = \frac{B_S}{H_k} \tag{2}$$

The permeability decreases dramatically as the material approaches the saturation state. The H field is generated when current is running through the copper windings of inductors. Larger currents lead to stronger magnetic fields. With a stronger magnetic field, magnetic cores are saturated easily, resulting in small permeability and inductance. To avoid saturation, advanced materials and appropriate inductor designs are needed.

Therefore, the requirements of miniaturization, high power efficiency and the limitations of magnetic materials as cores, lead to the objectives for this work as discussed in the next sub-section.

1.3 Research objectives

The primary objective of this work is to design and demonstrate miniaturized, substrate-embedded inductors with high inductance density and low DC resistance for low frequency (1-10 MHz) and high frequency (100-140 MHz) integrated voltage regulators. It also establishes the ideal material properties for ultra-high efficiency inductors. The metrics required to achieve the desired goals along with related prior art, main technical challenges and their associated research tasks are summarized in Table 1.1.

Table 1.1: Research objectives beyond prior art, technical challenges and associated research

	Low Frequency (1 – 10 MHz)		High Frequency (100 - 140 MHz)		Research Direction	
Metrics	**Prior Art**	**Objectives**	**Prior Art**	**Objectives**	**Challenges**	**Tasks**
Inductance (nH/mm^2)	1.7	10-20	3.2	6	**Material Challenge** Need materials that have trade-off between high permeability and frequency stability **Inductor Challenge** Inductor design for high inductance & current handling with low DC resistance **Integration Challenge** Lack of fabrication process to embed inductors	Model and design magnetic-cores with medium permeability and good stability at high frequencies Model embedded inductor topologies that meet target specifications Develop innovative process to fabricate and embed inductors into the substrate
DC resistance (mΩ)	20	5-20	36	5-20		
Current handling (A/mm^2)	1	2	1	2		
Thickness (mm)	2	0.5	0.7	0.2 – 0.3		
Type	Discrete	Integrated	Discrete	Integrated		

1.4 Technical challenges

The performance of magnetic inductors in power electronics is controlled largely by the permeability and loss tangent of the magnetic core used. This is given by equation (3):

$$L = \frac{t_m w_m N^2 \mu_r \mu_o}{l_m} \tag{3}$$

Where, N is the number of coil turns, w_m, l_m and t_m are the width, length and thickness of the magnetic core respectively. If a high permeability material is used for fabricating the inductor, it can result in a high inductance density keeping the number of windings same, provided it has low losses at the desired frequency of operation. However, this incorporation of magnetic materials as the substrate for formed inductors has some challenges:

1. **Magnetic material limitations:** Inductors are primarily an energy storage device. This energy is given by Equation (4):

$$E = \frac{1}{2}Li^2 \tag{4}$$

Where, L is the inductance and i is the current through the windings. When current passes through the windings, some energy is dissipated as heat due to the resistance of the copper windings. This reduces the efficiency of the inductors. Therefore, the ratio of inductance to DC resistance (L/R_{DC}) is the figure of merit (FOM) usually used to define the efficiency of an inductor. High permeability materials can be used to give a high L/R_{DC} ratio without increasing the number of windings. However, most of the materials used so far are limited in thickness to a few microns since they are deposited by thin-film technologies like sputtering (physical vapor deposition (PVD)). Due to the small thickness, these materials cannot be used to form the thick copper windings that are needed for a high L/R_{DC} value. Most applications use ferrites as the core, which have high resistivity and low eddy current loss, but have low M_s of 0.1-0.3 T [14]. Metal alloys have high M_s (0.8-0.3 T) but have low resistivity which leads to high losses [15]. Sputtered nano-films have permeabilities above 200 and an M_s of 2 T, but inadequate thickness of sputtered films make them unsuitable for power electronics applications [16]. It is observed that the high DC resistance eliminates the benefit of high inductance. Therefore, there is a lack of high permeability, high magnetization saturation, and low loss materials in the range of 100-300 microns for embedded inductors over a range of frequency from 1-100 MHz.

2. **Inductor topologies for high-current handling:** Saturation of magnetic cores is a major concern to the performance of inductors. As the load current increases, the inductance of the structure to power the module reduces. However, at high inductances, the cores saturate faster, which in turn reduces the permeability. This reduction in the relative permeability degrades the inductor performance. Therefore, inductor topologies must be designed such that early saturation can be avoided. Three different topologies can be explored, namely: planar, solenoid, toroid, each with its set of advantages and disadvantages. Planar topologies have high inductance density but low DC resistance. This is because of the random orientation of the magnetic field in the core. Solenoid and toroid inductors show good current handling with high efficiency because the magnetic field is enclosed in the core itself. Another important consideration in topology design is the hard and soft axis of the core material. In such cases, the inductor must be designed to work at maximum efficiency along the high permeability (hard axis). The lack thereof of topologies that suit magnetic materials to extract high inductance at low thickness profiles is a major challenge.
3. **Fabrication and integration:** The third objective is to miniaturize the power module. This entails embedding inductors into the substrate with a thickness of less than 500 μm. As explained before, the state-of-the-art inductor fabrication approach assembles them as surface mount inductors. This leads to long interconnections length, high associated parasitics and large real estate footprint, which results in high DC resistance and low efficiency. Therefore, advances in processes are required in order to fabricate the "formed" embedded inductors. One of the key challenges in the processing of inductors is to realize fully filled and/or conformal windings around the core material. Integration

is easier for thinner conformal windings, however since one of the objectives is to lower the DC resistance, thicker windings is a necessity for inductors. If the vias are not fully filled or the windings are not conformal, it results in an increase of the DC resistance. Additionally, the thickness of the magnetic core affects integration because formation of void free and uniform windings for higher aspect ratio is a bigger challenge [17].

1.5 Unique approach addressing technical challenges

The technical challenges in achieving ultra-high efficiency substrate embedded inductors for miniaturized power modules as described in the above section need to be addressed to realize the target objectives. The direct fabrication of such a formed inductor is achieved through the following tasks:

(i) Model and characterize magnetic materials with medium permeability and good stability at high frequencies

(ii) Design embedded inductor topologies that can give high inductance, high current handling and good stability according to the magnetic core properties

(iii) Develop innovative processes for fabricating and integration of inductors for miniaturization. Figure 1.6 shows the unique approach for meeting the target objectives set in Section 1.3.

As discussed in Section 1.4, ferrites have been the most used core till now. However, they suffer from high eddy current losses. There has been a gradual shift towards other materials such as nanocomposite films, alloys and metal-polymer composites (MPC). MPCs are composed of an epoxy resin filled with magnetic particles, which can be in the form of spheres, flakes or cylinders. The filler loading and filler shape have been optimized

while designing the material to have a target permeability for a frequency application. In this work, two materials have been modeled, one for low frequency (10 MHz) and one for high frequency (100 MHz) applications. These materials show lower eddy current losses because the permeability is suppressed in the metal fillers as compared to a bulk metal.

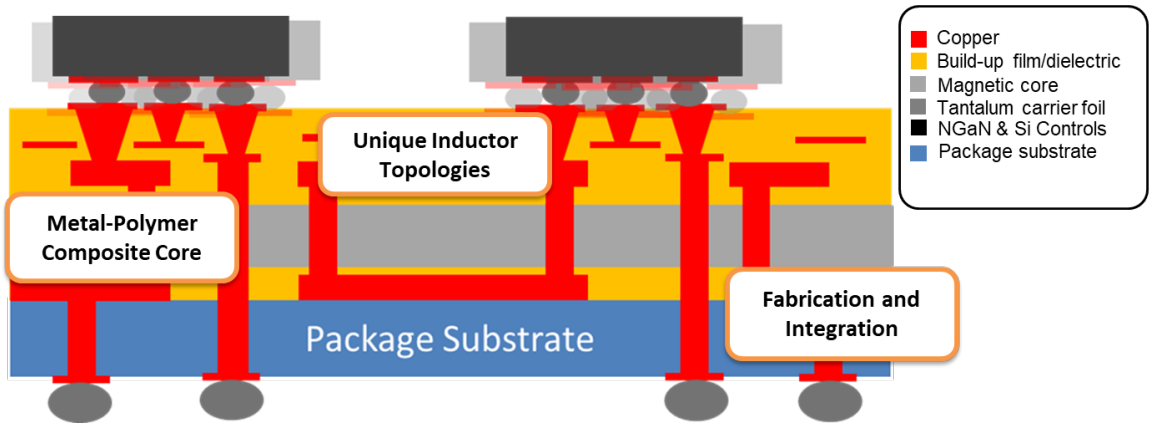

Figure 1.6: Unique approach for embedded inductors with magnetic cores for ultra-high efficiency inductors

Benefitting from this property of MPCs, inductor topologies can be designed as per the permeability of the material ranging from 1-100 MHz. The structures developed are planar, solenoid and toroid, out of which the toroid is shown to have maximum inductance and performance efficiency. Figure 1.7 shows the planar and 3D (solenoid and toroid) structures that have been designed and fabricated in this work.

As shown in Figure 1.6, the proposed structure consists of an MPC core that acts as the main substrate for the inductor structure. The core is laminated between layers of dielectric. The thickness of the magnetic layer controls the amount of dielectric to be used such that the skin depth effect is minimized. This reduces the eddy current losses and enhances frequency stability. The polymer dielectric acts as an insulating layer as well as

an adhesive to stack layers of different thermal expansion coefficients (CTE) in order to form the copper windings around the core material. The windings around the magnetic core are the most important and need to be conformal for good electrical characterization.

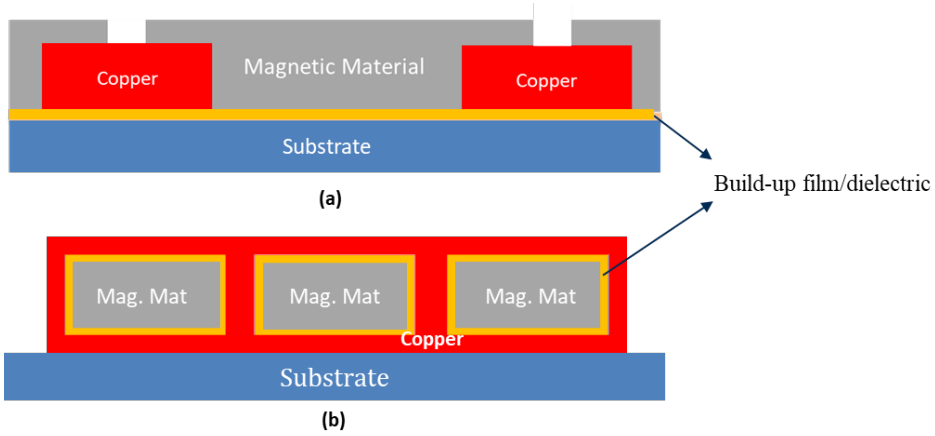

Figure 1.7: Schematics of inductor designs: (a) planar inductor (b) 3D (solenoid and toroid) inductor

This work demonstrates embedded inductors for low and high frequency applications. It compares the performance of the three topologies designed and establishes the toroid inductor as the best in terms of performance for IVRs. It also shows the effect of different filler loadings on the electrical performance and frequency stability of inductors.

1.6 Dissertation outline

This thesis document is divided into six main chapters. Chapter 1 introduces the power module, integrated voltage regulators, inductor architecture evolution, research objectives, challenges and unique approach to address the technical challenges.

Chapter 2 presents the literature review of the state-of-the-art inductor technologies. It also discusses the fundamental structure and properties of various magnetic materials

used as inductor cores and their challenges. The next 3 chapters discuss the research tasks associated with the objectives, which address the respective technical challenges.

Chapter 3 describes the properties of magnetic core materials in order to achieve the target specifications. This is followed by design of a material with the required properties and describes how the magnetic properties of the material affect the electrical performance of the embedded inductors. It also includes the characterization of materials for low and high frequency applications.

Chapter 4 describes electromagnetic (EM) based modeling techniques used to simulate various inductor topologies, namely, planar, solenoid and toroidal structures that can be embedded to achieve miniaturization at high power efficiency. This chapter also discusses the advantages of toroidal inductors over other topologies.

Chapter 5 presents the fabrication and characterization of the EM modeled topologies. The complete process details and structural characterization of the fabricated inductors are described in this chapter. The inductance and DC resistance characterization of the structure against frequency are also shown.

Chapter 6 summarizes the overall research, correlating the results obtained with the objectives that were set. It also provides the scope and suggestions for future work - coupled or tapped inductor in conjunction with the modeled materials in this work for 48V-1V IVR.

CHAPTER 2. LITERATURE REVIEW

This chapter review the role of inductors in power modules, the advances in magnetic materials for passive components, properties of the materials and their effect on the inductor performance. It also briefly describes the inductor topologies and their advantages and disadvantages.

2.1 Role of inductors in power modules

The inductor forms an essential part of a switching regulator. Figure 2.1 shows a simplified circuit for a buck converter. This reduces the input voltage to a lower output voltage. In this circuit, the inductor acts as an energy storage device. When the transistor is powered, current flows from the input source, through the transistor and inductor, to the output. The magnetic field in the inductor builds up, thus storing energy. The voltage drop across the inductor is proportional to the duty cycle of the transistor is in the direction opposite to the input voltage [18]. When this transistor is switched off, the inductor flips the electromotive force and supplies current to the load.

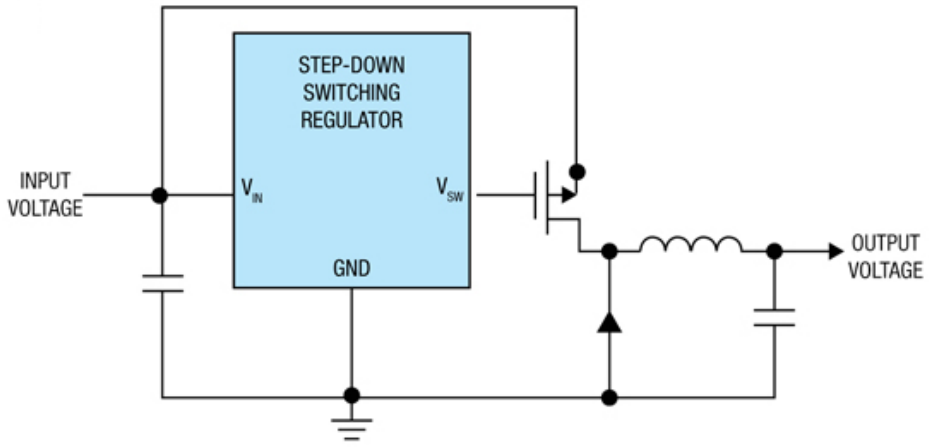

Figure 2.1: Simplified buck converter circuit

The amount of energy stored in the inductor is given by equation (4) discussed in Section 1.4. Inductors are made of winding copper coils that induce a magnetic field when current flows through them. The magnitude of this field is decided by the type of magnetic material, thus enhancing the inductor performance. Therefore, the key parameters that affect the inductance are the permeability of the magnetic core, the number and thickness of the copper windings. Another important parameter to be considered is the frequency of operation of the converter. This affects the frequency stability of the magnetic core.

These parameters make it important to understand how the properties of materials affect inductor performance. Target values must be determined for these properties, to meet the targets of inductance density and DC resistance for substrate-embedded inductors.

2.2 Fundamentals of magnetic properties

The magnetic properties that are critical to the performance of inductors are (i) permeability (μ) as a function of frequency (ii) loss tangent (iii) magnetization saturation (M_s). The permeability is defined as the degree of magnetization induced in a material on application of an external magnetic field. It depends on the type of material and temperature. As discussed in Section 1.4, the permeability of a material decreases with an increase in frequency due to M_s. M_s is an intrinsic property and is the maximum magnetic flux that can be induced under a magnetic field.

Losses in magnetic materials can be due to hysteresis, resonance, eddy current damping and ferromagnetic resonance. Eddy current is a current that circulates in the core induced by alternating magnetic field. They reduce the overall magnetic flux by generating a flux in the direction opposite to the induced magnetic flux by the applied magnetic field.

They shield the inner portion of the core's cross-section. This is called magnetic skin effect and depends on the skin depth of conducting materials, which is the core depth at which the flux decays to 1/e of the surface value, given by equation (5):

$$\delta = \sqrt{\frac{\rho}{\pi f \mu}} \tag{5}$$

Where, δ is the skin depth, ρ is the resistivity and f is the frequency of operation. Increase in the thickness of conducting surface, operating frequency and permeability of material decreases the skin depth and so thicker cores have higher eddy losses. This is depicted in Figure 2.2. Hence, thin and high resistivity materials are preferred for inductor cores.

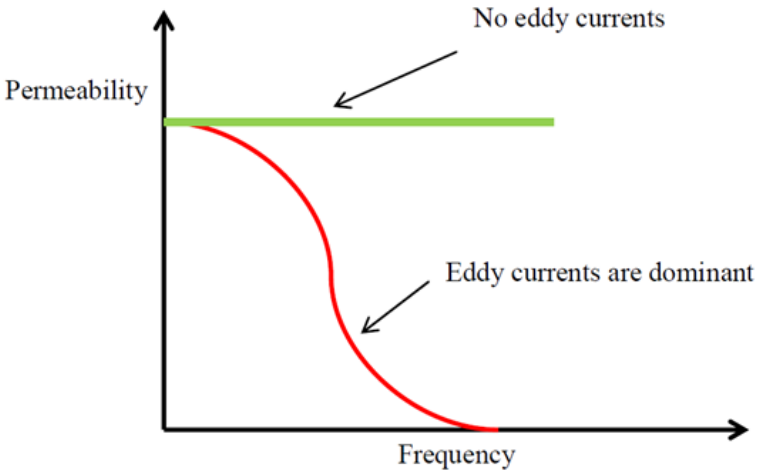

Figure 2.2: Effect of eddy currents on frequency stability and permeability

Shown in Figure 2.3 (a), is a hysteresis loop. The magnetization (B) increases as the applied magnetic field (H) increases. At the saturation point, when the magnetic field is at its peak (H_k), there is no further increase in the B-field. This results in a decrease of the

inductance due to a decrease in permeability, as seen in Figure 2.3. The said H-field is generated by current flowing through the inductor windings. Higher current implies stronger H-field. And so, materials with small H_k limit the operating power of inductors. Therefore, we can see that the three properties are interdependent, and materials need to be engineered such that there is a good trade-off between the properties. Materials have a hard axis and easy axis. Hard axis is the direction where a large magnetic field is needed to align magnetic spins in the direction and reach saturation. Easy axis is where a small magnetic field is enough to align the spins and reach saturation state. Hard axis is known to have a large H_k and can handle more current [19].

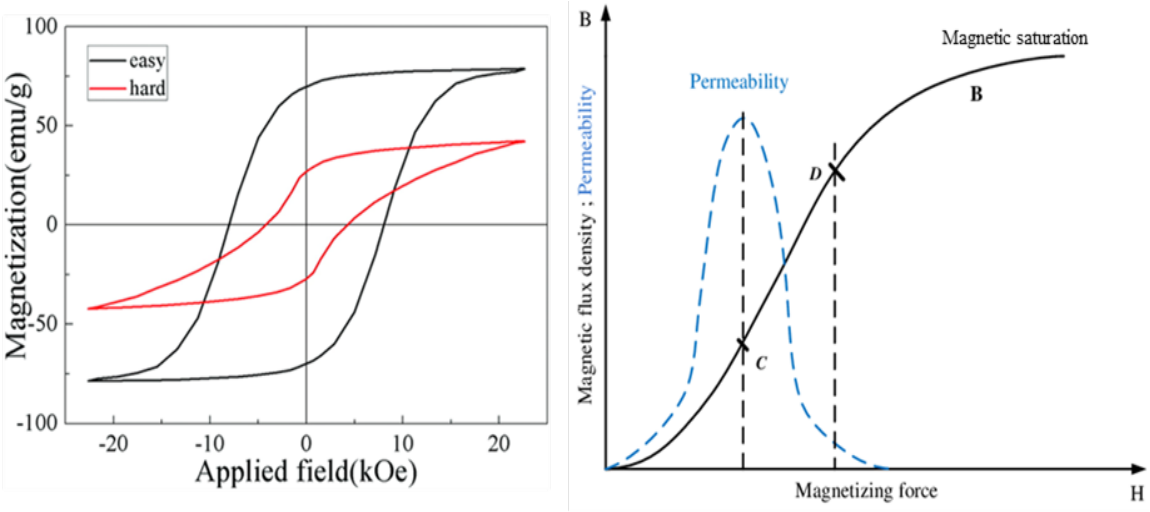

Figure 2.3: Interdependence of permeability, losses and magnetic saturation (a) hard and easy axis of magnetic materials (b) permeability as a function of magnetic field

In conclusion, the magnetic material must be modeled to have high resistivity, high permeability (along hard axis) with good frequency stability, high coercivity, and low losses at high frequencies with a thickness that supports high skin depth. This is done using

analytical finite-element models like Bruggeman's model and Landau–Lifshitz–Gilbert equation which is discussed in Chapter 3 of this work.

2.3 Advances in magnetic materials for power inductors

The commonly used materials for inductors are ferrites. But there have been advances and a shift towards materials such as nanocomposites films, metal alloys and metal-polymer composites with improved properties. The general classification of materials has been shown in Figure 2.4. These can also be grouped as per their frequency of operation: low frequency (1-50 MHz) and high frequency (50-150 MHz).

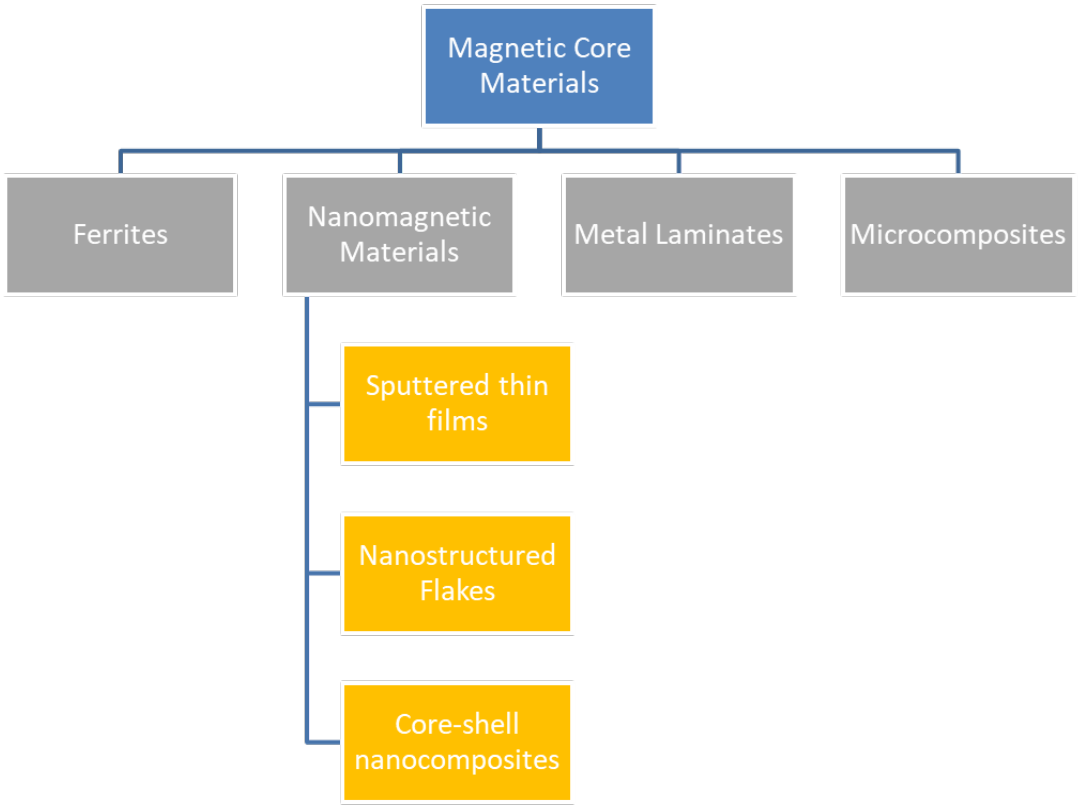

Figure 2.4: Classification of materials for passive applications

2.3.1 Low frequency materials

Ferrites have been used as magnetic core for decades for low frequency applications. This is due to the high resistivity of ferrites (> 1 Ω.m), which leads to lower losses [3, 18] as explained in Section 2.2. However, they suffer from several drawbacks such as low M_s of 0.5 T due to low H_k and low permeability, which limits them to a low frequency operation of around 1 MHz [3, 14]. Therefore, they exhibit low inductance density and current handling. With modifications, some ferrites can be used for up to 50 MHz frequency operations. Such a modification was shown by TDK, where a Manganese (Mn)-Zinc (Zn) based ferrite was optimized for 700 KHz-4 MHz range. The curie temperature of Mn-Zn ferrites is around 250 °C, which makes it suitable for a high temperature environment [21]. Table 2.1 in conjunction with Figure 2.5 summarizes the material performance of various ferrites in the market for the low frequency range.

Table 2.1: Performance of ferrites in the low frequency range [19–21]

Material	Operation Frequency (MHz)	Magnetization Saturation (T)	Core Loss (mW/cc)
Ferrite 3C90	0.5 1.0	0.10 0.02	700 70
Ferrite 3F5 MnZn	1.0	0.02	30
Sumida's ferrite	1.5 1.0 0.2	0.10 0.02 0.02	37 70 250
Virovac amorphous flakes ($Co_{67}Fe_4B_{11}Si_{16}Mo_2$)	0.1 0.1	0.10 0.20	30 200
Hitachi metals: Finemet-FT-3L, 3M	0.02 0.02	0.20 1.00	15.0 300
Kemet	1.0 2.0	0.02 0.02	4.00 1.00

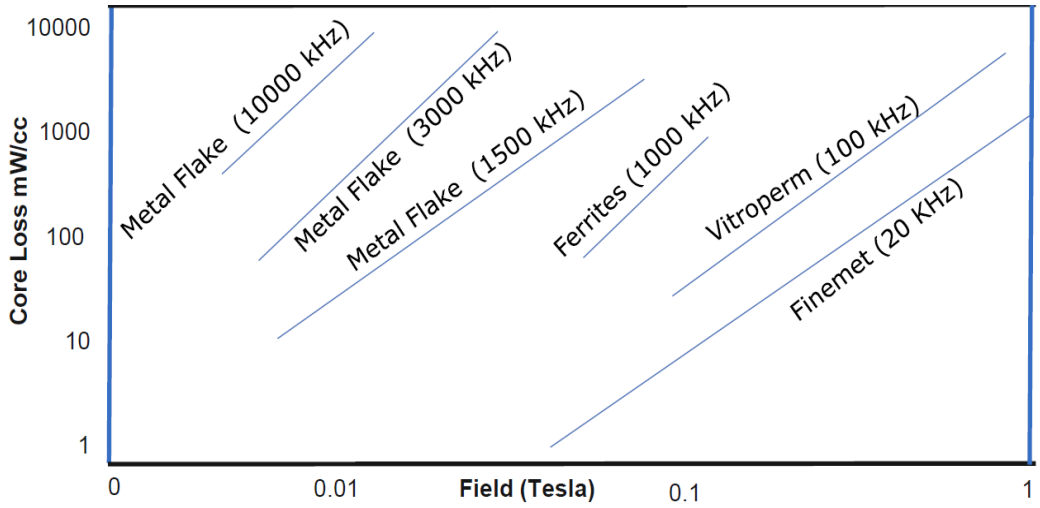

Figure 2.5: Core losses of different ferrites [21]

This led to a shift to using metal alloys as cores for low frequency applications. Compared to ferrites, metal alloys show a higher M_s and higher permeability. This allows better miniaturization. However, conductivity of the alloys increases the eddy current losses. This is mitigated by adding low conductivity elements like boron or phosphorous to reduce the eddy losses [3]. Hitachi has shown good soft magnetic properties (Metglass^{TM}), such as low coercivity, low loss and high permeability. This is attributed to absence of grain boundaries and inherent anisotropy. They are synthesized by rapid cooling which does not give atoms enough time to rearrange, resulting in a metastable amorphous structure [15]. These properties can be further worked on by synthesizing them in a nanocrystalline form. As the grain size decreases, the coercivity increases in the micron range (~ 1 μm). In the nanometer scale, the soft magnetic properties decrease with decrease in grain size as demonstrated by Herzer's model [15].

Metal powders showed by Taiyo Yuden are high M_s metal particles that can handle higher current in comparison to ferrites. Figure 2.6 shows the DC bias of the metal powders

and ferrites. The powder shows a smaller drop in inductance as the current increases. Metal powder cores have a thin oxide layer which isolates the conductive metal, improving permeability. This oxide layer has a thickness of 100-200 nm which provides good electrical insulation and mechanical strength between the powder particles.

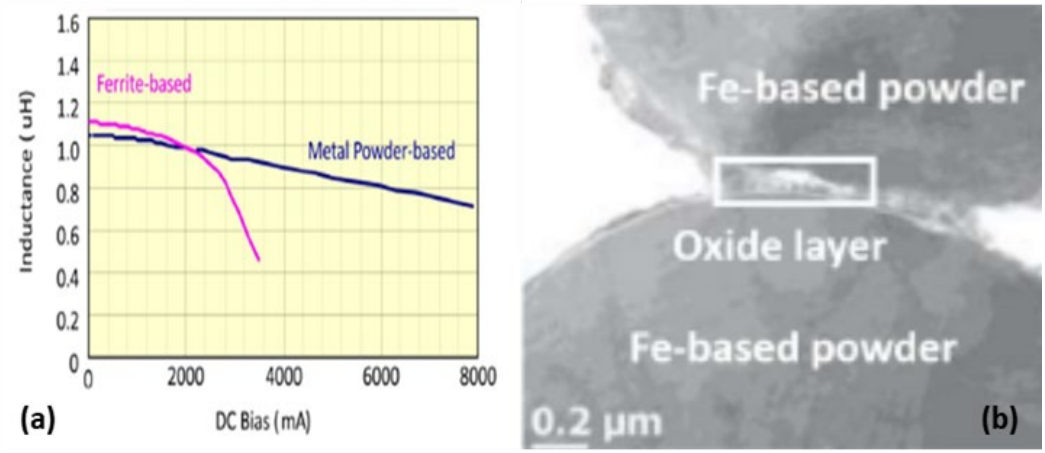

Figure 2.6: Taiyo Yuden's metal powder characteristics: (a) DC bias characterization comparison between ferrites and metal powders (b) TEM image showing thin oxide layer between metal particle cores [22]

MPCs go one step ahead and embed high M_s metal particles in an epoxy resin. This leads to low eddy current losses at high frequencies. The high M_s prevents early saturation of the core. Typical materials are Molypermalloy Powder, Sendust, High Flux and XFlux [22, 23]. The Center for Power Electronics, Virginia Tech showed composites with particles in the shape of flakes. At frequencies between 4-10 MHz, ferrites such as Ferroxcube show lower losses [26]. Nitto Denko also demonstrated metal-polymer composites with flake particles. Because of the shape anisotropy and orientation of the flakes, the composites from Nitto Denko show high in-plane permeability till 10 MHz [27].

2.3.2 High frequency materials

Thin films of magnetic materials have gained traction recently since they address the disadvantages of ferrites. These are more commonly used for high frequency applications owing to high magnetic particle content (Fe, Ni, Co) which give it high permeability and M_s [28]. NiFe thin-films have been used as the magnetic cores for on-chip inductors by Tydnall [26–28]. Typically, electroplating methods are used for depositing the thin films on the wafer. However, a noticeable drawback of these films is the generation of high eddy currents at high frequency due to the presence of highly conductive elements such as Ni and Fe, thereby restricting the range of applications of the films. To counter this limitation, the use B, P, and O elements, has been recommended in literature due to their low conductivity. These losses can be further decreased by the use of alternately laminating magnetic, and insulation films [3, 29–30].

Thin films can also be deposited by sputtering. These films display stable permeability at high frequencies and can be used as magnetic cores for high-frequency inductors. Koh et al. fabricated CoZrTaB thin films with the use of sputtering technology [33]. There is a relation between sputtering power and the magnetic film's properties – for example, a reduction in sputtering power was found to increase the ferromagnetic resonance (FMR) and the anisotropic field (H_k). High anisotropy is related to low permeability along the hard axis since magnetic moments are difficult to rotate from the easy to hard axes.

Apart from magnetic films, several ferrites also show good response up to GHz. Aided by sintering additives, ferrites are compatible with low-temperature co-fired ceramic

technology (LTCC), making them acceptable substrates for embedded inductors. Bierlich et al. presented an M-type ferrite with good high-frequency response [34]. The magnetic properties of the ferrite can be altered upon substituting Fe^{3+} by Co^{2+} and Ti^{4+} in $BaCo_xTi_xFe_{12-x}O_{19}$ ferrite. Increasing the x value decreases the coercivity (H_c) value significantly, resulting in low hysteresis loss, and making them suitable candidates for high frequency applications [34]. On the contrary, the reduction in H_c comes at the price of a corresponding decrease in Ms, thus causing the ferrite to saturate at weak field. This means that inductors with low Ms cores can only account for low DC bias current. The hysteresis loop at different x values is depicted in Figure 2.7. The complex permeability of the ferrite is analyzed, and a good high frequency response is inferred from Figure 2.7[35].

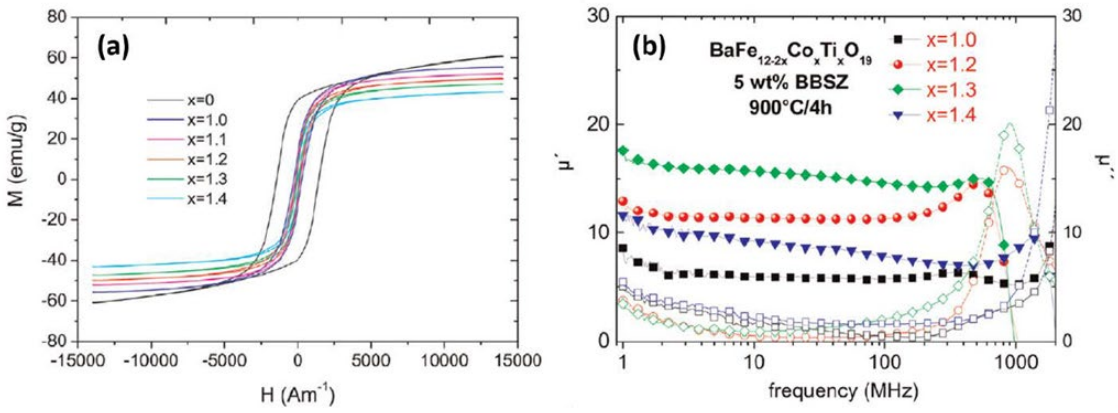

Figure 2.7: (a) Hysteresis loops (b) complex permeability of ferrites for different compositions [32–33]

2.4 Advances in inductor fabrication and integration

There are two ways to fabricate inductors. The first is to fabricate inductors separately as discrete inductors and then insert them into the substrates. The second method is to directly fabricate them as films into the substrate. These inductors are referred to as formed inductor. The two architectures are shown in Figure 2.8.

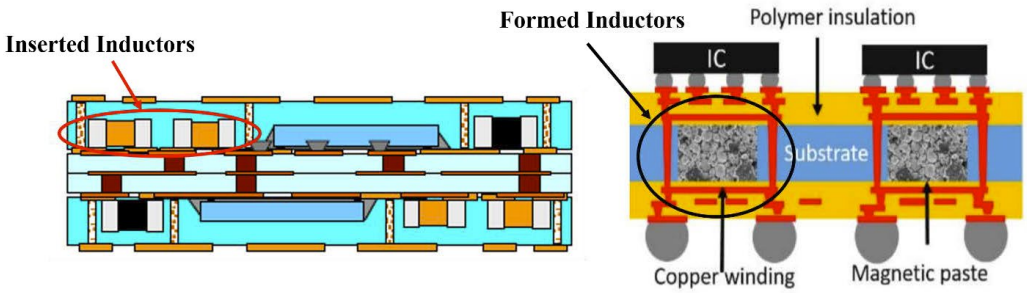

Figure 2.8: Cross-section of substrates with (a) inserted inductors (b) formed inductors [25, 34]

2.4.1 Discrete inserted inductors

Most of the discrete inductors which can be inserted into the substrate have been demonstrated by Taiyo Yuden, Murata, TDK and Coilcraft. These have a small footprint and are hence easy to insert directly. The biggest limitation is that these inductors do not have copper terminations for interconnecting to the rest of the package. This leads to solder connections which has reliability issues due to CTE mismatch. This can be avoided if the inductors have copper terminations, so interconnections can be made by thermocompression bonding or electroplating.

The thinnest inductors from Taiyo Yuden, Coilcraft, Kemet and TDK have been summarized in Table 2.2 along with their sizes and specifications. The thickness profile allows for insertion at high power densities. Coilcraft's thinnest inductors use magnetic composites as the core. Kemet's inserted inductors are ferrite-based chip inductors. However, the ferrites have a low M_s, due to which the saturation current is low and limits its application frequency. On the other hand, TDK's inductors have metal magnetic cores with high M_s which allows for high current handling applications. They also have a closed magnetic path to reduce leakage currents.

Table 2.2: Power inductors with low thickness profile from Taiyo Yuden, Coilcraft, Kemet and TDK [35–44]

Company (Series)	Inductance (μH)	Thickness (mm)	DC resistance (Ω)
Taiyo Yuden			
MCFK1608TR24M	0.24	0.6	0.050
MCFK1608TR47M	0.47	0.6	0.085
MCFK1608T1R0M	1.00	0.6	0.224
MCEK1608TR24MG	0.24	0.65	0.100
MCEK1608TR47MG	0.47	0.65	0.150
MCEK1608T1R0MG	1.00	0.65	0.340
Coilcraft			
XFL2005	0.15	0.5	0.098
XFL2006	1.00	0.6	0.169
Kemet			
L0603B100DWFT	10	0.8	0.36
L0603B220DWFT	22	0.8	1.00
L0603B470DWFT	47	0.8	2.50
	TDK		
TFM160808ALC-R47MTAA	0.470	0.8	0.062

Murata's inductors have the lowest thickness profile of 0.4 mm and can handle a current of 4.2 A because the core is magnetic material based with a total height of the structure as 0.8 mm. It was also one of the first to adopt thin-film inductor fabrication techniques and introduced the LQW15DN series for smartphones, with the smallest inductor (1.0x0.5 mm) having and inductance of 15 μH. They also developed the smallest inductor (0.25x0.125 mm) with Barium-Strontium Titanate thin films. These are multilayered ceramic thin film inductors [47].

As explained in Section 1.4, the figure of merit (FOM) of L/R_{DC} is a good metric to judge the performance of inductors. Figure 2.9 shows a plot of L/R_{DC} as a function of current density for several commercially available insertable inductors.

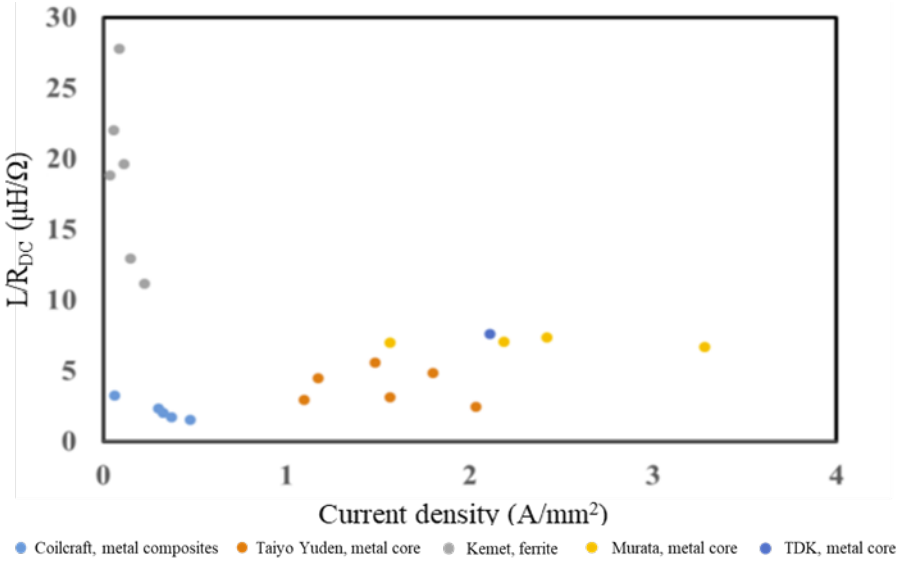

Figure 2.9: Performance plot of commercially available 'inserted' inductors

It is observed that metal core inductors have higher current handling compared to ferrite core inductors. This is due to the high Ms of metal elements. Ferrite-based inductors show higher L/R_{DC}, but lower current handling compared to metal-based inductors. However, metal-based inductors which give low inductance density can be utilized at much higher frequencies since the required inductance is much smaller.

2.4.2 Formed inductors

Formed inductors can have 3 topologies: planar, solenoid and toroid. Planar inductors have a structure where the copper windings are sandwiched between two magnetic layers, also known as Magnetic-Copper-Magnetic (MCM) inductor. The other type is Copper-Magnetic-Copper (CMC) inductors, where the magnetic cores are enclosed within copper

windings. Toroids and solenoid inductors come in this category. Figure 2.10 illustrates the difference between MCM and CMC inductors.

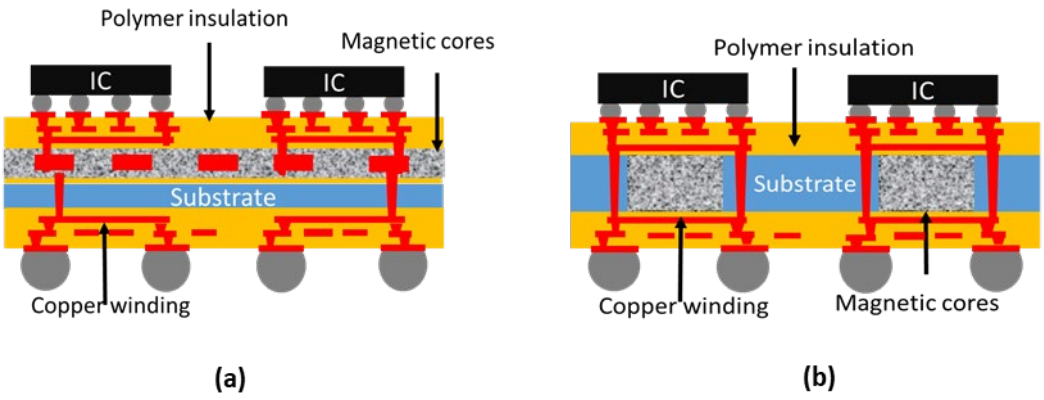

Figure 2.10: Schematic illustration of (a) MCM topology (b) CMC topology

The inductance for planar structures is decided by the number of copper windings. More windings correspond to higher inductance density. Thicker and wider traces lower the DC resistance. The magnetic field for planar structures is oriented randomly, and so it is not possible to align only in the hard axis direction. This lowers the current handling of MCM structures. To improve the working of planar structures, the windings are elongated in the longitudinal direction to increase the magnetic field transversely (racetrack inductor). The current handling can also be increased by reduction in the number of turns. Stripline inductors are planar inductors with one turn and show high current-handling because of weak magnetic fields. They also have high inductance density because of the small size.

Solenoid inductors comes under CMC topologies. The magnetic field is generated within the windings and is enclosed within the magnetic core that limits EM interaction. Like planar structures, they show high current handling when the field is oriented along the uniaxial hard axis [48]. Toroidal inductor structure also constrains all the magnetic field

within the winding loop. They require radial anisotropy [49], which is harder to obtain than uniaxial anisotropy as depicted in Figure 2.11.

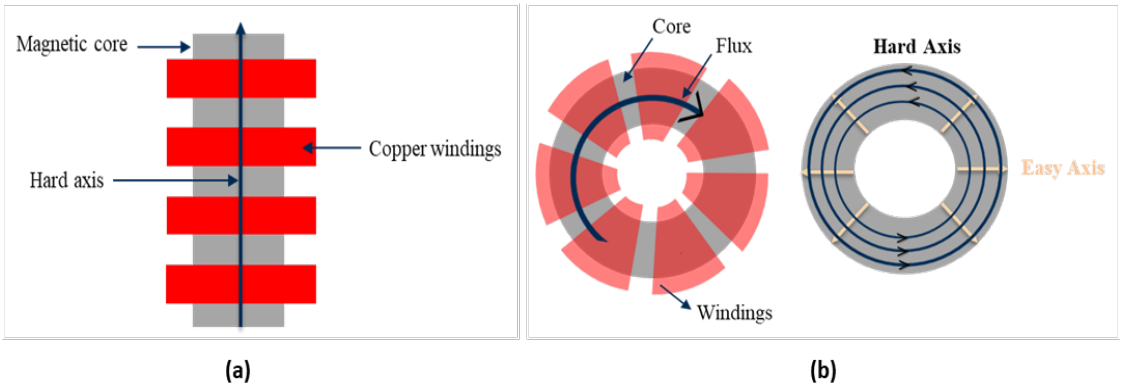

Figure 2.11: (a) Solenoid inductors with magnetic field along the hard axis of the magnetic cores (b) toroidal inductors with radial anisotropy

Planar inductors with magnetic cores

Planar inductors using ferrite laminates: the copper coils are fabricated on a polyimide film separate from the magnetic cores and then assembled to form a hybrid inductor structure [50]. This is shown in Figure 2.12.

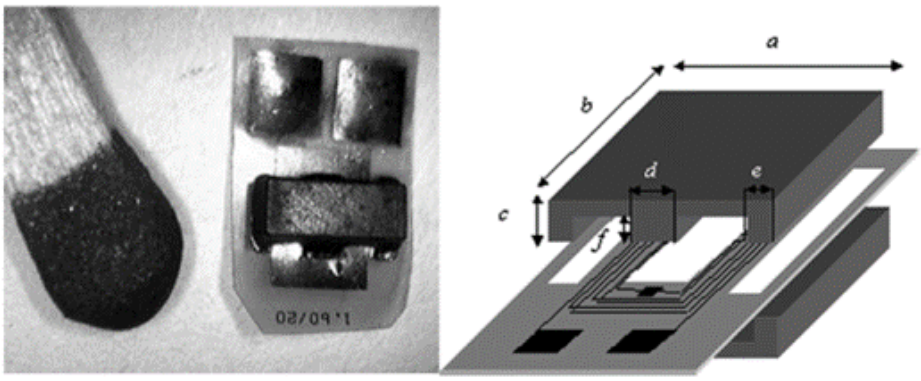

Figure 2.12: Hybrid inductors with planar coils with two ferrite laminate cores [50]

Spiral Inductors on PCB with metallic magnetic cores: the coils are directly patterned in the PCB and a magnetic core such as electroplated CoNiFe [51], NiFe [52] is introduced to increase the inductance as shown in Figure 2.13. However, they do not meet the size and performance targets for many applications [53].

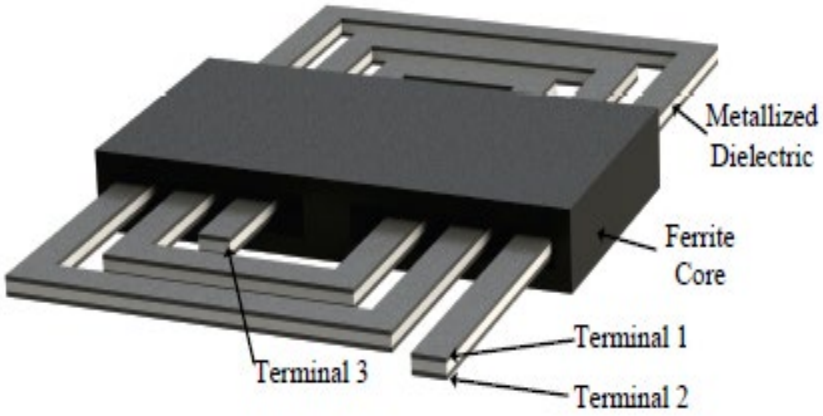

Figure 2.13: Cross-section of PCB with integrated inductors and capacitors [54]

Planar inductors on magnetic substrates

When the planar structures are fabricated on magnetic substrates, it reduces the space that is utilized by the core. The coils are electroplated on cores such as NiZn and coated with a conductive powder and polymer binder as shown in Figure 2.14 (a). A similar structure was also demonstrated by Intel, where coils were printed on CoZrTa laminates. This structure as shown in Figure 2.14(b) demonstrates a uniaxial anisotropic magnetic field, which results in a high current handling with high frequency stability, making it suitable for 100 MHz frequency operations [55].

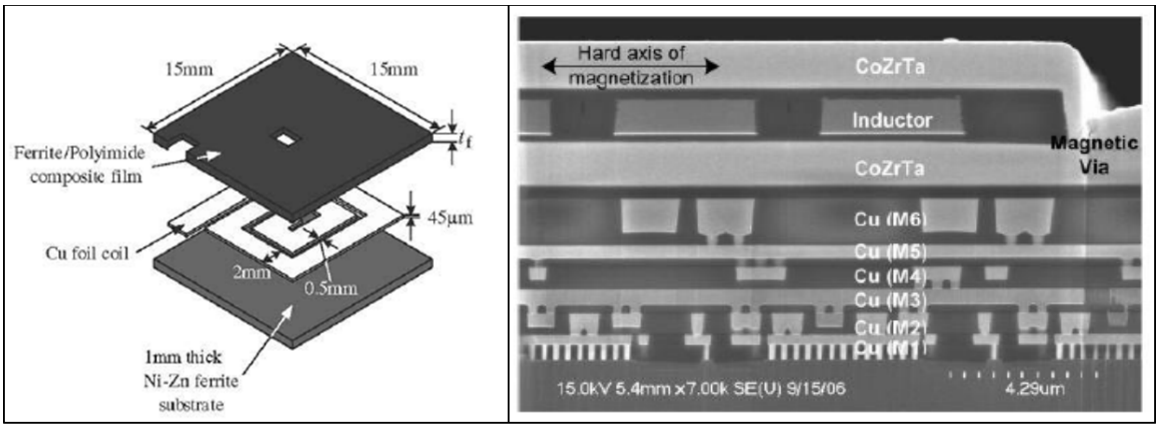

Figure 2.14: (a) Spiral inductors on magnetic substrates [56] (b) cross-section view of inductor integrated on CMOS [57]

Polyimide dielectric was used as a planarizing layer between two magnetic cores. Magnetic vias were formed to connect the top and bottom magnetic material. The inductance was shown to be 9 times as compared to air-core inductors.

Toroid inductors with magnetic cores

As discussed earlier, toroids show radial anisotropy, which improves its inductor performance. However, it requires two metal-layer patterns with vias which increases fabrication complexity. Toroidal inductors with ferrite substrate cores: vias are drilled through the core (substrate) and the vias are filled by electroplating to provide connections. It is then stacked with a power IC chip and packaged [57] as shown in Figure 2.15. Toroidal Inductors with Electroplated Metal Laminate Cores: laminated cores separated by a polymer layer show lower eddy current losses [58]. This approach is time consuming since it requires multiple deposition and electroplating steps. Furthermore, the seed layer needs to be etched after every electroplating step. An all-aqueous-based electro-chemical process was reported for laminating magnetic cores, using a electrodepositable photoresist

dielectric as shown in Figure 2.15. In this, the second electroless seed layer is selectively deposited which does not need seed layer etching [59].

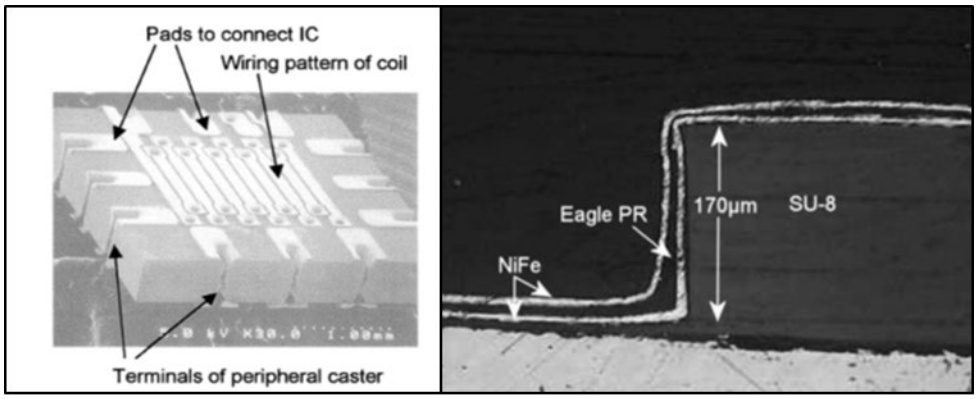

Figure 2.15: (a) Toroidal inductor on ferrite substrate [57] **(b) Laminated NiFe core by all aqueous-based electro-chemical process** [59]

2.5 Summary

Inductors are typically the largest components in a power converter that play a crucial role in determining the efficiency of the converter. Until recently, inductor technologies were limited to discrete ferrite inductors despite their low Ms that degraded their power density and frequency response. Nanocomposite films make up for this drawback by exhibiting high permeability and high frequency stability. However, the films are sputtered and cannot have a large thickness, which limits the inductance and affects the permeability at high frequencies. Advanced magnetic materials such as metal composites have emerged to enhance volumetric density, albeit their much higher losses. The desired magnetic material must have a good permeability with high frequency stability, high Ms, and low loss at in ultra-thin form factor (50-100 microns). It must also be substrate-process compatible and scalable for high volume manufacturing technologies. Different materials have been compared for the above requirements in Figure 2.16 by way of a stoplight chart.

Material	Ferrite	Sputtered thin-films	Metal-polymer composites
Freq. stability			
Loss			
Permeability			
Scalability			
Current handling			
Substrate compatibility			

Figure 2.16: Stoplight chart comparing the performance of different materials across specified parameters for inductor applications

The current discrete inserted inductors need to be replaced by formed inductors and be integrated with the active components in a miniaturized and ultra-thin form factor. This can be achieved by planar or toroidal topologies. Spiral inductors are more widely used because of their ease of fabrication while toroidal inductors offer higher power densities [60]. The advantages and disadvantages of each topology is summarized in a stoplight chart depicted in Figure 2.17.

	Inductance	Saturation Current	Process Fabrication	Design Complexity
Solenoid				
Toroid				
Spiral				
Stripline				

Figure 2.17: Stoplight chart comparing performance of different inductor topologies [60]

Building on the desired properties, a unique structure that integrates a magnetic material with high performance topology has been proposed in this work. The demonstration of a high inductance, high Ms, and low loss magnetic embedded structure will be discussed in the next chapters.

CHAPTER 3. DESIGN AND BENCHMARKING OF MAGNETIC MATERIALS FOR POWER INDUCTORS

This chapter sets the benchmark for the IVR i.e. efficiency, duty cycle for different switching applications. Building on this, the required properties of magnetic particles are deduced. It also discusses modeling and design of magnetic particles in order to obtain the target properties. The effect of filler loading and size on the performance of materials is studied.

3.1 Performance benchmarking for inductors in IVR applications

High efficiency-high voltage IVRs which have a stack-up as shown in Figure 3.1 are required in order to allow next generation data centers to operate with high efficiency. This will reduce both energy and resources for these infrastructures, enables miniaturization of power modules and their integration close to the System on Chip (SoC) [61].

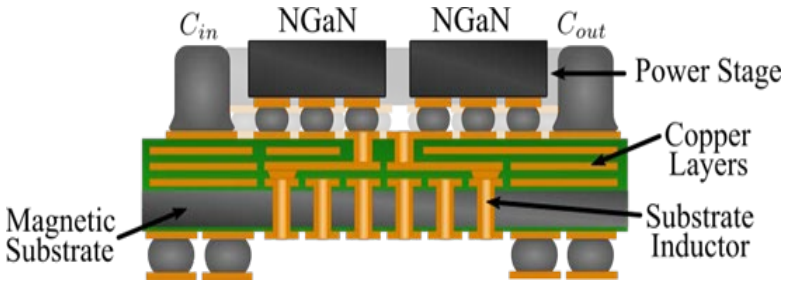

Figure 3.1: Single stage IVR dielet cross section

Different switching frequencies are of importance: 48V-1V, 12V-1V, 3.3V-1V and 1.7V-1V. However, single stage 48V to 1V ultra-high conversion ratio or 12V to 1V high conversion ratio present new challenges that are not seen in low voltage converters such as

3.3V or 1.7V to 1V. New metrics for magnetic materials and inductor technologies are required to describe their efficiency for different applications [62]. The focus of this work is on 48V to 1V and 12V to 1V for low frequency applications and 1.7V to 1V for high frequency applications [59-60]. However, material properties for all applications have been predicted for future work.

3.1.1 Inductor efficiency analysis

In a buck converter (Figure 2.1), there are various energizing and de-energizing stages. When the inductor is energized, its current increases as it stores energy. When it is drained, its current decreases as it releases energy. This builds up current which is equal to the current that is consumed by the load. It also generates an AC current ripple. The typical current waveform is shown in Figure 3.2, where I_o is the output load current, Δi_L is the current ripple and is the energizing duty cycle (D), and $T_s = 1/f_s$ is the switching period.

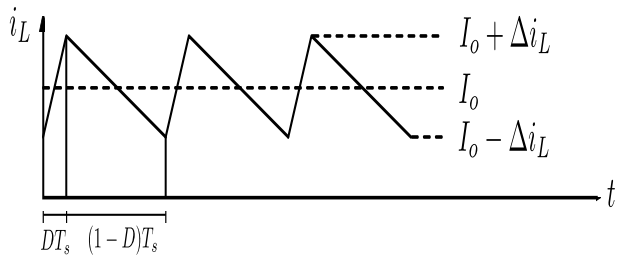

Figure 3.2: Inductor current waveform

The inductor losses due to the DC and AC current can be expressed as given by equation (6), where $R_{acx}(D, f_s)$ corresponds to the effective AC resistance per inductance with dimension Ω/nH and is a function of the duty cycle and frequency, R_{DC} is the inductor DC resistance, and $L(f_s)$ is the inductance at the switching frequency.

$$P_L = I^2 R_{DC} + \Delta i^2 L(f)_s R_{acx}(D, f_s) \quad (6)$$

The minimum requirement that an inductor needs to meet in order to have an efficiency of 95% is determined from the above waveform analysis. In this analysis, we consider a DC-DC converter with I_o = 2.5A of output current, output voltage V = 1V, and frequency f_s = 10 MHz. In Figure 3.3 different values of R_{acx} and Δi_L are plotted versus the inductance L for the conversion ratios of $D = k/48$, with value of $k = 1, 2, 4$. The parameter k corresponds to the duty cycle extension provided by the converter.

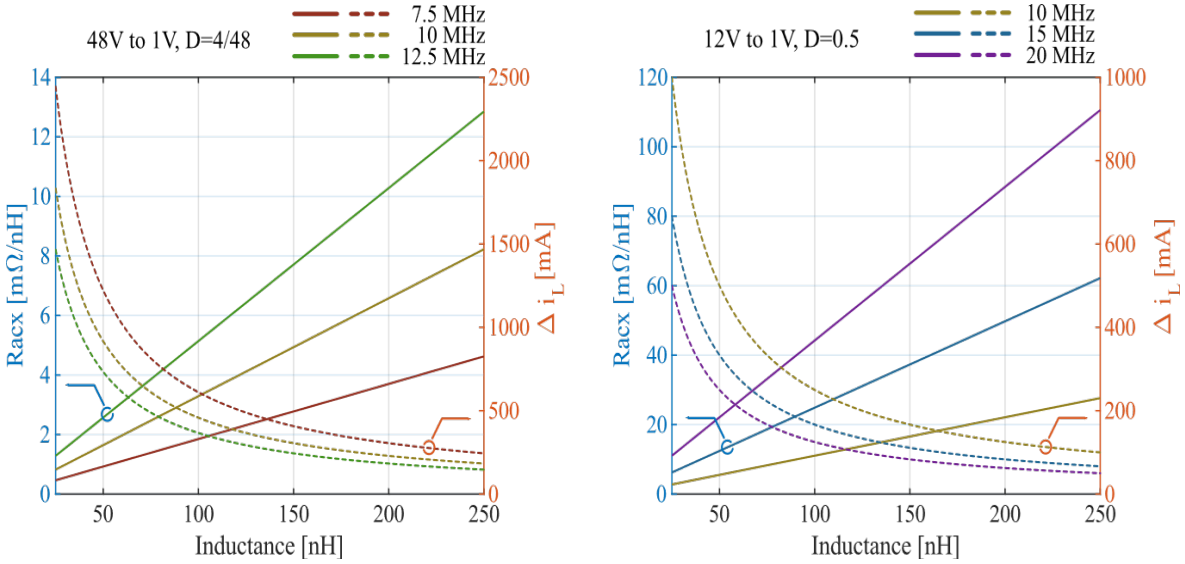

Figure 3.3: Racx for D = k/48 and k = {1, 2, 4}

We observe that if a duty cycle extension by a factor of 4 is provided for 48V to 1V conversion ratio, with an inductance of 91 nH at 10 MHz, the R_{acx} must be less than 3 mΩ/nH. The same analysis shows that for a conversion ratio from 1.7V to 1V at 50MHz, the required inductance is 8 nH and R_{acx} is 32.6 mΩ/nH. This shows the difficulty in achieving 48V to 1V compared to low voltage converters. Table 3.1 summarizes the required inductor performance for different conversion ratios. With the converter

delivering 2.5A of current, we should allow the inductor to have a saturation current of 3.5A. These numbers set the requirement of a total inductance L = 91 nH in a single inductor configuration for 48V to 1V and a total inductance of 10nH for 1.7V to 1V configuration. As it can be observed, at higher frequencies we can use inductors with higher effective AC resistance and lower inductance.

Table 3.1: Required inductor performance for different conversion ratio applications from IVR efficiency analysis

Conversion ratio	Inductor topology	Operation frequency (MHz)	Required inductance (nH)
48V – 1V	Single	10, 20	91, 73
48V – 1V	Coupled	10	364
12V – 1V	Single	10, 15, 20	45, 33, 25
3.3V – 1V	Single	50-100	20
1.7V – 1V	Single	50-100	8

From this analysis and the required inductor performance, the required material property can be predicted in order to achieve the set objectives.

3.1.2 Material property analysis

As discussed in Section 2.2, the magnetic materials must have the following generic properties:

- High permeability: this is crucial for the miniaturization of power inductors as a high permeability results in high inductance thus allowing a small footprint.

- High-frequency stability: permeability drops with increasing frequency of operation. Therefore, magnetic materials are expected to have stable and high permeability for inductors operating at such frequencies.
- Scalability: Thick magnetic cores are desired because for the same size, structures, thicker magnetic cores lead to lower reluctance and higher inductance. Thus, a higher L/RDC value can be achieved without changing the structure and DC resistance of inductors.

These properties are subject to change as per the conversion ratio applications. Different materials will be designed and characterized in the next sub-section. Based on the inductor requirements in the above sub-section and analysis of the designed materials, the required properties for various applications will be discussed. A conclusion will be drawn about the best application for the modeled materials at the end of this chapter.

3.2 Design methodology

In order to design materials to match the required properties and enable the desired performance, different parameters that affect material properties need to be studied. The particle shape plays an important role in understanding the anisotropy of properties. Similarly, the losses in magnetic materials depend on the ferromagnetic resonance which is decided by the particle size.

3.2.1 Effect of particle shape on permeability of magnetic materials

From the comparison of properties in Figure 2.16, the material of interest is MPC. The permeability of MPCs depends on the particle shape of the filler used. As expected,

spherical particles, show an isotropic permeability (same along all directions). For disk shaped particles, the permeability along out-of-plane direction is smaller than in-plane direction, resulting in anisotropic permeability. This is due to demagnetization that arises from shape anisotropy. Under external applied field, magnetic particles are magnetized to induce magnetic poles on the particle surface [65]. These poles generate internal fields, referred to as demagnetizing fields, and oppose the external field as shown in Figure 3.4.

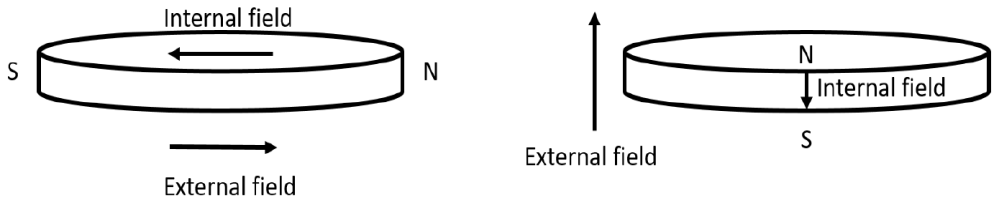

Figure 3.4: Magnetized particle with induced demagnetizing field

Because of the magnetic field induced in the reverse direction, the effective field experienced by the particles is reduced, resulting in lower magnetization and permeability. The strength of the internal field depends on the distance between magnetic poles. For disk particles, the in-plane demagnetizing field is weaker than the out-of-plane field due to the longer distance. As a result of the weak demagnetization, the effective field ($B_{eff} = B_{ext} - N$, where N is the demagnetizing factor) along the in-plane direction is stronger than out-of-plane direction [66]. Thus, the permeability is higher along in-plane direction than out-of-plane direction. Therefore, the in-plane direction with higher effective field is called the easy axis and the out-of-plane direction is the hard axis. Based on this, for long rods, the permeability in the z direction is higher than the in-plane permeability. Similarly, for thin films the permeability is higher in the film/flake plane [67].

By solving the Landau-Lifshitz-Gilbert (LLG) in equation (7), the permeability spectrum can be obtained [68]:

$$\frac{dM}{dt} = -|\gamma| M \; x \; H_{eff} - |\gamma| \frac{\alpha}{M_s} M \; x \; [M \; x \; H_{eff}] \tag{7}$$

Where, M is the magnetization, H_{eff} is the effective field, $\bar{\gamma}$ is the Landau-Lifshitz gyromagnetic ratio, and α is the damping constant. The solutions of LLG equation are given by [69], which can be modified further by assuming that the particles saturate along z-axis. Thus, permeability along z-axis is 1. At low frequency (ω=0), the equations can be simplified, as shown below, to study the effect of shape on permeability.

$$\mu_x = \frac{M_s}{H_k + M_s(N_x - N_z)} + 1 \tag{8}$$

$$\mu_y = \frac{M_s}{H_k + M_s(N_y - N_z)} + 1 \tag{9}$$

The frequency stability, given by the ferromagnetic resonance (FMR), is also affected by the particle shape. It was observed that by changing the shape from sphere to rod or disk, FMR frequency is increased [70]. In this work, magnetic particles in the spherical shape are designed and embedded in an epoxy resin to design MPCs for target applications.

3.2.2 Effect of particle size on loss tangent of magnetic materials

For conductive magnetic particles, eddy-currents play an important role in determining the frequency stability of magnetic particles. To design the right particle size and filler loading, eddy current loss needs to be discussed. Eddy current losses are

proportional to the size, resistivity and operation frequency as stated in [63, 64] equation (10):

$$\mu'' = \frac{2\pi(\mu')^2\sigma d^2 f}{3} \tag{10}$$

Where σ is the conductivity, d is the particle size and f is the operation frequency. Since high-permeability metal particles is a requirement for magnetic cores, the conductivity is fixed and cannot be changed. Thus, the only way to lower the eddy current loss is to use smaller particles. In addition, the eddy current losses are also reduced by isolating each particle with an oxide layer. Because of the insulation film, eddy currents are unable to circulate on wide arcs, resulting in low eddy current loss. The spherical particles chosen to have a particle size of less than 30 μm in order to ensure a trade-off between the permeability and frequency stability. These particles are then embedded in an epoxy resin with different filler loadings in order to synthesize materials with different permeabilities and losses.

3.3 Magnetic material characterization and design validation

Two materials (MPC 1, MPC 2) were synthesized (courtesy Panasonic), in the form of MPCs. The spherical metal fillers were chosen to have a particle size of less than 30 μm. For MPC 1, the metal fillers coated with a metal oxide were embedded in an epoxy resin with a filler loading of 91 wt. % (~60 vol. %). It is then scaled up to make sheets of thickness 100 μm. For MPC 2, the filler loading was kept at 97.8 wt. % and a final sheet thickness of 100 μm. These materials can directly be used as magnetic cores for fabrication of inductors. The performance of the two materials was compared with MPC 3 with a

thickness of 200 µm (available in the public domain). This comparison is to understand the permeability-conversion ratio application dependence and to extrapolate the required material properties for different conversion ratios. Figure 3.5 shows the SEM image of the three materials.

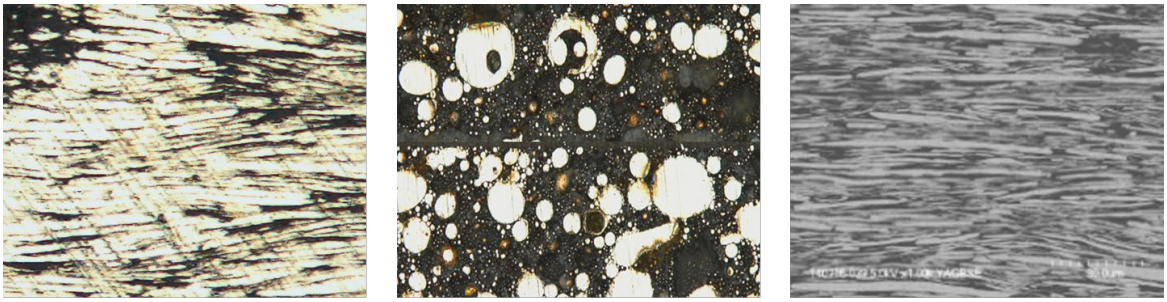

Figure 3.5: SEM image of synthesized (a) MPC 1 (b) MPC 2 (c) MPC 3

For the suggested stack-up discussed in the unique approach of this work shown in Figure 3.6, an insulating layer of dielectric is introduced around the magnetic core.

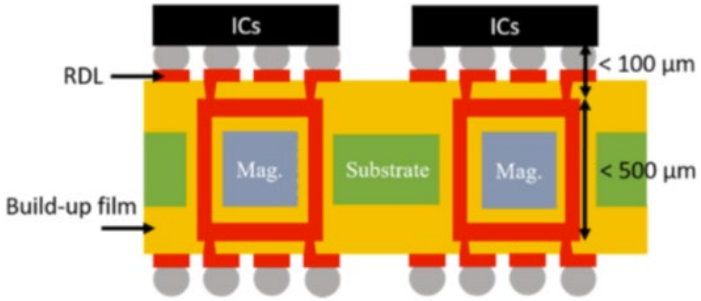

Figure 3.6: Substrate-embedded inductor stack up

Therefore, the adhesion of build-up film/dielectric to the magnetic materials is important to the fabrication and reliability of the architecture. Improper adhesion between the core and the build-up film can lead to delamination during processing. In addition, difference in the coefficient of thermal expansion (CTE) between the two layers can also

lead to warpage due to a CTE mismatch. This can further add to delamination at the interface during fabrication. The adhesion is measured by laminating a 15 µm ABF™ buildup film on the two synthesized magnetic films and conducting a peel test on them. Figure 3.7 shows the adhesion strength, which confirms excellent bonding properties. The average adhesion strength of MPC 1 to buildup film is 900 g/cm and that of MPC 2 is 1000 g/cm.

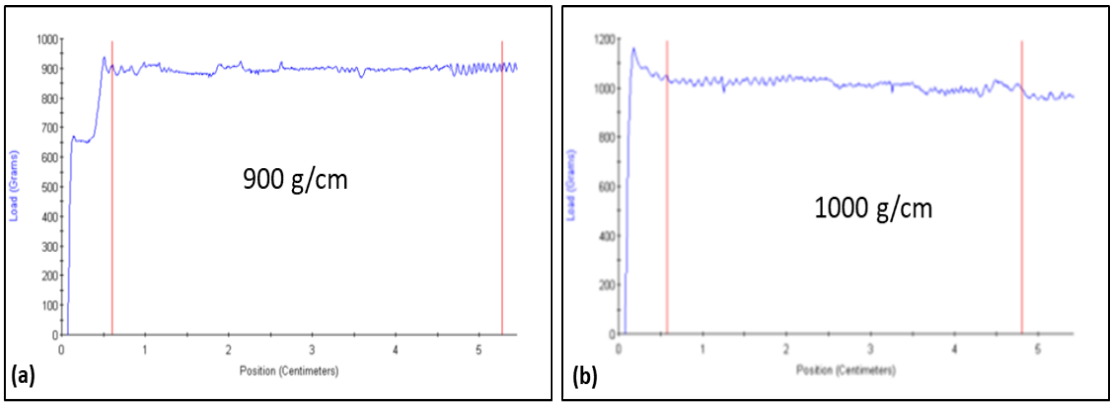

Figure 3.7: Peel strength of ABF laminated magnetic cores for (a) MPC 1 (b) MPC 2

The complex permeability spectrum of the two MPCs and the reference MPC 3 are measured using a vector network analyzer (VNA) and impedance analyzer. The quasi-static M-H loop for the materials was measured, where M and H are related by equation (11).

$$B = \mu_o(H + M) = \mu_o(1 + x_{mo})H \tag{11}$$

The results for MPC 1, MPC 2 and MPC 3 are shown in Figure 3.8, Figure 3.9 and Figure 3.10 respectively. The measured permeability is shown in green and compared to the modeled permeability in black.

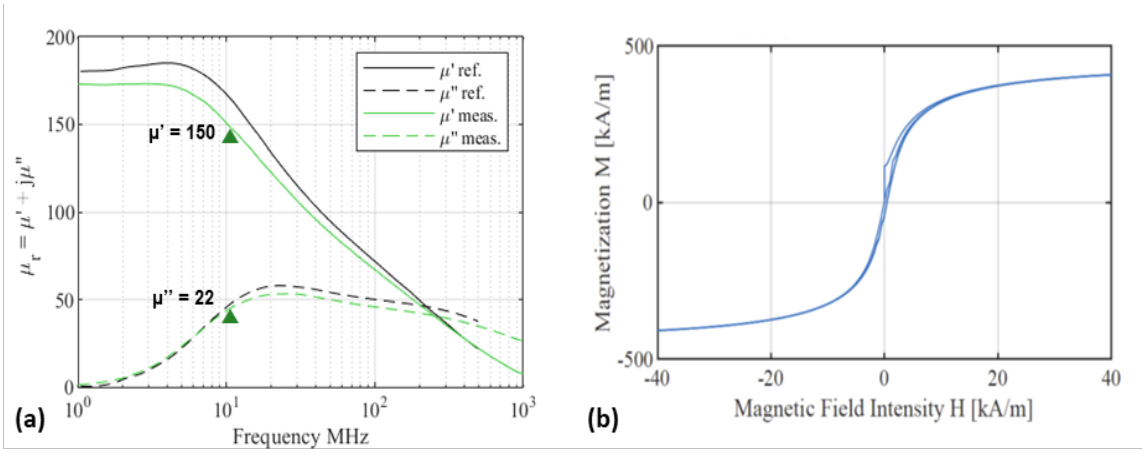

Figure 3.8: Characterization of MPC 1 (a) permeability, measured in green and modeled in black (b) M-H curve

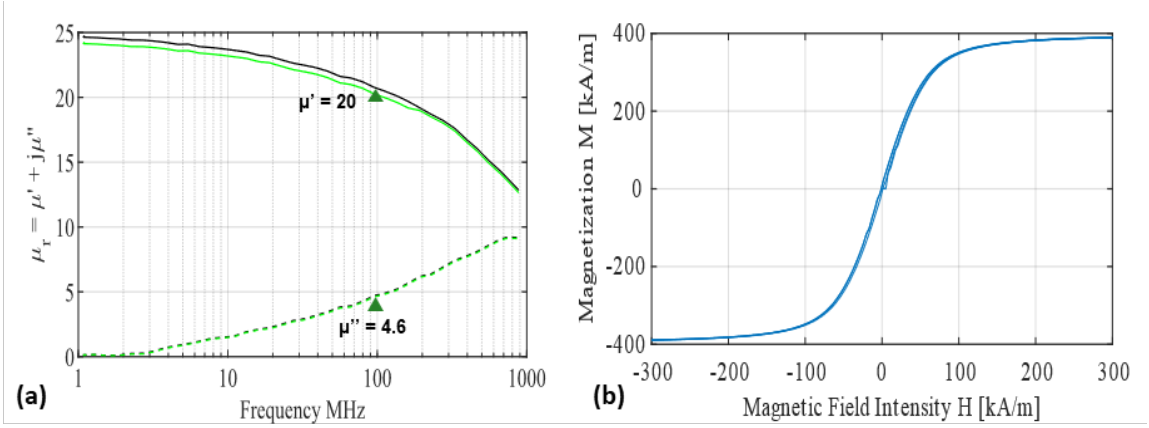

Figure 3.9: Characterization of MPC 2 (a) permeability, measured in green and modeled in black (b) M-H curve

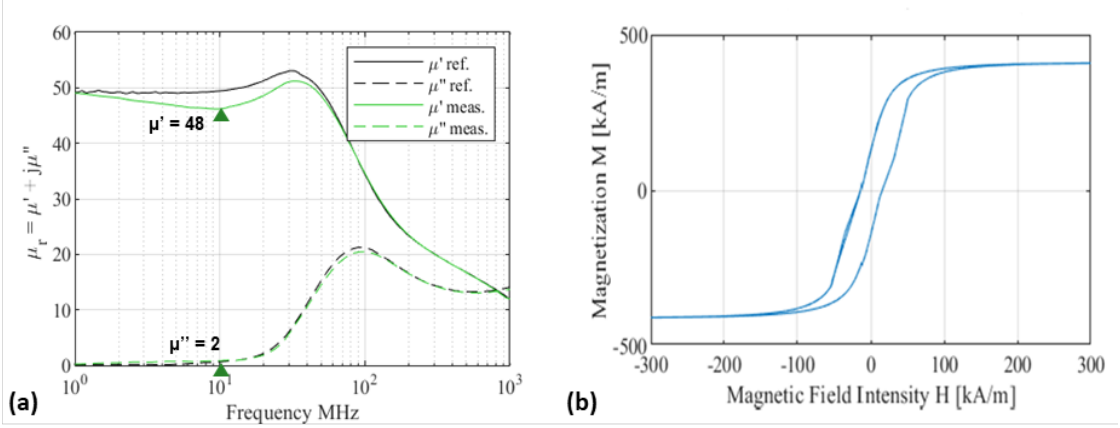

Figure 3.10: Characterization of MPC 3 (a) permeability, measured in green and modeled in black (b) M-H curve

From Figure 3.8 we see that MPC 1 starts to saturate at a magnetic field of H = 4.5 kA/m and is almost hysteresis-less. MPC 2 starts to saturate at a magnetic field of 200 kA/m. From Figure 3.10, MPC 3 starts to saturate at H = 20 kA/m and has a much larger B-H hysteresis window. But with a current ripple of 500mA, the H field span is less than 1.5kA/m which still produces very low core losses in both materials. The properties relevant to inductor performance are tabulated in Table 3.2.

Table 3.2: Properties of synthesized materials

Material	Permeability (μ)	Operation frequency (MHz)	Loss tangent (δ)	Resistivity (Ω.cm)
MPC 1	150	10	0.146	$4x10^3$
MPC 2	20	100	0.230	$5x10^3$
MPC 3	48	10	0.041	$1x10^7$

As seen from the above table, although the modeled materials show a very good permeability, the materials are highly lossy. MPC 2 shows good stability at high frequencies and so can be used for low voltage conversion ratios where the inductance requirement is low. In order to benchmark the synthesized materials, a FOM is defined for materials based on the permeability and thickness of the sheet, as given in equation (12):

$$FOM = \frac{Thickness\ of\ magnetic\ sheet\ (\mu m)}{Loss\ tangent\ (\delta)} \tag{12}$$

Figure 3.11 shows material benchmark of the permeability vs FOM for the synthesized materials as compared to magnetic materials that are available in the market [14, 57, 68–71]. It also highlights the GT-PRC region of interest and current work.

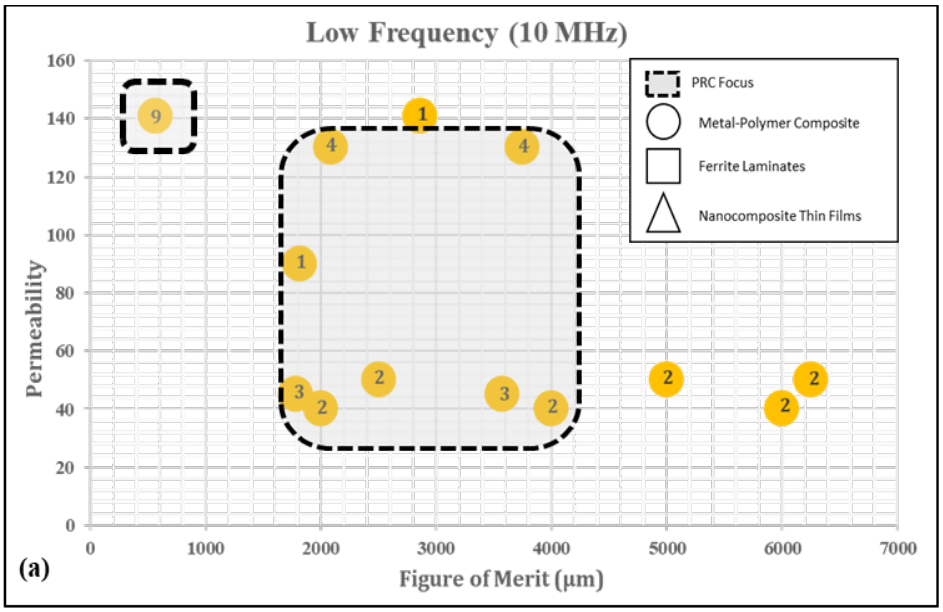

[1] Nitto Denko [2] Kemet M4, RM4A [3] TDK IFL04 [4] TDK IBF15 [5] Ferric [6] Fe-based nanocomposites [7] NiFe-based nanocomposites [8] Co-based nanocomposites [9] GT-PRC

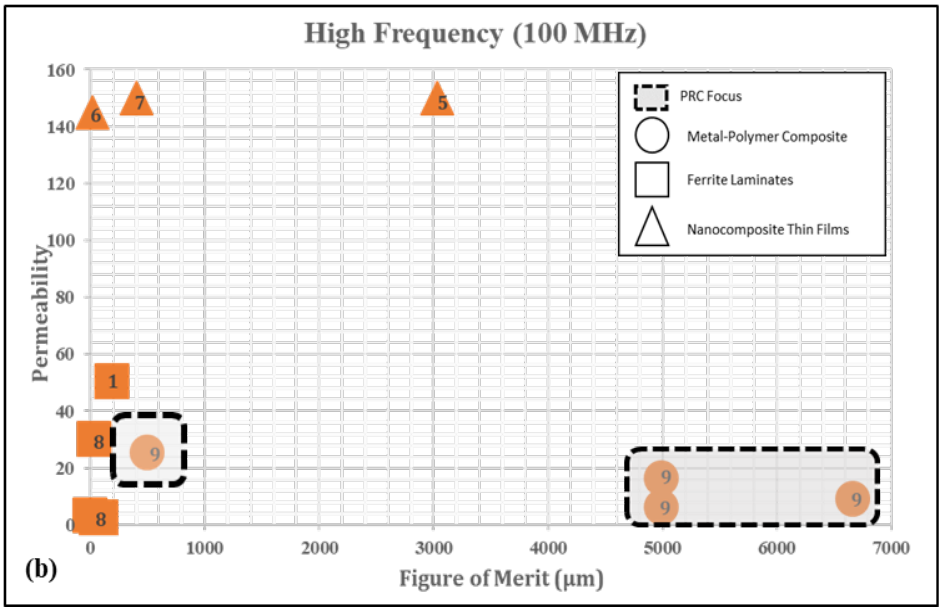

Figure 3.11: Material benchmark of synthesized materials compared to commercial magnetic materials for (a) low frequency applications (b) high frequency applications

Based on these properties and the inductor efficiency analysis, the next section discusses the frequency range in which the above materials can be used. It also predicts properties of materials for high conversion ratio applications.

3.4 Material benchmarking

Table 3.1 shows the required inductor performance for different conversion ratios. For determining the efficacy of MPC 1 and MPC 3 in 48V to 1V and 12V to 1V applications, a FOM R_{acx} vs duty cycle of one common single inductor topology was simulated and plotted, shown in Figure 3.12. • represent the targets for 48V to 1V with 4 times duty cycle extension, and × are the targets for 12V to 1V with duty cycle of 0.5.

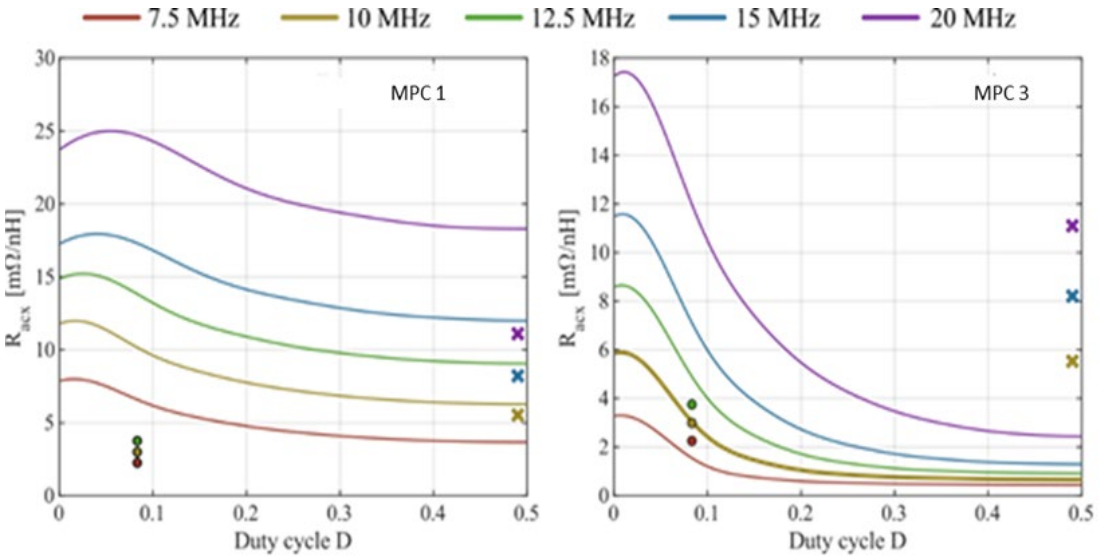

Figure 3.12: Effective AC resistance for inductors using MPC 1 and 3 at different frequencies (dots – 48V to 1V; cross – 12V to 1V)

In order to satisfy the minimum AC resistance, the • and × must be above the lines of the same color. From the above plot, it can be observed that for 48V to 1V, neither MPC 1 not MPC 2 can be utilized. However, MPC 1 is good to a certain extent for 12V to 1V up to 10 MHz, although materials with higher permeability can improve the performance. MPC 1, 2, 3 are good for 3.3 V to 1V applications as well, however for lower voltage conversions (3.3 V to 1V & 1.7V to 1V), MPC 2 is a better option since the inductance requirement is low and the frequency of operation can be increased up to 100 MHz.

For 48V to 1V to work, a material with a permeability somewhere between MPC 1 and MPC 3 is required, with the low losses of MPC 3, and the hysteresis curve of MPC 1. In order to determine the exact value of the required material properties, the LLG equation (7) was used in conjunction with the same inductor topology used to obtain Figure 3.12. To obtain a starting point for the model, the MPC 3 was used as a representative example to analyze the accuracy of this model. Figure 3.13 shows the fit obtained by equation 7 for MPC 3, and it shows a very good correlation. Therefore, it can be established that the equation can be used with an inductor topology to accurately predict the inductor performance as well as the material properties needed to achieve it.

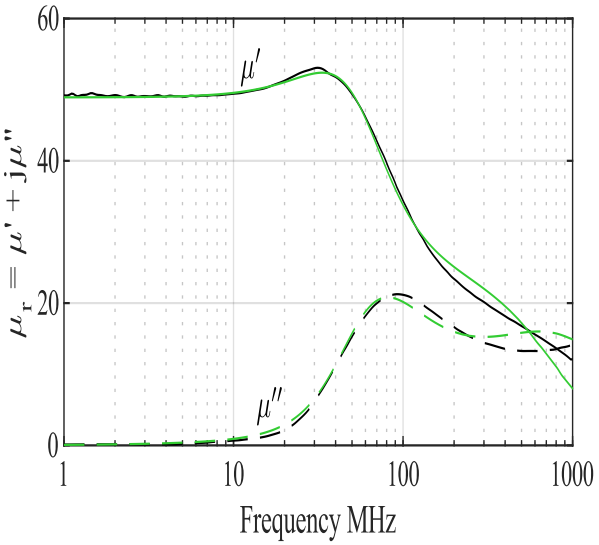

Figure 3.13: MPC 3 fitted with model of equation (7)

Figure 3.14 shows that a material for 48V to 1V should have a permeability around 90 and a loss tangent less than 0.033 at 10MHz and stable up to 50MHz (called CA90u33Lt), and for 12V to 1V it needs a permeability of 110 and a loss tangent of 0.162

at 20 MHz (called CA110u160Lt), and stable up to 40 MHz (although MPC 1 also gives a good performance).

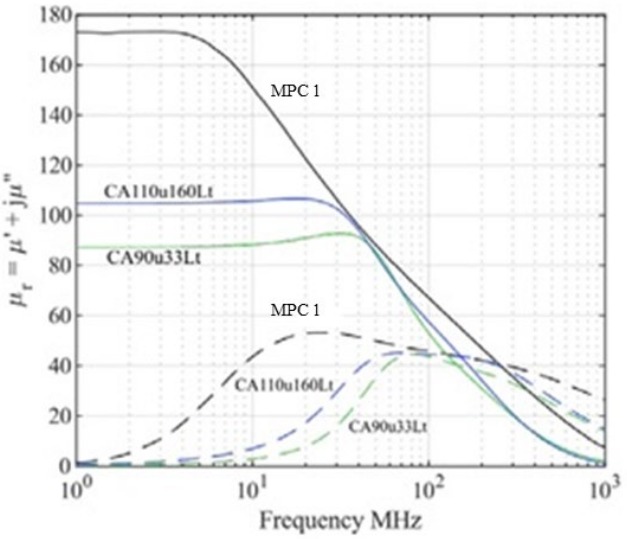

Figure 3.14: Comparison of permeability and loss tangent between synthesized MPC 1 and modeled materials CA90u33Lt (green) and CA110u160Lt (blue)

These materials should drive the design of future magnetic materials for high frequency high efficiency ultra-high conversion ratio IVR. Figure 3.15 shows the performance of the new modeled materials in Figure 3.13 for 48V to 1V and 12V to 1V conversion ratios. It is observed that the × and • are above the frequency response of the materials and hence satisfy the required inductance and AC resistance values.

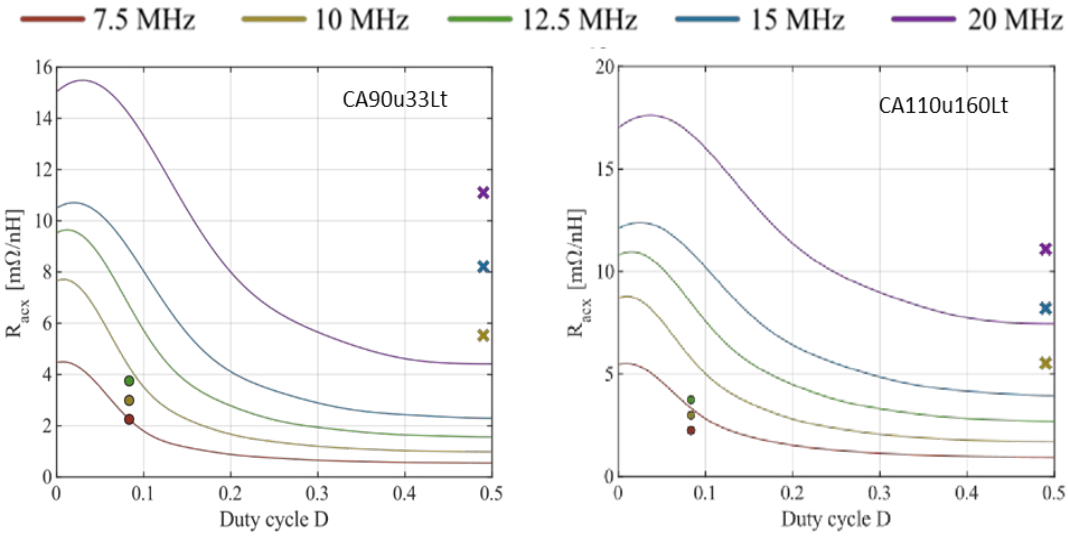

Figure 3.15: Effective AC resistance for inductors using the modeled materials (CA90u33Lt & CA110u160Lt) at different frequencies (dots – 48V to 1V; cross – 12V to 1V)

Therefore, the different inductor requirements and the materials that have the required properties in the desired range of operation and conversion ratios have been summarized in Table 3.3.

Table 3.3: Required inductor performance and the corresponding required material properties for different conversion ratio applications

Conversion ratio	Inductor topology	Operation frequency (MHz)	Required inductance (nH)	Required material properties, permeability (μ) & loss tangent (δ)
48V – 1V	Single	10, 20	91, 73	μ = 75, δ = 0.034
48V – 1V	Coupled	10	364	μ = 90, δ = < 0.033
12V – 1V	Single	10, 15, 20	45, 33, 25	**MPC 1:** μ = 150, δ = 0.146
3.3V – 1V	Single	10	20	MPC 1: μ = 150, δ = 0.146 MPC 3: μ = 48, δ = 0.041 **MPC 2:** μ = 20, δ = 0.230
1.7V – 1V	Single	50-100	8	**MPC 2:** μ = 20, δ = 0.230

In this work, the focus is on inductor design and fabrication with MPC 1, MPC 2 and MPC 3 and demonstrating that the required inductance and resistance value can be obtained for the corresponding conversion ratios. MPC 1 and MPC 3 are used for low frequency applications and MPC 2 is used for high frequency applications.

3.5 Summary

The modeling and characterization of magnetic particles are discussed in this chapter. Three major particle shapes, sphere, rod and film, are emphasized. Particles with spherical shape are preferred because of the good combination of high-permeability and high-frequency stability. A spherical particle size of less than 30 μm is chosen to be mixed with epoxy resin, with filler loading of 91 wt. % and 97.8 wt. %, to synthesize two magnetic composites. The composites are scaled up to obtain composite sheets with a thickness of 100 μm. An inductor efficiency vs duty cycle analysis gives the required inductance and resistance values for different conversion ratios. Furthermore, new materials are modeled in order to satisfy the established inductor performance requirements. It was also concluded that material with high permeability at low frequency can be used for 12V-1V applications and material with low permeability and high frequency stability is used for low voltage conversion ratios.

CHAPTER 4. INDUCTOR TOPOLOGY DESIGN

This chapter describes the design of different inductor topologies by incorporating magnetic cores for low and high frequency applications. Planar, solenoid and toroid inductors are designed for MPC 1 and MPC 2 which were introduced in Chapter 3. An analysis is conducted between the three topologies in order to determine the topology which produces maximum efficiency and meets the target objectives defined in Chapter 1 for the respective conversion ratio applications. The inductors are designed using finite-element method in ANSYS HFSS and Maxwell.

4.1 Electromagnetic simulation methodology

The magnetic circuit concept behind the design of inductors in ANSYS is based on a simple buck converter circuit as shown in Figure 2.1. In a buck converter, there are various energizing and de-energizing stages. When the inductor is energized, its current increases as it stores energy and a magnetic field is generated [77]. The amount of energy that is stored is given by equation (4), mentioned below for reference:

$$E = \frac{1}{2}Li^2 \tag{4}$$

Here, L is the inductance which as mentioned earlier is strongly dependent on the number of copper windings. The flux that is generated is dependent on the cross-sectional area of the windings. When it is drained, its current decreases as it releases energy. This builds up current which is equal to the current that is consumed by the load. Electric and magnetic circuits being analogous, the magnetic flux can be defined by equation (13):

$$\emptyset = \frac{Ni}{\mathcal{R}} \tag{13}$$

Where, $\emptyset$ is the magnetic flux, $\mathcal{R}$ is the reluctance in a magnetic circuit (like resistance in an electric circuit). This shows that an increase in the current will result in an increase in the magnetic flux. However, due to saturation of magnetic cores, after a certain value this flux will cease to increase. The saturation current depends on the given by equation (12).

$$i_{sat} = \frac{\emptyset\mathcal{R}}{N} = \frac{M_s A\mathcal{R}}{N} \tag{13}$$

A higher value of saturation current is desired and can be achieved by increasing the reluctance. This is best achieved by introducing air-gaps in the circuit or around the magnetic core as shown in Figure 4.1

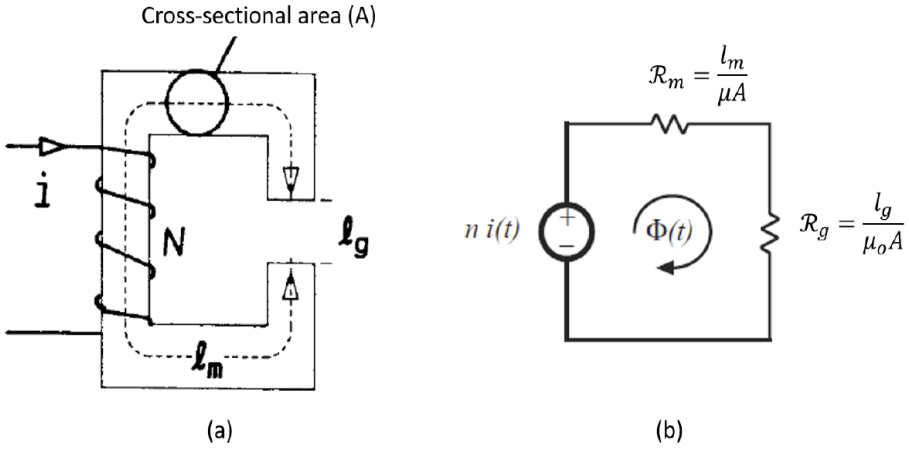

Figure 4.1: Magnetic core inductors with air-gaps to facilitate high current handling [72, 73]

While air-gaps improve the current handling, they have an adverse effect on the inductance, since an additional reluctance is added due to the air-gap reluctance in equation (13). For simple geometries, the equations for showing the effect of reluctance on the saturation current and inductance can be derived easily and used to calculate the saturation current and inductance. For complex structures, finite-element modeling is needed.

In addition to the magnetic core losses, inductor windings also contribute to the overall loss. At low frequency, the major contribution to the winding loss is DC loss. This is calculated as per equation (14). For small inductors, smaller wires are usually used. This leads to higher DC loss due to the smaller cross-sectional area since the resistance for smaller wires is higher. For high-inductance inductors, larger number of windings is used, resulting in a higher DC loss [80]. When applications require larger amount of current (1000s of amperes), DC losses become considerably more significant. During inductor design, thicker traces/windings, a smaller number of windings and high-resistivity conductors need to be used whenever possible.

$$P_{DC} = I_{DC}^2 R_{DC} \tag{13}$$

At higher frequency, another important term, loss due to alternating current (AC), starts to contribute to the overall loss. This is known as AC loss. The losses here are due the root mean square (I_{RMS}) current depends on the current ripple and load current in an inductor waveform [81]. Figure 4.2 shows the rectangular current waveform in an inductor, which is used to define I_{RMS}.

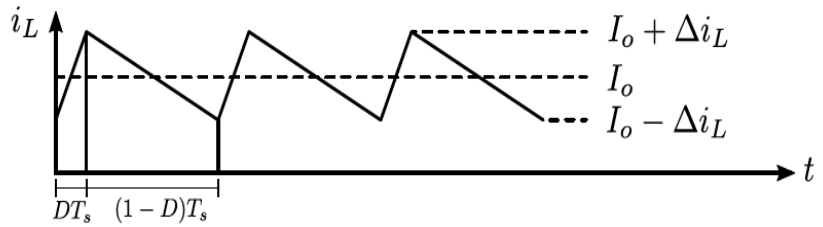

Figure 4.2: Inductor current waveform

$$I_{ripple} = I_{top} - I_{bottom} = \Delta i_L \tag{14}$$

$$I_o = \frac{I_{top} + I_{bottom}}{2} \tag{15}$$

$$I_{RMS} = \sqrt{I_o^2 + \frac{I_{ripple}^2}{12}} \tag{16}$$

The AC loss is calculated as equation 15, where R_{AC} is the AC resistance of the inductor windings at a given frequency [81].

$$P_{AC} = I_{AC,RMS}^2 R_{AC} \tag{17}$$

The skin effect is where alternating current tends to avoid travel through the center of a solid conductor, limiting itself to conduction near the surface. Faraday's law of induction states that an alternating current flowing through a wire induces a flux which is in a direction perpendicular to the alternating current. This changing flux induces eddy currents in the conductor, in the direction opposite to the initial current, which pushes the current towards the conductor surface [67]. This effectively limits the cross-sectional conductor area available to carry alternating electron flow, increasing the resistance of that

conductor above what it would normally be for direct current. The difference between AC and DC losses due to difference in current flow is illustrated in Figure 4.3.

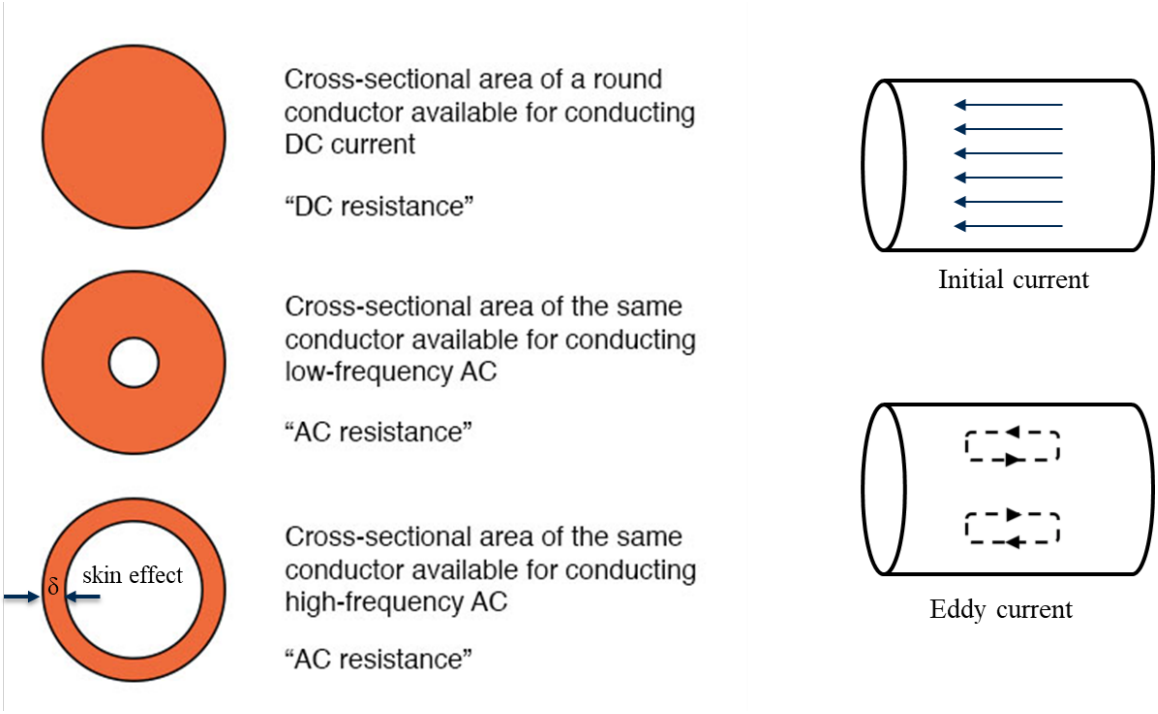

Figure 4.3: Difference between DC and AC loss due to skin effect

The AC losses can be calculated if the skin depth is known. The skin depth depends on the frequency of application, resistivity and permeability as discussed in Section 2.2.

$$\delta = \sqrt{\frac{\rho}{\pi f \mu}} \tag{5}$$

The resistivity depends on the conductor material and so cannot be changed. Therefore, the ratio of R_{AC} to R_{DC} is the ratio of the area of the ring due to skin depth, with to the area of the entire cross-section due to direct initial current. The AC resistance of a circular conductor with radius of r is then calculated as equation (18) [81]. To reduce the

AC loss, a flat wire is preferred since it has more surface area as compared to circular conductor assuming both have the same cross-sectional area [82]. The more surface area leads to smaller AC resistance and lower AC loss.

$$\frac{R_{AC}}{R_{DC}} = \frac{\pi r^2}{\pi r^2 - \pi(r-\delta)^2} \tag{18}$$

The proximity effect plays a far greater role for transformers, whereby neighboring conductors generate fields displaced by current. This results in an increase in the eddy current losses. This reduces the area for the flow of current more than that defined by the skin depth. Therefore, the AC resistance is higher than the resistance caused only by the skin effect. If the conductors carry the current in the same direction, then the magnetic field of the halves of the conductors which are close to each other is cancelling each other and hence no current flow through that halves portion of the conductor. The current is crowded in the remote half portion of the conductor. This is illustrated in Figure 4.4 below.

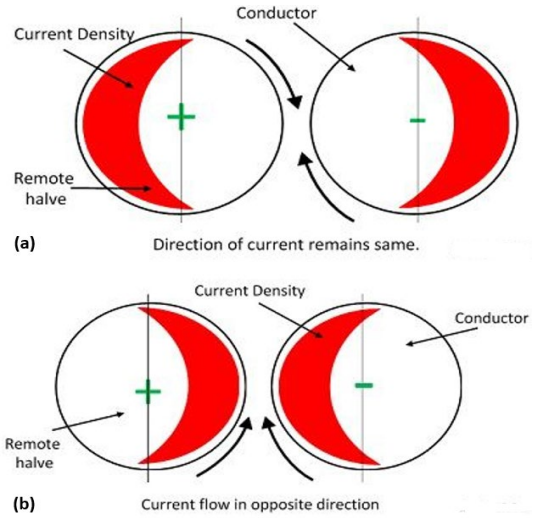

Figure 4.4: Proximity effect (a) current in same direction (b) current in the opposite direction

If direct current flows on the surface of the conductor, then the current is uniformly distributed around the cross-section area of the conductor. Hence, no proximity effect occurs on the surface of the conductor. The proximity effect mainly depends on the factors like conductor's material, conductor diameter, frequency and conductor structure.

- Frequency – The proximity increases with an increase in the frequency
- Diameter – The proximity effect increases with an increase in the diameter
- Material – If the material is made up of high ferromagnetic material then the proximity effect is more on their surface

A possibility for calculating eddy current losses for simple geometries is described by Dowell. The AC resistance under proximity effect shows strong dependence on the skin depth (δ), winding height (h) and number of winding layer (N) [80]. The DC resistance is mostly independent of these parameters. As the number of windings increase, the AC resistance increases dramatically. But it also increases the alternating current. A combination of high alternating current and AC resistance results in high AC losses. For transformers, the multi-layer needs to be avoided since the AC component is stronger than DC component. For inductors, the AC component is usually a small fraction of DC component. Thus, the inductors can be designed with multi-layer despite the proximity effect [80]. In this research, therefore, proximity effects are not considered during inductor design.

4.2 Inductor design using finite-element modeling

In ANSYS Maxwell, the permeability spectrum and the hysteresis loop of magnetic cores are required to simulate the frequency-response and current-response of power inductors respectively. Various inductor structures are designed to achieve the specifications list in the Introduction. Table 4.1 re-captures the objectives for the inductors.

Table 4.1: Inductor objectives

	Low Frequency (1 - 10 MHz)	**High Frequency (100 - 140 MHz)**
Metrics	**Objectives**	**Objectives**
Inductance density (nH/mm^2)	10-20	6
DC resistance (m**Ω**)	5-20	5-20
Thickness (mm)	0.5	0.2 – 0.3

4.2.1 Planar topology

Initially, 2D planar inductors were designed to achieve the objectives. As discussed earlier, planar inductor is an MCM topology. Traces are designed to be thick and wide in order to reduce the DC resistance. Such a planar structure is called spiral inductor. However, the magnetic field is randomly oriented in all directions which results in lower current handling for anisotropic magnetic cores. To maximize the current handling, the hard axis needs to be aligned in the direction of the magnetic field. This structure is called a “racetrack inductor”. The copper windings are elongated longitudinally to enhance the transverse magnetic field strength [83]. The current handling of planar inductors can be improved with reduced number of windings. Planar inductors with one turn are called stripline inductors and show high current-handling because of weak magnetic fields. In

addition to the high current handling, the stripline inductors also have high inductance density because of the small size. The different planar topologies have been summarized in Figure 4.5.

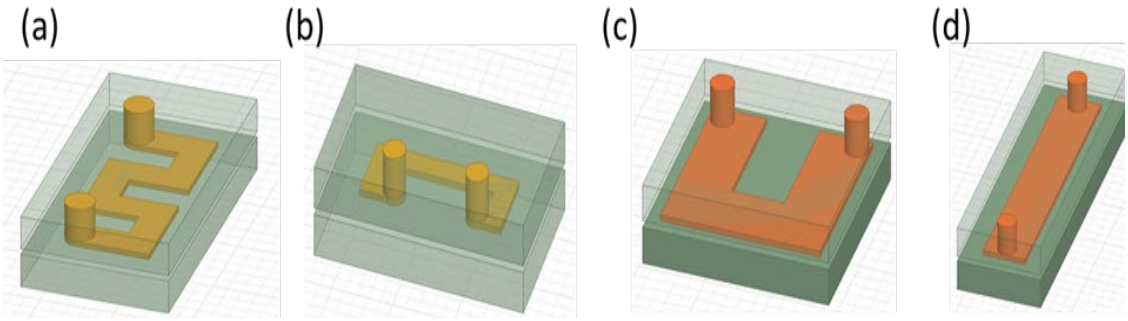

Figure 4.5: Isometric views of four planar inductor designs (a) Meander inductor (b) Spiral inductor (c) Spiral inductor (d) Stripline inductor

Different planar inductors were designed for low frequency (MPC 1) and high frequency (MPC 2) applications. Figure 4.6 show the detailed inductor design with dimensions for the low frequency material. The copper windings are sandwiched between two magnetic sheets to form a closed magnetic loop, without any air-gaps, for high inductance with low DC resistance.

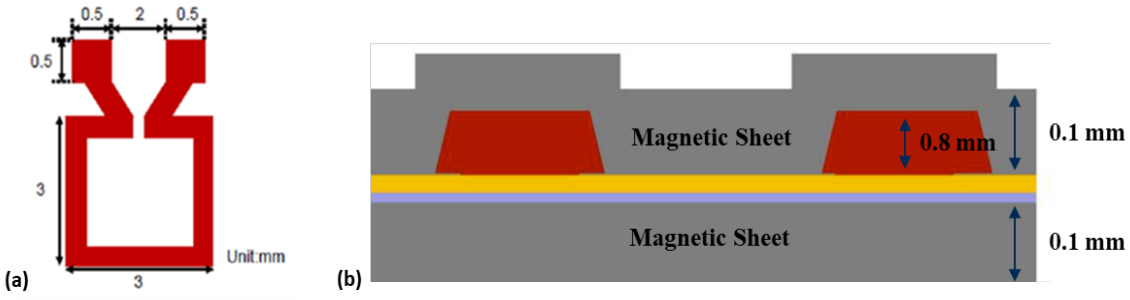

Figure 4.6: Detailed inductor design and stack-up for low frequency applications (MPC 1-courtesy Panasonic)

Table 4.2 shows the performance of the designed topology for low frequency as compared to the target objective. This inductor has an inductance of ~95 nH and a DC resistance of 10 mΩ. The total thickness and size of the inductor is ~ 300 µm and ~ 9 mm^2.

Table 4.2: Designed planar inductor for low frequency application (MPC 1)

	Low Frequency – MPC 1 (1 - 10 MHz)	
Metrics	**Objectives**	**Designed performance**
Inductance density (nH/mm^2)	10-20	10.5
DC resistance (mΩ)	5-20	10.0
Thickness (mm)	0.5	0.28

Figure 4.7 shows the detailed dimensions of the inductors for high frequency applications, which determines the inductor performance for specific applications.

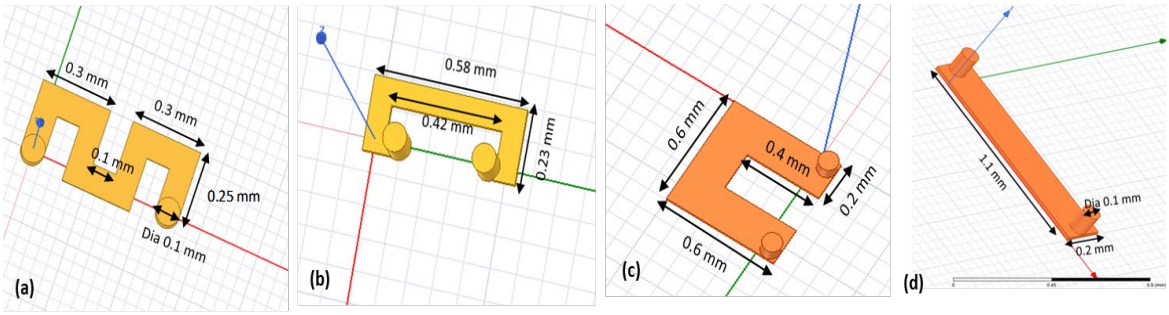

Figure 4.7: Top views of four planar inductor designs (a) Meander inductor (b) Spiral inductor (c) Spiral inductor (d) Stripline inductor (MPC 2-courtesy Panasonic)

Of the four designs, the stripline inductor was found to give the maximum inductance with lowest DC resistance as shown in Table 4.3. This is due to weak magnetic field and small inductor size as explained earlier. The DC resistance is low due to only one turn of the copper windings.

Table 4.3: Designed planar inductor for high frequency application (MPC 2)

	High Frequency – MPC 2 (100 - 140 MHz)				
Metrics	**Objectives**	**Designed performance**			
		Meander	**Spiral**	**Spiral**	**Stripline**
Inductance density (nH/mm^2)	6	7.04	6.89	7.75	7.27
DC resistance (mΩ)	5-20	9.79	8.91	5.34	4.74
Thickness (mm)	0.2-0.3	0.26	0.26	0.26	0.26

4.2.2 Solenoid topology

Next, 3D solenoid inductors were designed to achieve the objectives for low and high frequency applications. As discussed earlier, solenoid inductor is a CMC topology. These have a high current handling because of oriented magnetic fields [84]. The optimal design is shown in Figure 4.8.

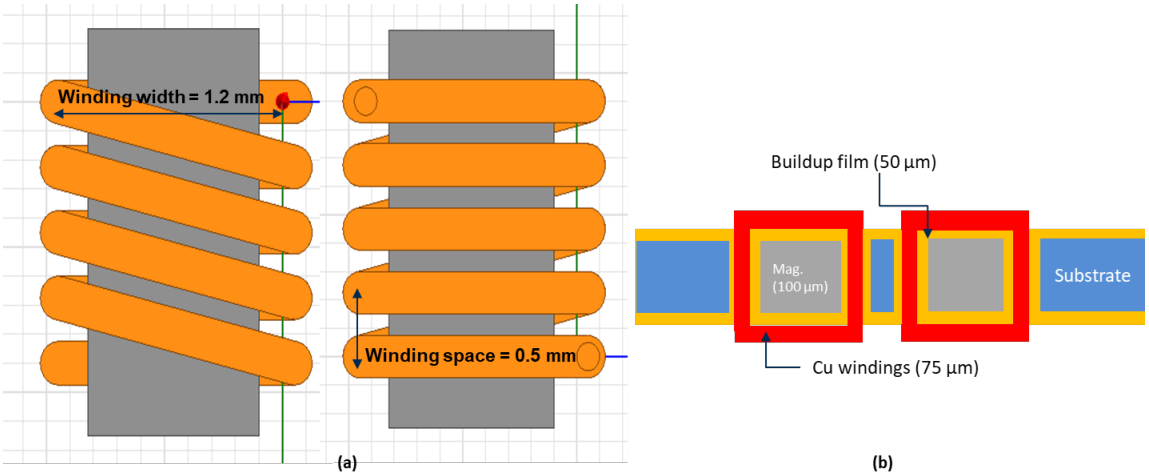

Figure 4.8: (a) Top and bottom view of detailed solenoid inductor design (b) solenoid inductor stack up

The inductance here depends on the number of windings around the magnetic core. In the design shown in Figure 4.8, the solenoid has 5 turns. Higher turns results in a higher DC resistance. For low frequency, the inductor has an inductance of 100 nH with a DC resistance of 14.94 mΩ. For high frequency, the inductor has an inductance of 84.95 nH with a DC resistance of 13 mΩ. A comparison in solenoid inductor performance for low and high frequency applications is done in Table 4.4.

Table 4.4: Designed solenoid inductor for low and high frequency applications

	Low Frequency – MPC 1 (1 - 10 MHz)		**High Frequency – MPC 2 (100 - 140 MHz)**	
Metrics	**Objectives**	**Designed performance**	**Objectives**	**Designed performance**
Inductance density (nH/mm^2)	10-20	11	6	7.92
DC resistance (mΩ)	5-20	14.94	5-20	13
Thickness (mm)	0.5	0.27	0.2-0.3	0.23

4.2.3 Toroid topology

Toroid inductor is another type of 3D inductor. In order to compare the difference between the performance of embedded solenoid and toroid inductors, both topologies were simulated [85]. Also, each structure was simulated for different number of turns. The simulated structures for the initial comparison are shown in Figure 4.9.

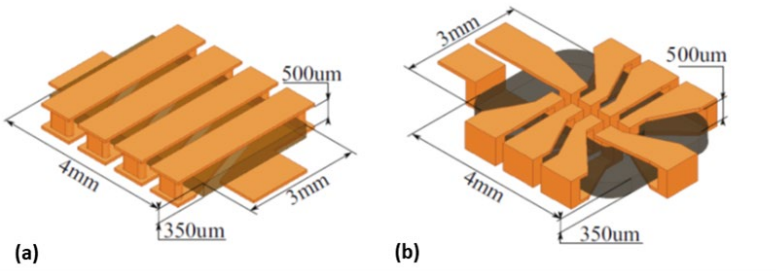

Figure 4.9: Solenoidal and toroidal inductor models [85]

Through simulation, the inductance vs. frequency with 3, 4, and 5 turns for solenoid is shown in Figure 4.10 [85]. It is observed that when the inductor is embedded (placed between two conducting planes) the inductance drops significantly [65]. This also affects the quality factor Q, which is the ratio of inductance to the resistance, as shown in Figure 4.11.

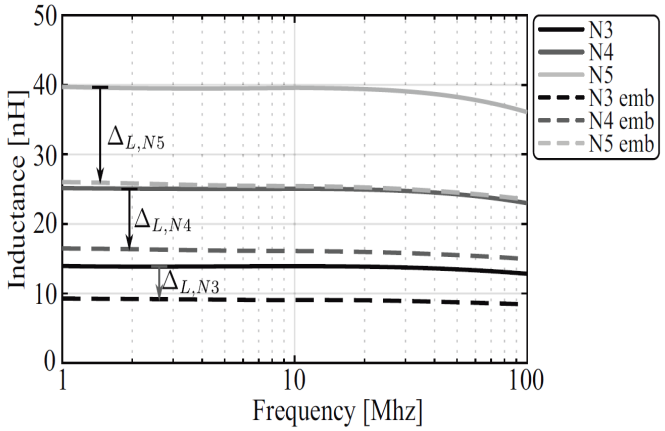

Figure 4.10: Solenoidal inductor: inductance vs frequency [85]

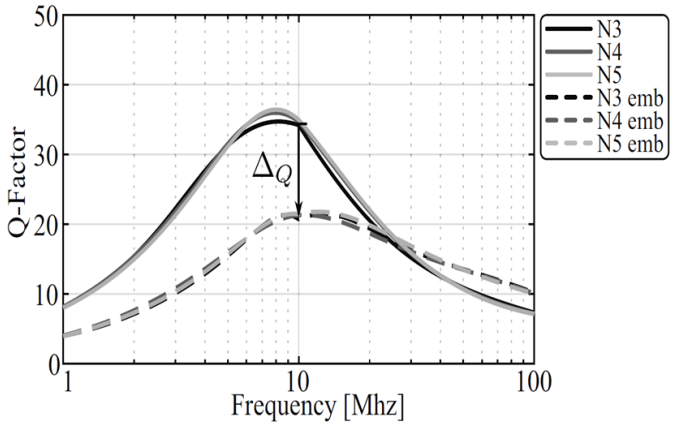

Figure 4.11: Solenoidal inductor: Q-Factor vs frequency [85]

Similarly, the toroid structure was simulated, and the inductance and Q-factor vs frequency is shown in Figure 4.12 and Figure 4.13. The solenoid inductance and Q-factor decrease by 35% when it is embedded, whereas the toroidal design is only affected by less

than 5%. Also, the toroid provides 50% more inductance, 33% higher Q-factor, for the same R_{DC}. This makes the toroidal design more suitable for heterogeneous package integration [85].

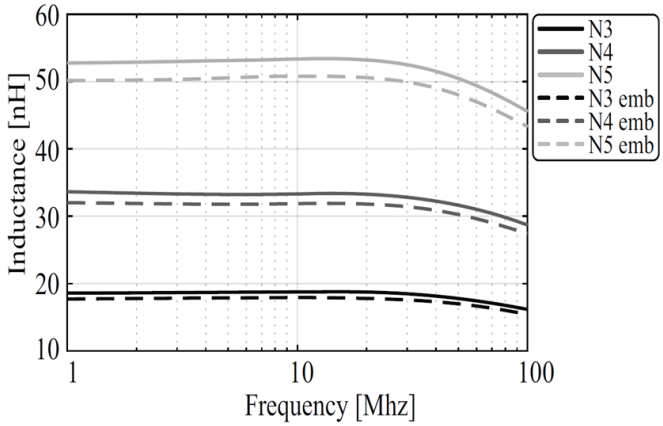

Figure 4.12: Toroidal inductor: inductance vs frequency [85]

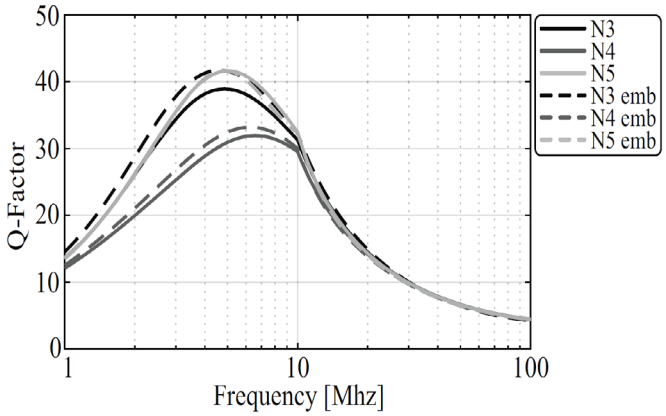

Figure 4.13: Toroid inductor: Q-Factor vs frequency [85]

In both the solenoid inductor scenarios – surface and embedded, the conduction planes reduce the field intensity and decreases the inductance. For both toroidal inductor scenarios, the conduction planes do not have a significant impact over the field intensity, as most of the energy is stored inside the toroid.

Therefore, a novel toroid inductor is designed for low and high frequency applications, which shows superior performance compared to the planar and solenoid designs (see support acknowledgements in the end). The basic toroidal cell of the inductor is shown in Figure 4.14. The core of the cell is the magnetic sheet with through vias that connect the top and bottom traces. A via (conductor line) is the simplest structure that has a close magnetic field. The magnetic field is produced by the vias and is shaped to look like an elongated toroidal inductor [86].

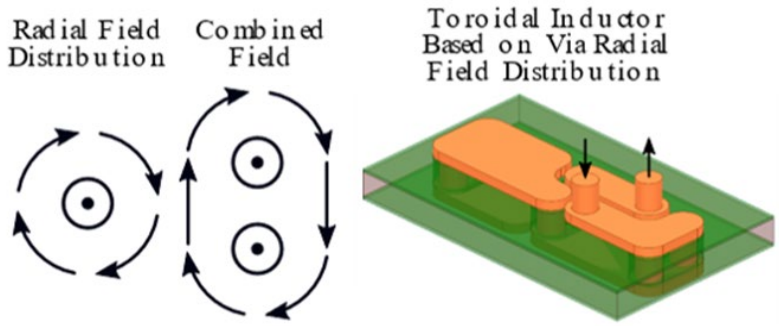

Figure 4.14: Basic toroidal inductor cell

The inductor cell presents a toroidal field distribution (Figure 4.15). This basic toroid cell can be extended to increase the number of toroidal inductors with minimum number of features. The magnetic field is not only contained within the magnetic core, but is also conformed around the inductor cell, even if the magnetic core used is much larger. This toroid design is referred to as 'interleaved toroid' or 'via expandable interleaved toroidal inductor cell with vias-in-slot thru magnetic sheet' [86].

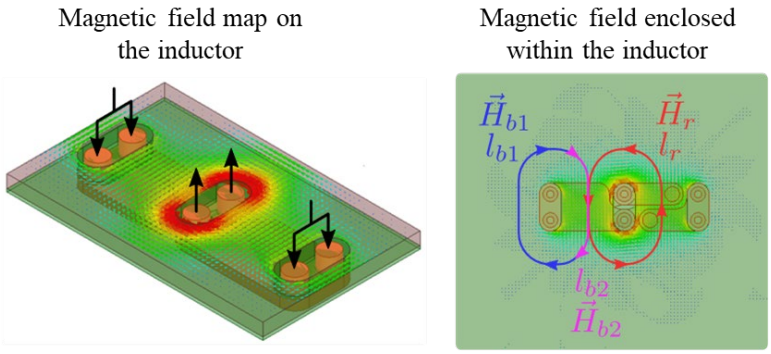

Figure 4.15: Inductor magnetic field distribution

Next, 3D toroid inductors were designed to achieve the objectives for low and high frequency applications. Four toroidal configurations were designed, each differ in size by extending the inductor cell in the X and Y direction. These are shown in Figure 4.16. The designs include a shunt which allows for meausurement of the inductor properties using a VNA. As discussed earlier, properties of MPC 1 are used for designing low frequency application inductors and MPC 2 properties are used for high frequency application inductors.

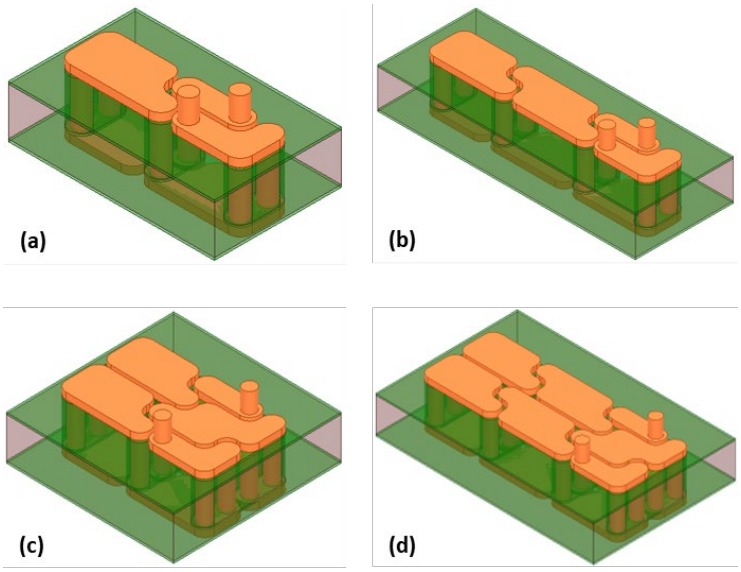

Figure 4.16: Four configurations of toroidal base cell

The trade off is between the DC resistance, inductance, inductance density, and saturation current. Each design is suitable for a particluar application frequency. For low frequency application of 12V to 1V conversion ratio, the single inductor configuration (c) and (d) are found to give the required results, shown in Figure 4.16. The entire inductance from the structure is attributed to the vias. The inductors that have been fabricated in this work are shown in Figure 4.17. The inductance due to the traces on the top and bottom is negligible. The simulated vs. objectives for these configurations are discussed in Table 4.5 and Table 4.6.

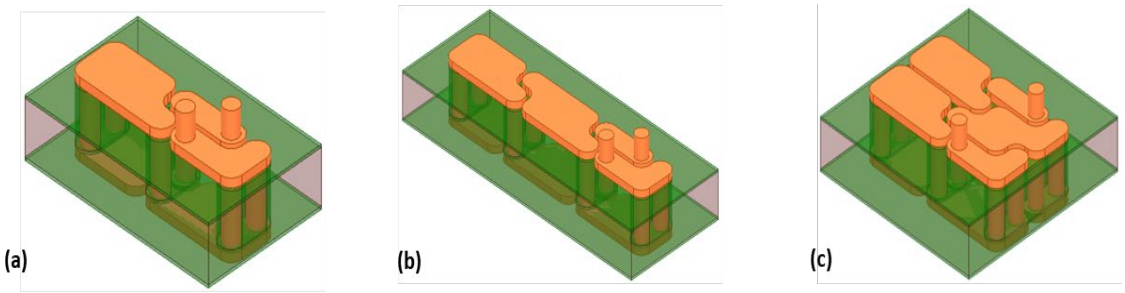

Figure 4.17: Inductor configurations for low and high frequency applications

Table 4.5: Designed toroid inductor for low frequency application (MPC 1)

	Low Frequency – MPC 1 (1 - 10 MHz)			
Metrics	**Objectives**	**Configuration A**	**Configuration B**	**Configuration C**
Inductance (nH)	45	22.23	38.10	52.8
Inductance (nH/mm^2)	10-20	10.8	13.25	17.11
DC resistance (mΩ)	5-20	6	10.2	12
Thickness (mm)	0.5	0.170	0.170	0.170
Surface area (mm^2)	-	1.8x1.15	2.5x1.15	1.8x1.7

Table 4.6: Designed toroid inductor for low frequency application (MPC 3)

	Low Frequency – MPC 3 (1 - 10 MHz)			
Metrics	**Objectives**	**Configuration A**	**Configuration B**	**Configuration C**
Inductance (nH)	45	13.02	22.27	30.8
Inductance (nH/mm^2)	10-20	6.5	7.2	11
DC resistance (mΩ)	5-20	6.6	11.4	13.3
Thickness (mm)	0.5	0.3	0.3	0.3
Surface area (mm^2)	-	1.8x1.15	2.7x1.15	1.8x1.7

For high frequency application of 3.3V to 1V and 1.7V to 1V conversion ratios, the single inductor design simulated is shown in Figure 4.15. The simulated vs. objectives for these configurations are discussed in Table 4.7.

Table 4.7: Designed toroid inductor for high frequency application (MPC 2)

	High Frequency – MPC 2 (100 - 140 MHz)			
Metrics	**Objectives**	**Configuration A**	**Configuration B**	**Configuration C**
Inductance (nH)	6-20	4.2	8.0	11.75
DC resistance (mΩ)	5-20	5.5	8.6	9.7
Thickness (mm)	0.5	0.170	0.170	0.170
Surface area (mm^2)	-	1.8x1.15	2.5x1.15	1.8x1.7

4.3 Summary

This chapter discusses the concept behind electromagnetic modeling of inductors to meet the objectives set in Chapter 3 for low and high frequency applications. The designs require a trade off between the number of inductor windings and the thickness of winndings in order to optimize the inductance density and DC resistance. Air gaps are introduced to improve the current handling, but it degrades the inductance. The EM modeling is affected by eddy current losses, skin effect and proximity effect. These parameters are optimized using FEM.

Different inductor topologies are desgined: planar, solenoid and toroid inductors. The simulated results show that inductors with spiral structure barely meet the required objectives. Inductors with solenoid structure show a slightly better performance than planar structures. On embedding, toroid inductors show the best performance compared to the other topologies. The solenoid inductance and Q-factor decrease by 35% when it is embedded, whereas the toroidal design is only affected by less than 5%. Also, the toroid provides 50% more inductance, 33% higher Q-factor, for the same R_{DC}. This makes the toroidal design more suitable for heterogeneous package integration. Therefore, the major focus of the next chapter is on the fabrication and characterization of toroid inductors in order to achieve low and high frequency objectives.

CHAPTER 5. INDUCTOR FABRICATION AND CHARACTERIZATION

This chapter discusses the basics of inductor fabrication via the semi-additive process (SAP). It describes fabrication process flow and characterization of planar and solenoid inductors. For the proof of concept of the interleaved toroid inductors, a substrate compatible novel process was established. Details of the fabrication processes are also presented. The electrical characterization of the fabricated inductors is performed to demonstrate the advantages of the toroidal structure. The measured performance results of fabricated inductors are compared to the simulated results to demonstrate the performance improvements with the proposed designs, materials and stack up. This validates the accuracy of FEM models and unique approach proposed in this work.

5.1 Microfabrication technologies

There are different microfabrication processes to form copper windings. Depending on the critical dimensions in the structures, these processes can be modified in order to fabricate the designed inductors.

The technologies in the marketplace to enable heterogeneous integration are subtractive etching process, semi-additive process (SAP) and damascene process. The simplest method is the subtractive patterning. It does not require a seed layer plating. But it results in tapered side walls with high impedance. The SAP method deposits a seed layer which is followed by electrolytic plating in order to form copper windings. The copper pattern is developed using a photoresist which transfers the circuit design from a mask to

the substrate. After metallization, the seed layer is removed using an etchant. With high resolution photolithography and optimized seed layer etch, this method has been demonstrated down to 1.6 μm pitch on organic interposers [87] and can achieve an I/O density of about 40 IOs/mm/layer [88]. The three process flows are shown in Figure 5.1.

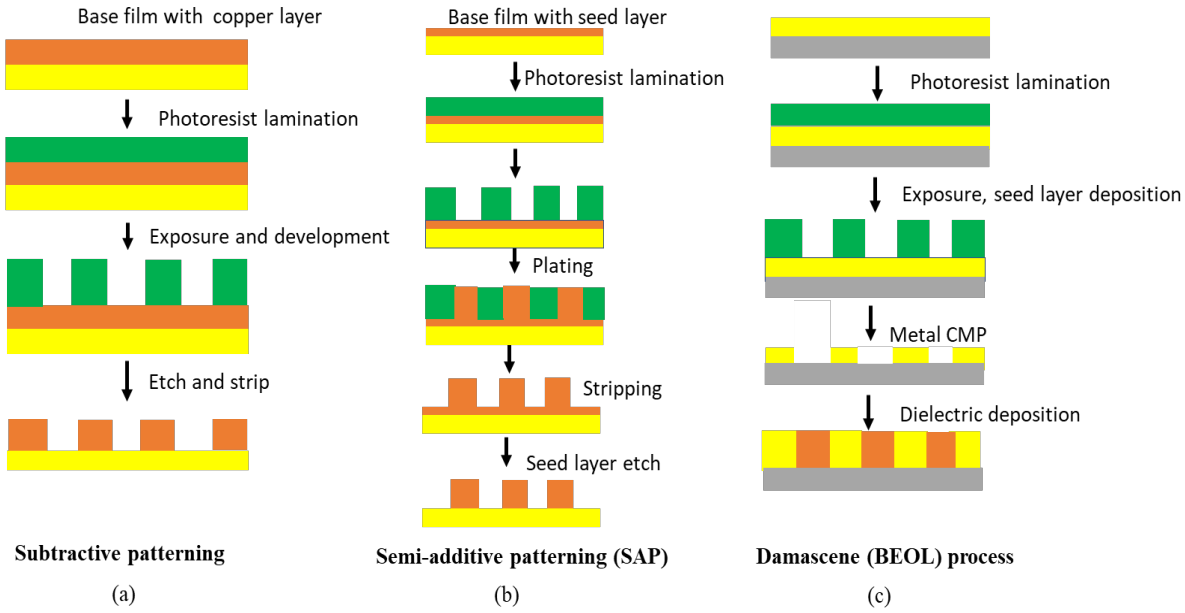

Figure 5.1: Process flow for (a) semi-additive patterning (b) subtractive patterning (c) Damascene process

However, the challenges associated with SAP process include: (i) rough surface due to the desmear of the polymer (ii) trace delamination due to narrow contact area (iii) copper trace electroplating height non-uniformity and (iv) thin dielectric film lamination to achieve planar surfaces for multi-layer RDL. The Damascene process etches vias and patterns using the deep reactive ion etching. Since this process eliminates copper etch, it results in highly precise sub-micron lines and spaces. This technology can scale to I/O densities of greater than 200 I/Os/mm/layer, at relatively higher costs [89]. However, they have high resistance and low line length for chip-to-chip interconnections.

5.2 Electrical characterization set-up

For the inductance measurement, RF probes ACP40-GSG-500 from Cascade Microtech™ were used. To measure in the range of 10 MHz and 500 MHz, a VNA from Agilent Technologies™ model E8363B was used, shown in Figure 5.2.

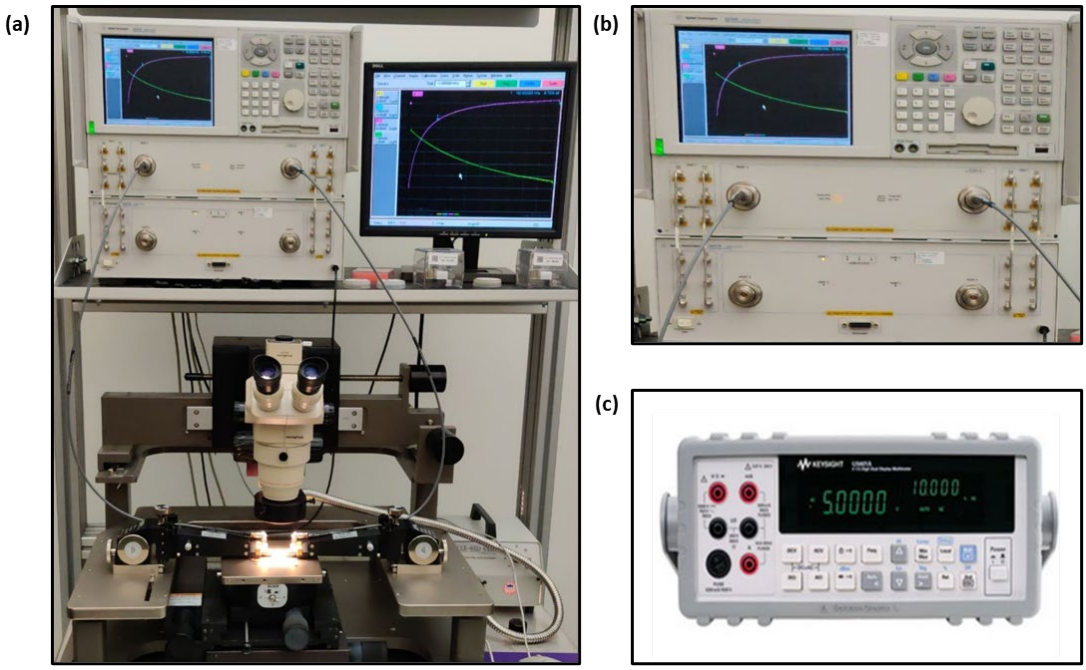

Figure 5.2: (a) VNA-probe set-up for inductance characterization (b) VNA (c) multimeter for R_{DC} measurement

To measure in the range of 1 MHz to 50 MHz an open source low frequency VNA was used. To measure the DC resistance a 4-wire method with DC probes DCP-150K-50 and multimeter from Hewlett Packard model 34401A was used, shown in Figure 5.2. The inductance is extracted by converting S-parameter into Y-parameter after 2-port measurements. This is calculated by equation (19):

$$L = \frac{imag(\frac{1}{Y - parameter})}{2\pi f} \quad (19)$$

Where, Y is the measured Y-parameter, f is the frequency and L is the inductance.

5.3 Fabrication and electrical characterization of inductor topologies

The different microfabrication processes discussed are modified and optimized for the designed inductor topologies, in the subsequent sections.

5.3.1 Planar inductor

Planar inductors have thick copper traces. This makes subtractive patterning the preferred process for fabrication. While the process is less time consuming, the copper traces are etched vertically as well as horizontally. This is because liquid etchants have low selectivity and form an undercut such that the top trace is narrower than the bottom. The resulting DC resistance is lower due to smaller cross-sectional area [90]. Therefore, the SAP process is chosen for the fabrication of planar inductors.

In this process, no organic substrate is utilized. The fabrication starts by laminating a 100 μm magnetic sheet with 10 μm dielectric at 100 °C and 0.3 MPa for 60s. The dielectric film is cured in an oven at 130 °C for 30 minutes to assist polymer flow and 180 °C for another 30 minutes to assist the formation of cross-linking in the dielectric. A copper seed layer is deposited by PVD. First a 50 nm layer of titanium, followed by a 150 nm layer of copper seed layer is deposited. Next, the copper windings are formed by Ultraviolet (UV) lithography with a 25 μm photoresist followed by electroplating. Another 100 μm

thick magnetic sheet with dielectric is laminated onto the copper windings. Layers of dielectric is used to ensure planarization. UV laser was used for via-in-via drilling to access the metallization for probing, testing and forming redistribution layers (RDL) for package integration. The process flow is summarized in Figure 5.3.

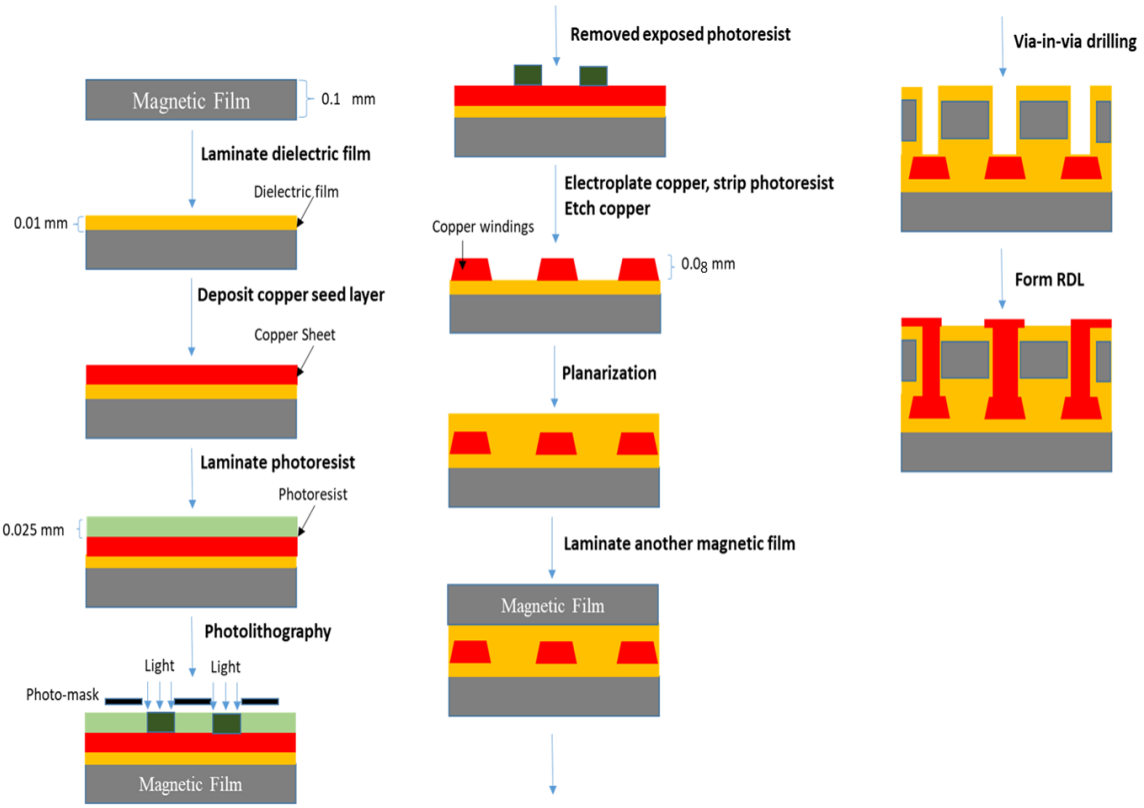

Figure 5.3: Fabrication process flow for planar inductor with magnetic core

Planar inductors were fabricated using both the low and high frequency material for all the designed topologies. The fabricated inductor is depicted in Figure 5.4. These were characterized using the set-up as discussed earlier. The measured inductance for the low frequency application is ~112 nH at 10 MHz for an inductor area of 9 mm^2, and the DC resistance is measured to be ~9.8 mΩ, compared to a simulated R_{DC} of 10 mΩ.

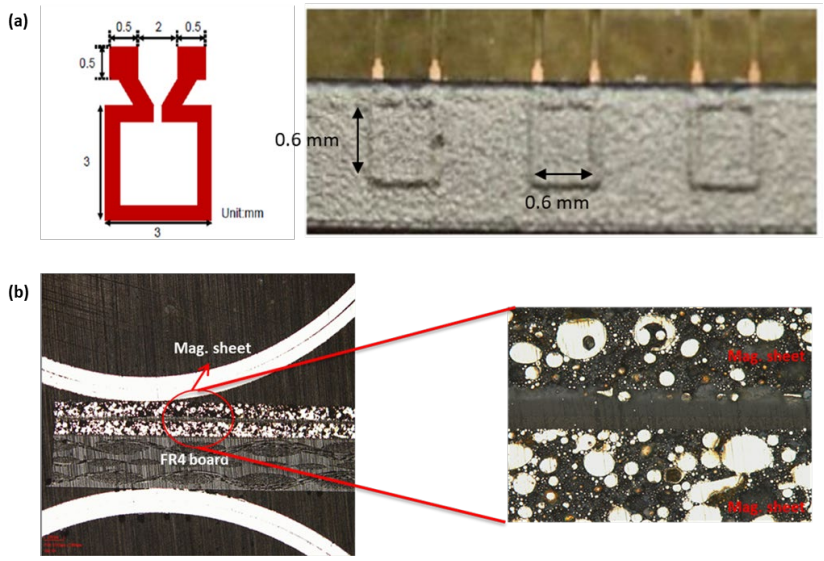

Figure 5.4: (a) Top view of fabricated planar inductor for low frequency applications (b) cross-section of fabricated planar inductor for high frequency applications

The fabricated value shows a very good correlation to the simulated value since the copper windings are thick and wide and do not require via filling. Formation of such windings is easier and results in a low R_{DC} value. Similarly, the measured inductance for the high frequency application is ~18.62 nH at 100 MHz, and the DC resistance is measured to be ~4.72 mΩ, compared to a simulated R_{DC} of 4.7 mΩ. The simulated and measured values for planar inductors are compared in Table 5.1 for low and high frequency applications.

Table 5.1: Comparison of measured and simulated values for planar inductors

	Low Frequency – MPC 1 (1 - 10 MHz)			High Frequency – MPC 2 (100 - 140 MHz)		
Metrics	**Objectives**	**Simulation**	**Measured**	**Objectives**	**Simulation**	**Measured**
Inductance density (nH/mm^2)	10-20	10.5	12.38	6	7.27	7.9
DC resistance (mΩ)	5-20	10.0	9.83	5-20	4.74	4.72
Thickness (mm)	0.5	0.28	0.30	0.2-0.3	0.26	0.26

5.3.2 Solenoid inductor

In the case of solenoid inductors, the copper windings are wound around the magnetic sheet. However, the core is formed by an organic substrate which holds the magnetic sheet. This structure requires via filling in order to form the copper windings. The SAP process is modified and optimized for the same, shown in Figure 5.5. The magnetic sheet is cut into small bars. Cavities are made in an organic substrate by CO_2 drilling. A 50 µm dielectric was laminated on one side of the organic substrate at 100 °C and 0.3 MPa for 60s. The magnetic bars and placed within the cavities.

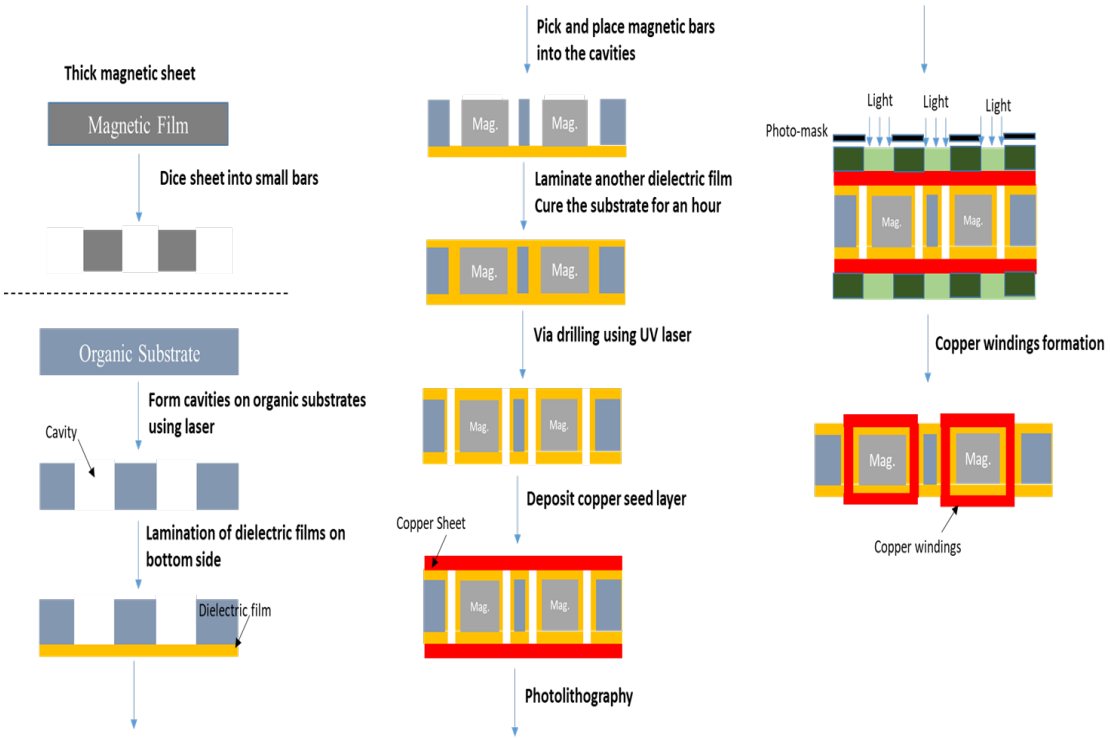

Figure 5.5: Fabrication process flow for magnetic core based solenoid inductors with organic substrate

This is followed by lamination of another 50 µm dielectric on the other side at the viscoelastic temperature such that the dielectric flows in the cavity. After curing, vias are drilled using the UV laser (6 W power) in the cured polymer. Without the side cavities, vias need to be drilled in organic substrates, which require much more power to be drilled through. This step is shown in Figure 5.6. For solenoid structures, the vias need to be filled with copper forming the windings. PVD of seed layer will not deposit the copper conformally along the via sidewalls. In this case, the seed layer is deposited by electroless method. Electroless deposition is preferred for high-aspect ratio cores and via filling.

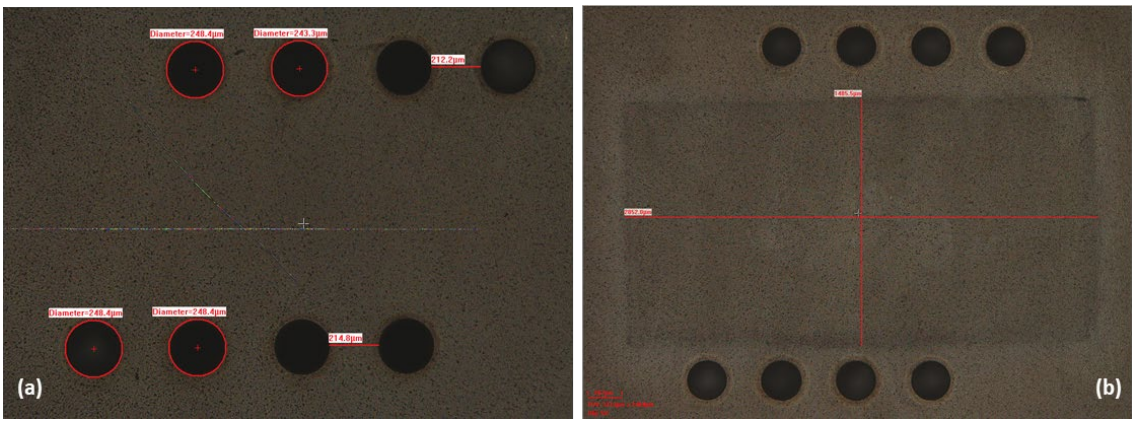

Figure 5.6: Laser-drilled vias on dielectric films

After this, photoresist is laminated on both sides in order to expose the vias and pattern traces connecting the vias on the top and bottom. This is followed by electroplating for metallization of vias, photoresist stripping and seed layer etching. Solenoid inductors were fabricated using both the low and high frequency material for all the designed topologies. Figure 5.7 shows the cross-section of the solenoid inductor fabricated with MPC 1 and MPC 2.

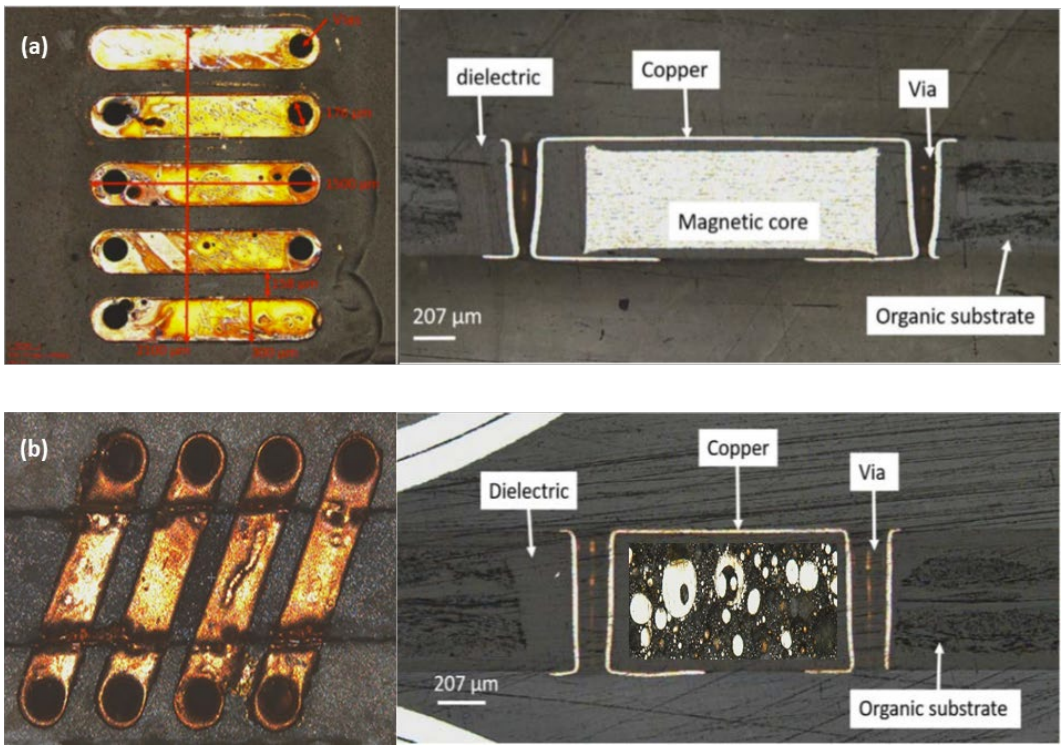

Figure 5.7: Top view and cross-section of fabricated solenoid inductor for (a) low frequency applications (MPC 1) (b) high frequency applications (MPC 2)

The measured inductance density for the low frequency application is 13.5 nH/mm^2 at 10 MHz for an inductor area of 3.5 mm^2, and R_{DC} is measured to be 18 mΩ, compared to a simulated R_{DC} of ~ 15 mΩ. This is because the designed copper thickness is 50 µm with filled vias, whereas conformal windings of 25 µm thickness were fabricated. In order to reduce the R_{DC}, the vias must be filled completely or the conformal windings must be made thicker.

Similarly, the measured inductance density for the high frequency application is 8 nH/ mm^2 at 100 MHz, and the DC resistance is measured to be 20 mΩ, compared to a simulated R_{DC} of 13 mΩ. The simulated and measured values for solenoid inductors are compared in Table 5.2 for low and high frequency applications.

Table 5.2: Comparison of measured and simulated values for solenoid inductors

	Low Frequency – MPC 1 (1 - 10 MHz)			High Frequency – MPC 2 (100 - 140 MHz)		
Metrics	**Objectives**	**Simulation**	**Measured**	**Objectives**	**Simulation**	**Measured**
Inductance density (nH/mm^2)	10-20	11.0	13.5	6	7.92	8.0
DC resistance (mΩ)	5-20	14.94	18.0	5-20	13	20
Thickness (mm)	0.5	0.27	0.18	0.2-0.3	0.23	0.16

5.3.3 Interleaved toroid inductor

Inductors with a high inductance density but low DC resistance entails a trade-off between the thickness and number of copper windings. Inductors with high inductance density can be easily achieved with large number of windings. This inevitably leads to a large form factor and high DC resistance. A low resistance is imperative for power modules to reduce joule heating and stresses induced in the package due to thermal loading.

By incorporating advanced high-permeability magnetic composites as the core, the inductors can achieve high-inductance density without the need for large number of windings. Magnetic-core toroid inductors were designed for high conversion ratio converters and to ensure package embedding and thereby reduce interconnection lengths and associated parasitics.

It was shown in Chapter 4, that the toroid design shows best performance towards achieving the target objectives. The major focus of this is on the demonstration of these interleaved toroids.

Unlike the planar and solenoid inductors, the toroid is truly embedded and does not have any organic substrate or carrier. The inductor can be directly fabricated in the magnetic sheet, and the sheet itself can be assembled directly in the IVR module, shown by the dotted area in Figure 5.8. This saves real estate in the module which is occupied by the organic substrate in other topologies.

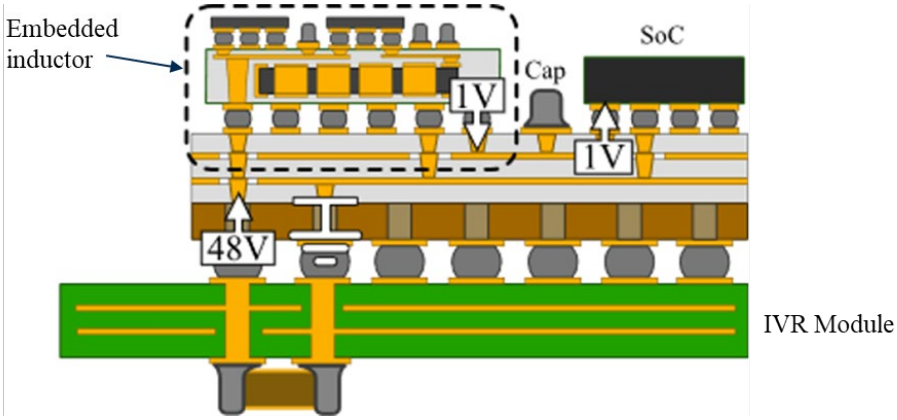

Figure 5.8: Power distribution network with embedded inductor incorporating magnetic core

Like the fabrication of solenoid inductors, toroidal designs also require via drilling and filling. This is to be fabricated using a magnetic sheet as substrate. In this, substrate slots are first drilled to make sure no magnetic material is between the vias and the coupling between them is maximized. This is important to achieve coupled inductors at this level of integration. The slots are then filled with dielectric and the vias are drilled in the slots to form the inductor. As explained earlier, the inductance of the structure is mostly due to the vias, the top and bottom traces have a negligible contribution to the total inductance of the structure. A process was developed to fabricate the designed inductors, as shown in Figure 5.9.

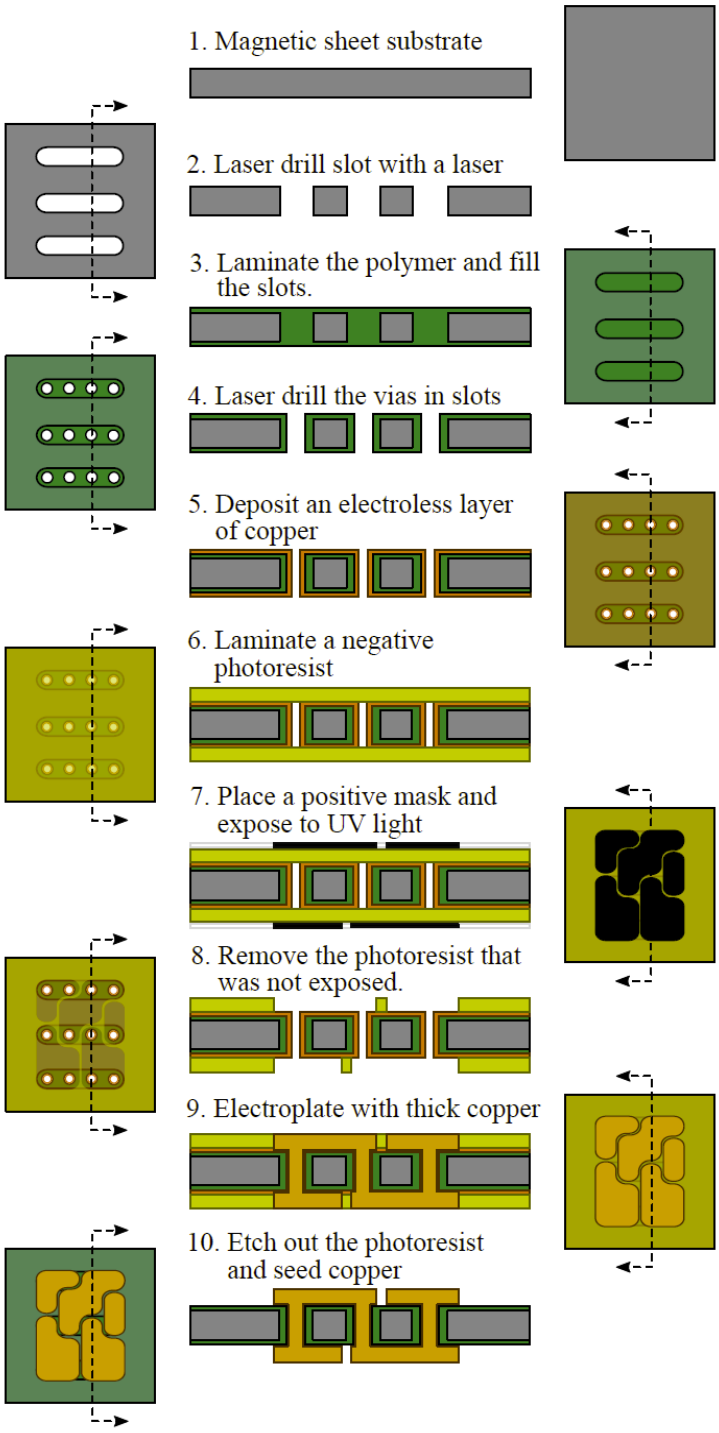

Figure 5.9: Fabrication process flow for magnetic core based solenoid inductors with organic substrate

First a magnetic sheet is used as the substrate/core and ellipsoidal slots are drilled with a femto-second laser (steps 1 and 2). The femto-second laser thermally ablates the material by impinging excited electrons on the core surface that ionizes the material. The material evaporates in the form of plasma, creating the desired pattern. The size of the slots is controlled by optimizing the laser power, speed and drill repetitions. Figure 5.10 shows the initial attempts at drilling slots in the core, by only increasing the number of laser pulses. The process was optimized by pulsing laser repeatedly at high speeds in incremental steps, downward (z direction) through the core, keeping the laser power low. This prevents local heating of the material, which causes burning of the edges and flaking of magnetic particles in the core. The thickness of the core controls the accuracy and cleanliness of the slot. As expected, thicker cores need high power for the through slots, causing more error in the cuts. Figure 5.10 shows the slots drilled using the optimized drilling process.

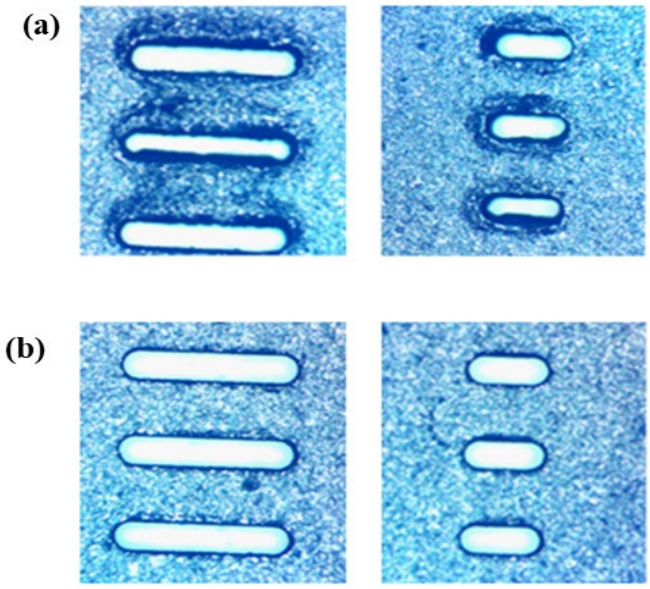

Figure 5.10: Top view of (a) initial slots in the core showing burnt edges and flaking of magnetic particles, due to thick core, high laser power and low speed (b) slots in core using optimized laser drilling process

In step 3, the slots are filled with a 15 μm ABF^{TM} dielectric film, by hot pressing under vacuum at the viscoelastic temperature of the dielectric, allowing it to flow into the slots. Thicker cores require thicker films to fill the slots completely in order to avoid voids and sagging of the dielectric within the slots. Next (step 4), the vias are laser drilled in the polymer-filled slots (via-in-via drilling). This allows the vias to be separated from each other by dielectric, leading to a toroidal structure around the top and bottom copper traces through the isolated vias. Therefore, the vias need to be perfectly aligned within the slot. This process was optimized in a similar fashion as the slots. The top view of the vias drilled in the polymer-filled slots are shown in Figure 5.11.

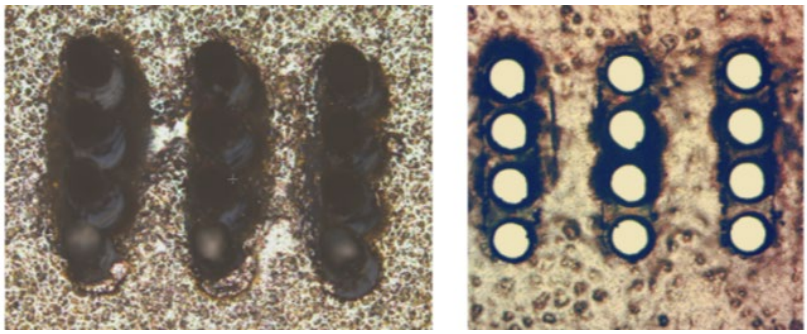

Figure 5.11: Top view of (a) initial vias in the polymer filled slots showing burnt edges and misalignment (b) vias in slots using optimized laser drilling process

In step 5, a thin layer of electroless copper seed layer is deposited. This is followed by UV lithography process, where a negative photoresist is vacuum laminated over the copper seed layer (step 6) and a positive mask is used to pattern the top and bottom layers (step 7). A problem encountered while lamination and development of the photoresist was the clogging of the photoresist inside the vias. The development solution was unable to remove this, leading to incomplete copper plating in the vias.

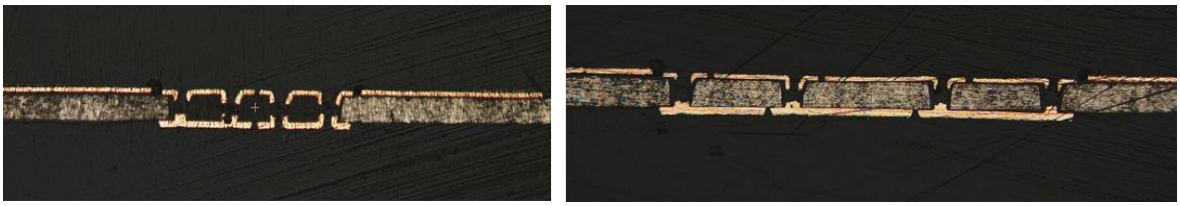

Figure 5.12: Cross-section depicting incomplete plating and no connection between top and bottom traces due to photoresist clogging

This resulted in no connection between the top and bottom traces, depicted in cross-section shown in Figure 5.12. To avoid this, the photoresist was hot rolled at low temperature and pressure. This formed an air bubble in the middle of the vias, preventing the photoresist from clogging them, shown in Figure 5.13.

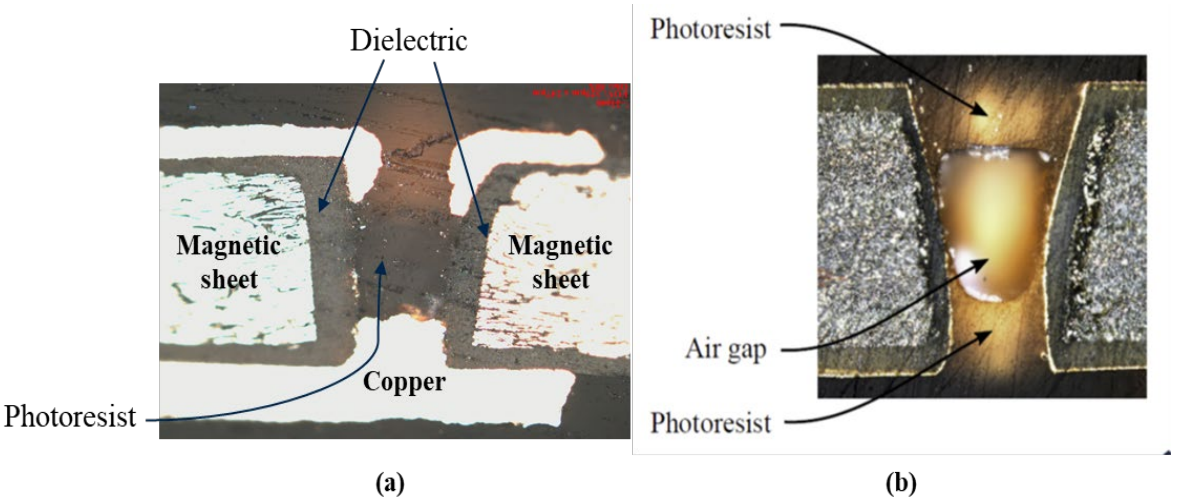

Figure 5.13: Cross-section of (a) photoresist in vias due to vacuum lamination (b) hot rolled photoresist to prevent via clogging

The photoresist is removed (step 8) and the inductor pattern becomes visible as shown in Figure 5.14. Then the copper top layer, bottom layer, and vias are electroplated (step 9). The remaining photoresist is stripped. The plated copper is annealed to remove residual copper stress and finally the copper seed layer is etched using a differential etching process leaving behind the fabricated inductor (step 10).

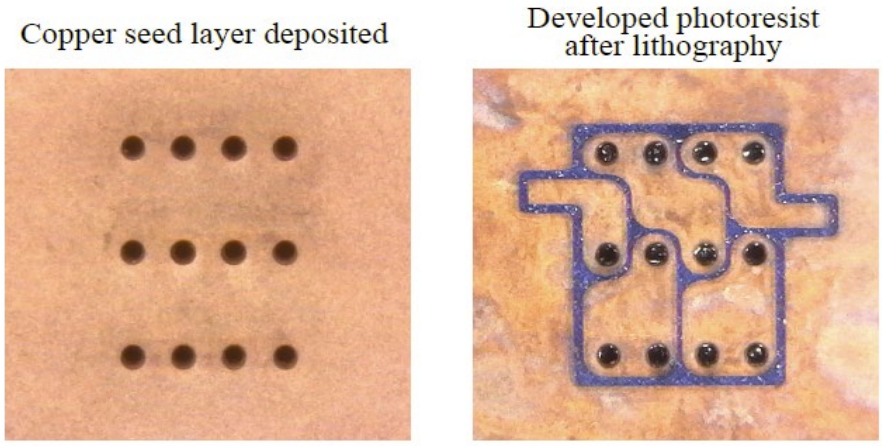

Figure 5.14: Top and bottom view after the photoresist development, exposing copper seed layer

Figure 5.15 shows one of the inductor configurations after the fabrication. The simulation model in ANSYS HFSS was adjusted to match the fabricated results.

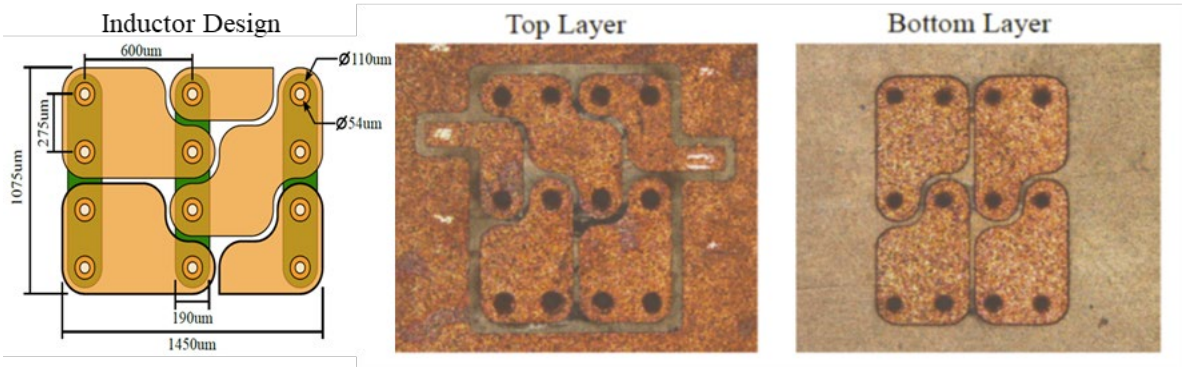

Figure 5.15: Top and bottom view of one of the fabricated inductor configurations, adjusted simulation of the fabricated inductor design (MPC 1)

Several processing challenges were encountered during the fabrication. Cross-sections were taken to study the challenges. Figure 5.16 shows two directions along which cross-sections. The first challenge is the formation of conformal vias as could be seen from the cross-sections in Figure 5.17. The vias need to be filled completely to ensure a low DC resistance.

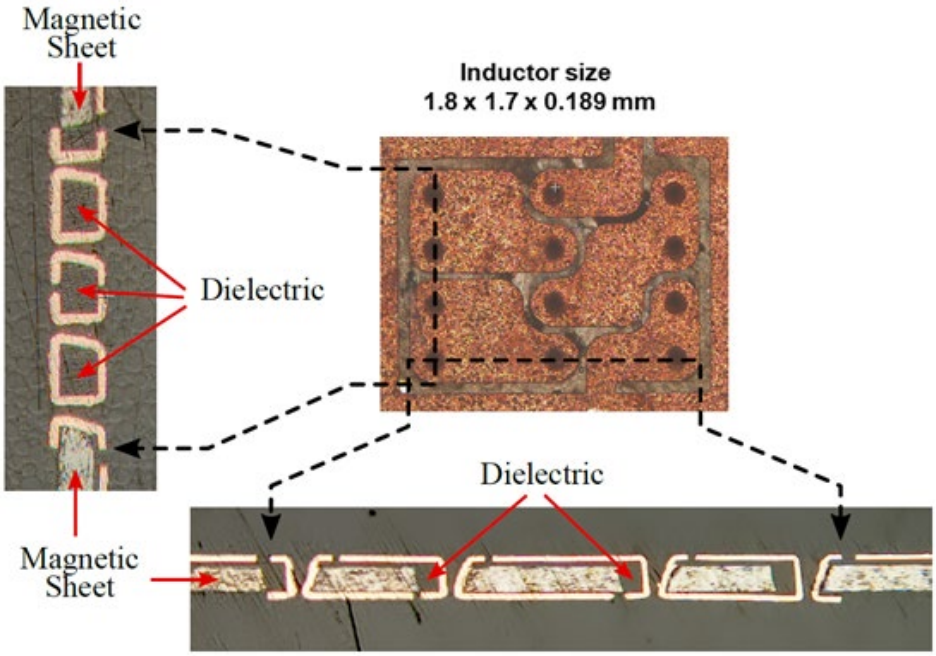

Figure 5.16: Cross-section directions of fabricated inductor using MPC1 (configuration C)

After electroplating for 90 minutes, the large vias with diameters of ~100 µm could not be filled. It is possible to completely fill the vias with longer electroplating time or changing the plating bath. However, this requires electroplating solutions with specific additives that suppress the growth of copper on the surface and promotes the growth of copper inside the vias, which out of the scope of GT-PRC facilities.

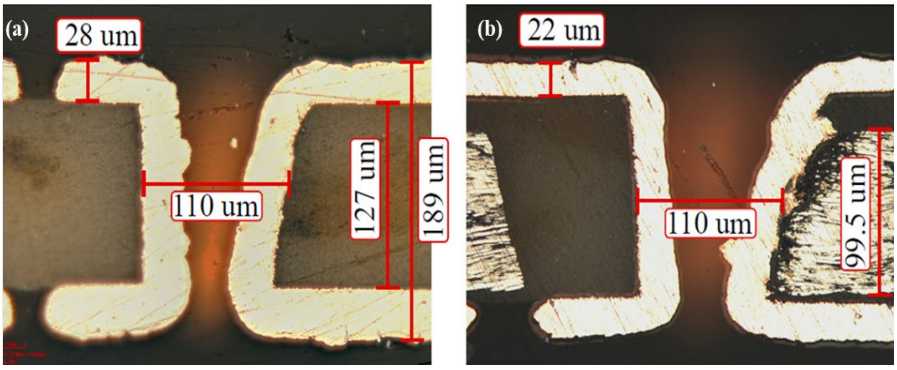

Figure 5.17: Fabricated inductor cross sections of MPC 1 along (a) slot direction (b) via direction showing conformal windings formation

The average copper thickness from the via cross-section is found to be 25 µm. Another way to completely fill the vias is to use copper paste, by using vacuum to suck the paste into vias using a squeegee followed by sintering to remove organics. The third challenge is the tapering of vias. This is because thermal ablation is higher at the surface as the beam travels downward through the core. Higher local heating spots on the surface leads to larger via opening on the top surface as compared to the bottom. To avoid tapering, two-side drilling can be optimized. The alignment marks need to be through the core for precise location of the vias from the bottom.

Once the process was optimized, the two toroid inductor configurations designed in Chapter 3 were fabricated for MPC 1 and 3. The electrical characterization was conducted as explained earlier. Figure 5.18 shows the fabricated inductor using MPC 1 with structures for shunt measurements and DC probe measurements.

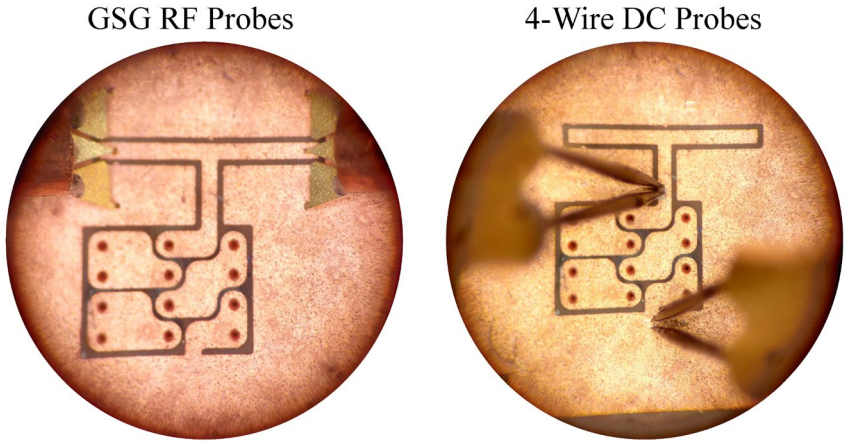

Figure 5.18: Electrical characterization of MPC 1: probes setup for measurements of inductance, AC resistance, and DC resistance

Figure 5.19 shows the inductor layout fabricated with MPC 1 which meets the 12V to 1V requirement and its corresponding inductance and AC resistance measurements. It shows a good correlation between the simulation model and the measurements using the fabricated inductor. The measured $R_{DC, meas}$ is 16 mΩ and the simulated value $R_{DC, sim}$ is 12 mΩ.

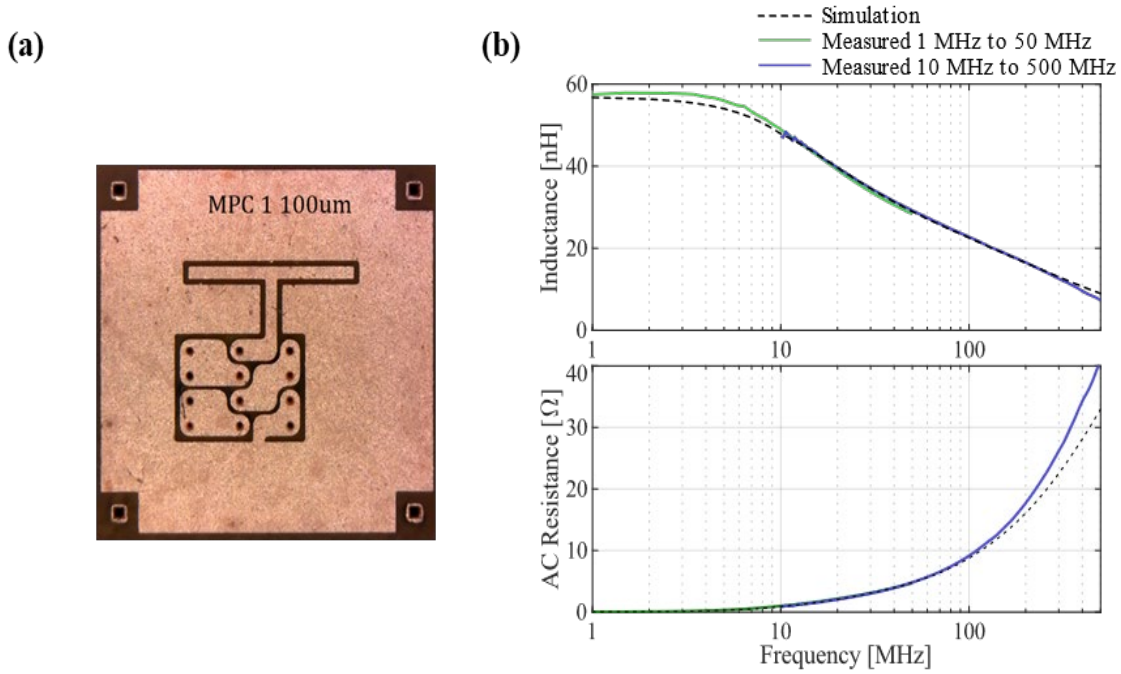

Figure 5.19: Comparison between simulated and measured inductance and resistance for MPC 1: configuration C

The measured value of inductance is seen to be higher than the simulated value below 10 MHz. This can be attributed to variation in the measured permeability value below 10 MHz which was used for the extraction of the inductance. This is because the equipment shows a lot of noise below 10 MHz.

Similarly, the remaining inductors were characterized for MPC 1 and MPC 3, as shown in the Figures below. The DC resistances have been tabulated for MPC 1 and R in Table 5.3.

Table 5.3: Comparison of simulated vs. measured DC resistance values for MPC 1 and MPC 3

R_{DC}	MPC 1		MPC 3	
	Simulated	**Measured**	**Simulated**	**Measured**
Configuration A	6	10.5	6.6	10.2
Configuration B	10.2	14.8	11.4	15.0
Configuration C	12	16.0	13.3	18.7

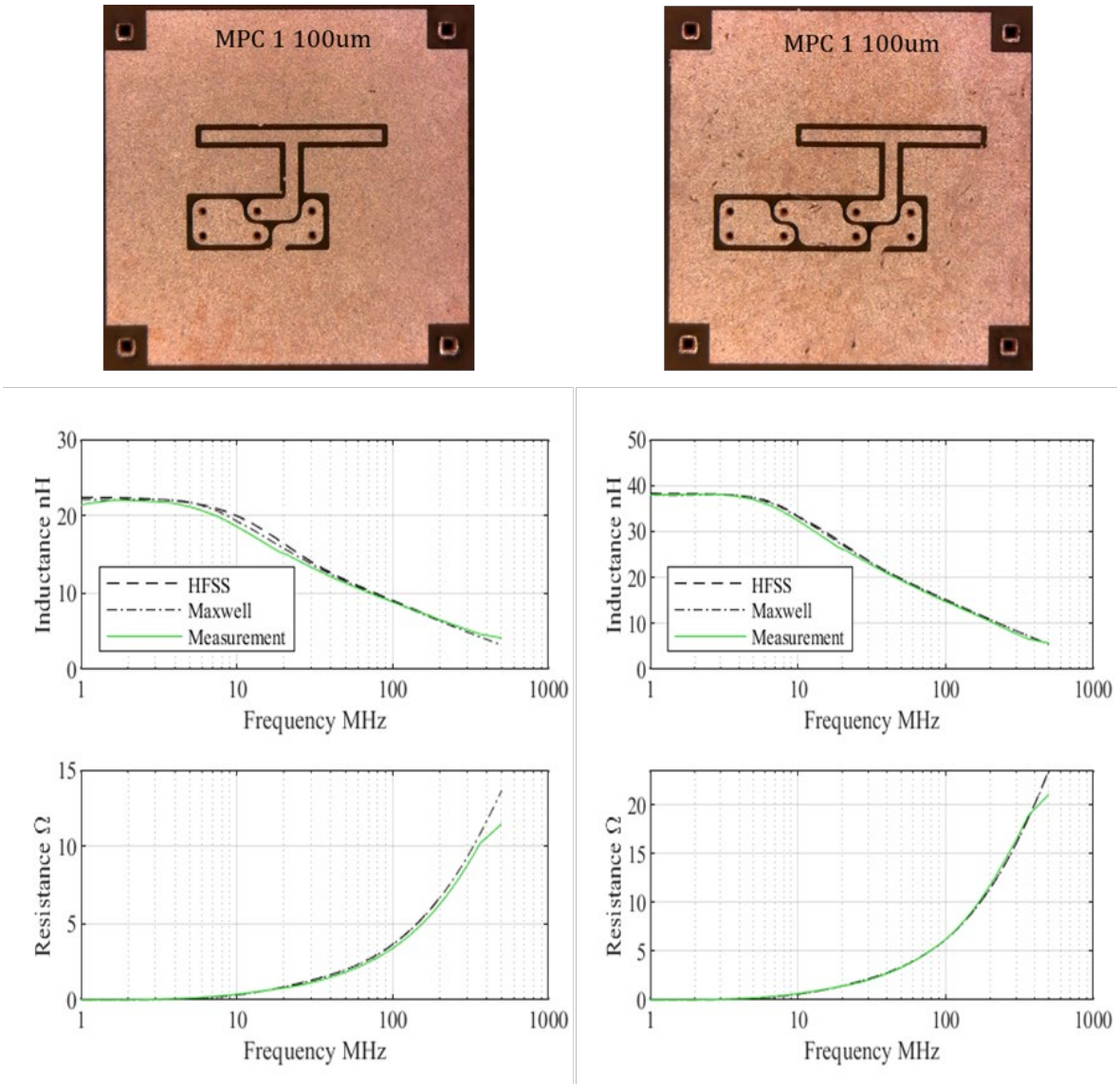

Figure 5.20: Comparison between simulated and measured inductance and resistance for MPC 1: configuration A and configuration B

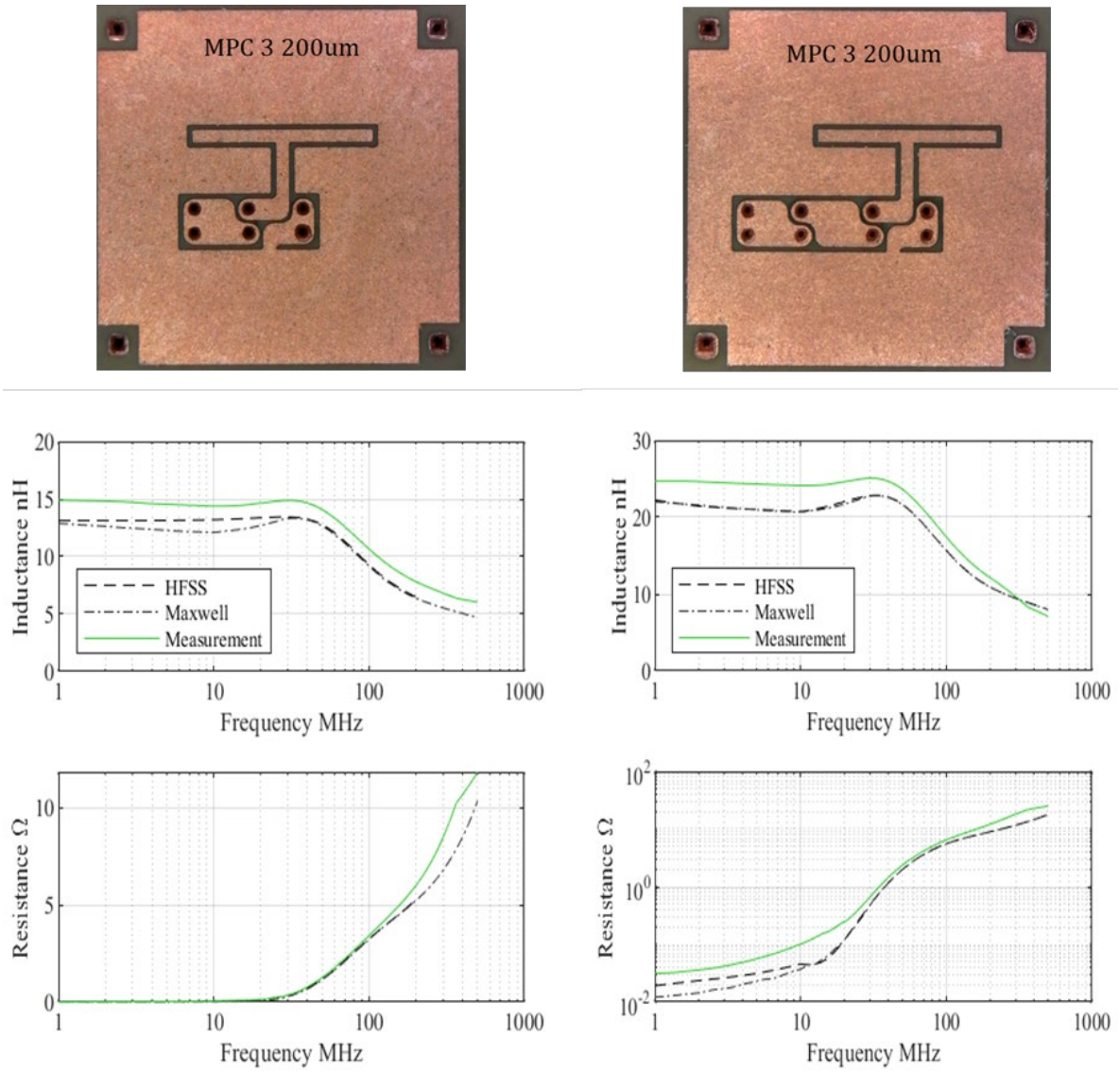

Figure 5.21: Comparison between simulated and measured inductance and resistance for MPC 3: configuration A and configuration B

The performance of MPC 1 and MPC 3 for low frequency conversion ratios measures up to the required inductance values determined in Chapter 3. The toroid configurations give much higher inductance densities and low DC resistance for smaller inductor size and lower thickness profile.

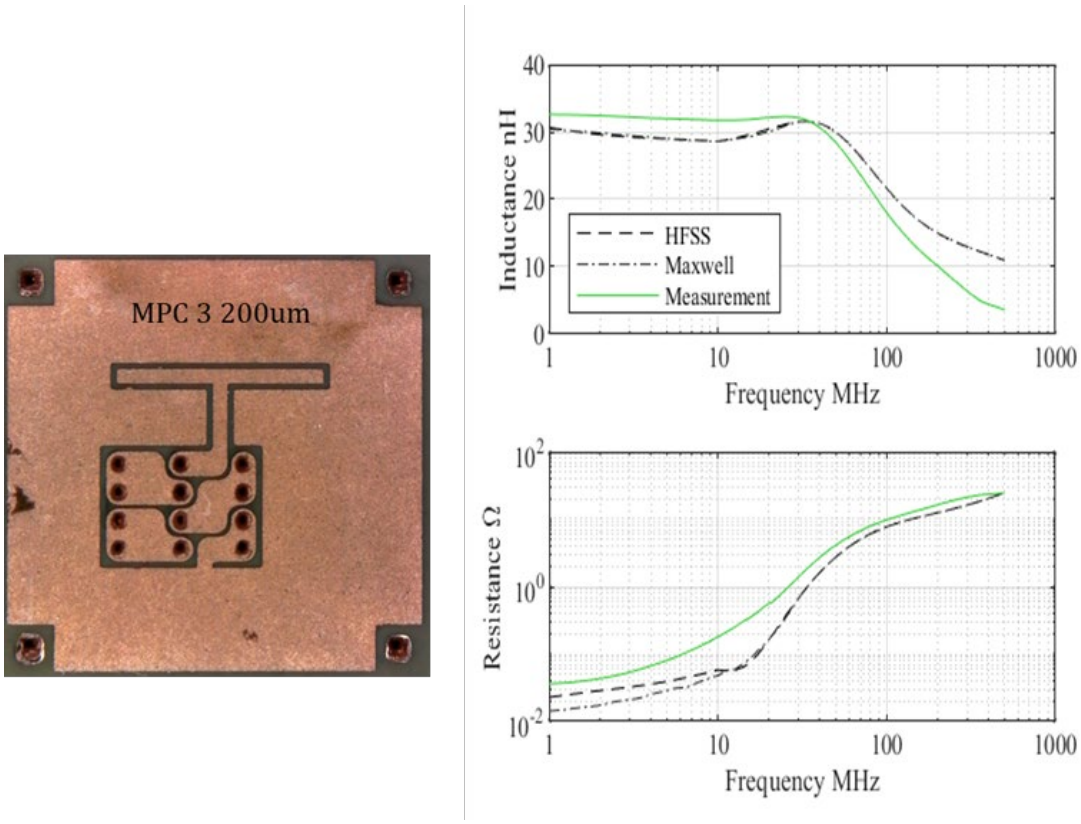

Figure 5.22: Figure 5.21: Comparison between simulated and measured inductance and resistance for MPC 3: configuration C

5.4 Summary

Fabrication of the designed planar, solenoid and toroid inductors is presented in this chapter. Various processes for microfabrication of the composite structure were explored. The frequency response of inductance and DC resistance are characterized as well. It was observed that the planar inductors showed the required inductor performance, with comparatively simpler fabrication process. However, it suffers from the formation of undercuts due to copper etching. The solenoid and toroid inductors were fabricated by SAP process, which gave higher inductances compared to the planar but had several processing limitations. The formation of conformal windings instead of fully filled vias was observed,

which resulted in a higher than expected DC resistance. Compared to the solenoid inductors, the interleaved toroids show a much higher inductance density at smaller inductor sizes and thickness profiles. The inductance density for low frequency voltage conversion was found to be 17.5 nH/mm^2 with a DC resistance of 16 mΩ for an inductor size. of 1.8 mm x 1.7 mm x 0.179 mm This makes the toroid design the better choice for embedding and package integration. The measured values were found to correlate well with the simulated values in Chapter 4. This shows that the integration of magnetic cores, combined with materials with high permeability, low loss and high frequency stability can help improve the inductor performance while keeping the footprint low.

CHAPTER 6. SUMMARY AND FUTURE WORK

This chapter summarizes the overall research work carried out in this work, to design and demonstrate a miniaturized, substrate-embedded inductor with high inductance density and low DC resistance for different voltage conversion applications. An IVR efficiency analysis was conducted in order to determine the required inductor performance for one step converters. This will allow the next generation of data centers and servers to operate with higher efficiency while delivering more computing power. The critical parameters governing the size and performance of power inductors are its inductance density and power handling capability. These parameters are determined by the permeability (μ) and saturation magnetization (Ms) of the inductor core materials. The material is needed to have a high permeability, low loss and high frequency stability. Based on the required material properties, two magnetic materials were synthesized. From the IVR analysis and synthesized material properties, inductor topologies were designed using finite-element based electromagnetic simulations. Out of the topologies that were designed and fabricated, the interleaved, embedded toroid inductor gives the maximum inductance at small footprints.

In summary, this work highlighted the importance of incorporating magnetic sheets as cores for embedded inductors. Directions for future work are briefly discussed to build upon these preliminary results and demonstrate a working inductor for 48V to 1V switching frequency power module. Based on the objectives defined in Chapter 1, three technical challenges were defined along with their associated research tasks. These research tasks performed to address the challenges are summarized in Table 6.1.

Table 6.1: Summary of the technical challenges addressed through associated research

Challenges	Tasks
Material Challenge Need materials that have trade-off between high permeability and frequency stability	Model and design magnetic-cores with high permeability, low loss and good stability at high frequencies
Inductor Challenge Inductor design for substrate-embedded inductors high inductance & current handling with low DC resistance.	Model embedded inductor topologies that meet inductance density, DC resistance requirements for an IVR efficiency of 95 % at different conversion ratio applications
Integration Challenge Lack of fabrication process to embed inductors	Develop innovative process to fabricate and embed inductors into the substrate

6.1 Summary of task 1 results

An IVR efficiency analysis was conducted to determine the required inductor performance by way of analyzing the inductor waveform. The required inductance and DC resistance for obtaining an inductor efficiency of 95% were established for 48V-1V, 12V-1V, 3.3V-1V and 1.7V-1V conversion applications. Based on these parameters, the required material properties were extrapolated. Metal polymer composites were chosen to be the magnetic cores due to high permeability, low loss tangent and good frequency stability. Two materials were synthesized to meet the specifications. A spherical particle size of less than 30 μm is chosen to be mixed with epoxy resin, with different filler leadings. The composites were scaled up to obtain composite sheets with a thickness of 100 μm. An inductance vs duty cycle analysis was conducted for the synthesized materials which established that the material with high permeability of 150 at low frequency can be used

for 12V-1V applications and material with low permeability of 25 at 100 MHz and high frequency stability is better used for low voltage conversion ratios. Using the LLG equation, the permeability vs frequency response for a known material in the market was modeled, to give a good correlation to the actual permeability response as reported. For a proposed future work, the LLG model was further used to model new materials with properties better suited for the 48V-1V and 12V-1V applications.

6.2 Summary of task 2 results

This task focused on the electromagentic design of different inductor topologies in order to meet the required inductance and DC resistance values determined from the previous task. The basic magnetic cirucit concepts that dictate different effects determing inductor performance were discussed. Larger number of windings increase the inductance, but also results in an increase in the DC resistance. Thicker windings increase the DC resistance. However, the skin effect plays an important role in the eddy current effect and losses. Higher eddy currents increase the AC resistance. It is observed that air gaps are introduced to improve the current handling, but it degrades the inductance. Therefore, the designs require a trade off between the number of inductor windings and the thickness of winndings in order to optimize the inductance density and DC resistance. The design takes into account all the parameters.

Different inductor topologies are designed: planar, solenoid and toroid inductors. Planar topologies show a high current handling but at the expense of low inductance density. They were designed to have an average inductance density of 12 nH/mm^2, DC resistance of 10 mΩ from an inductor surafce area of 9 mm^2. Solenoid inductors provide

higher inductances. On embedding, toroid inductors show the best performance compared to the other topologies. The solenoid inductance and Q-factor decrease by 35% when it is embedded, whereas the toroidal design is only affected by less than 5%. Also, the toroid provides 50% more inductance, 33% higher Q-factor, for the same DC resistance. This makes the toroidal design more suitable for heterogeneous package integration.

6.3 Summary of task 3 results

In this task, several microfabrication processes were explored and a novel process to fabricate and integrate the designed inductors was developed. The frequency response of inductance and DC resistance are characterized as well. Planar inductors do not need a support substrate, the magnetic sheet itself acts as the base core. In this, the copper windings are sandwiched between two magnetic sheets. These were fabricated by the SAP process. However, undercuts were formed which affected the DC resistance of the structures. The planar inductors show an average inductance density of 12.38 nH/mm^2 with a DC resistance of 9.8 mΩ for an inductor size of 9 mm^2, for high voltage conversions. For low conversion voltages, they show an average inductance density of ~ 7.9 nH/mm^2 with a DC resistance of 4.72 mΩ for an inductor size of ~ 3 mm^2. The size needed for low voltage applications is less because the inductance requirement is very low.

For solenoid inductors, a cavity-embedding approach was employed to achieve the objective. In this approach, the magnetic bars were embedded in cavities made in an organic substrate. The organic substrate forms the base core of the structure. As compared to the standard surface-mounted technology, this truly integrates inductors into substrates without adding any additional height to the architecture. The difference between the toroid and

solenoid is that there is no need for an additional organic substrate in the toroid structure. Both solenoid and toroid require fully filled vias for forming the copper windings for the formation of the copper-magnetic-copper topology. However, processing challenges encountered was the formation of conformal windings, which results in a higher than expected DC resistance. The solenoid inductors show an average inductance density of 13 nH/mm^2 with a DC resistance of 18 mΩ for an inductor size of 2.1 mm x 1.5 mm for high voltage conversions. For low conversion voltages, they show an average inductance density of 8 nH/mm^2 with a DC resistance of 20 mΩ for an inductor volume of 3 mm x 2 mm.

The inductance density for low frequency voltage conversion toroids was found to be 17.5 nH/mm^2 with a DC resistance of 16 mΩ for an inductor volume of 1.8 mm x 1.7 mm x 0.179 mm. Compared to the solenoid inductors, the interleaved toroids show a much higher inductance density at smaller inductor sizes and thickness profiles. The toroid design is the better choice for embedding and package integration. There was a good correlation between the measured and simulated values. This shows that the integration of magnetic cores, combined with materials with high permeability, low loss and high frequency stability can help improve the inductor performance while keeping the footprint low.

6.4 Future work

This research demonstrates substrate-integrated miniaturized inductors with high inductance and low DC resistance. The inductors show high efficiency of 10 nH/mΩ and a low thickness of 190 μm. The inductors demonstrated in this work lower the thickness, integrating the power module closer to the SoC. This lowers the parasitics increasing the power delivery network efficiency. Magnetic cores with high permeability, low loss and

high frequency stability combined with novel interleaved toroid topology and fabrication process are crucial to realize high efficiency inductors for package-integrated IVR. The inductor performance can be further enhanced by further advances in materials and design. The following directions are suggested for future research in this area:

- **Magnetic materials**: In order to realize inductors for 48V to 1V switching applications, materials with high permeability, high roll offs are needed. The permeability should be around 90 at 10 MHz with a loss tangent of 0.033. Such materials have been modeled for future work in this research. In order to synthesize these materials, trade-off must be made between the filler loadings, particle shape, size and material type.
- **Coupled and tapped inductor designs**: Innovative inductor structures with coupled or tapped toroid designs need to be analyzed to improve inductance density and current handling without the need for thick inductor cores.
- **Processing of fully-filled vias:** Challenges with conformal vias need to be addressed while fabricating inductor structures that require vias. Filling the vias with conductive paste is one solution to address this challenge. However, the residual porosity, high stresses and incompatible sintering temperatures causes other challenges to the inductor fabrication. The feasibility of various via-filling options needs to be further studied. The other solution is electroplating for longer times (~ 3 hours), which makes the process cumbersome.

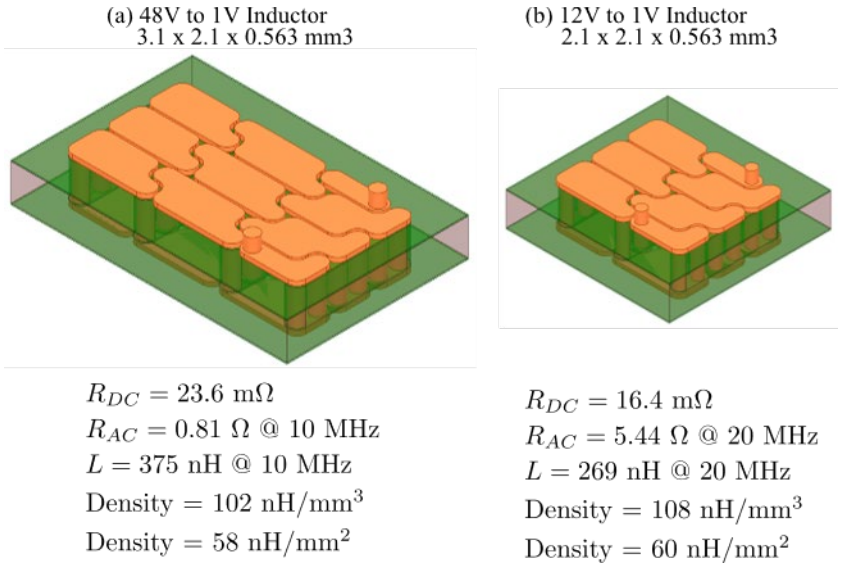

Figure 6.1: Coupled toroid design using newly modeled materials

Support Acknowledgments

The toroid inductor designs (Claudio Alvarez) were supported by ASCENT, one of six centers in JUMP, a Semiconductor Research Corporation (SRC) program sponsored by DARPA. Toroid inductor simulations and measurements were courtesy of Claudio Alvarez. This work was supported by the GT-PRC industry consortium and would not be possible without help from Panasonic Corp and Intel.

REFERENCES

[1] R. R. Tummala, "SOP: What is it and why? A new microsystem-integration technology paradigm-Moore's law for system integration of miniaturized convergent systems of the next decade," *IEEE Trans. Adv. Packag.*, vol. 27, no. 2, pp. 241–249, May 2004.

[2] R. R. Tummala, "Moore's Law meets its match," *IEEE Spectr.*, vol. 43, no. 6, pp. 44–49, Jun. 2006.

[3] C. Ó. Mathúna, N. Wang, S. Kulkarni, and S. Roy, "Review of integrated magnetics for Power Supply on Chip (PwrSoC)," *IEEE Transactions on Power Electronics*, vol. 27, no. 11. pp. 4799–4816, 2012.

[4] M. Swaminathan, J. Kim, I. Novak, and J. P. Libous, "Power Distribution Networks for System-on-Package: Status and Challenges," *IEEE Trans. Adv. Packag.*, vol. 27, no. 2, 2004.

[5] L. D. Smith, "Power distribution system design methodology and capacitor selection for modem cmos technology," *IEEE Trans. Adv. Packag.*, vol. 22, no. 3, pp. 284–291, 1999.

[6] U. Chaudhry, S. Kummerl, and C. H. Lim, "Powerful solutions come in small packages Innovative SiP power modules simplify and accelerate system development."

[7] R. C. N. Pilawa-Podgurski and D. J. Perreault, "Merged two-stage power converter with soft charging switched-capacitor stage in 180 nm CMOS," *IEEE J. Solid-State Circuits*, vol. 47, no. 7, pp. 1557–1567, May 2012.

[8] H. P. Le, S. R. Sanders, and E. Alon, "Design techniques for fully integrated switched-capacitor DC-DC converters," *IEEE J. Solid-State Circuits*, vol. 46, no. 9, pp. 2120–2131, Sep. 2011.

[9] J. Chen, "Resonant Switched Capacitor DC-DC Converter with Stackable Conversion Ratios," 2016.

[10] N. Wang, T. O'Donnell, R. Meere, F. M. F. Rhen, S. Roy, and S. C. O'Mathuna, "Thin-film-integrated power inductor on Si and its performance in an 8-MHz buck converter," in *IEEE Transactions on Magnetics*, 2008, vol. 44, no. 11 PART 2, pp. 4096–4099.

[11] Y. Su, W. Zhang, Q. Li, F. C. Lee, and M. Mu, "High frequency integrated Point of Load (POL) module with PCB embedded inductor substrate," in *2013 IEEE Energy Conversion Congress and Exposition, ECCE 2013*, 2013, pp. 1243–1250.

[12] W. Liu, Y.-F. Liu, L. Wang, and D. Malcolm, *A 3D Stacked Step-Down Intergrated Power Module*. .

[13] E. A. Burton *et al.*, "FIVR - Fully integrated voltage regulators on 4th generation Intel® Core™ SoCs," in *Conference Proceedings - IEEE Applied Power Electronics Conference and Exposition - APEC*, 2014, pp. 432–439.

[14] R. P.M., D. Mishra, H. Sharma, M. Swaminathan, and R. Tummala, "Nanomagnetic Materials and Structures, and their Applications in Integrated RF and Power Modules," in *Nanomagnetism*, 2014, pp. 13–16.

[15] M. S. Ryłko, K. J. Hartnett, J. G. Hayes, and M. G. Egan, "Magnetic material selection for high power high frequency inductors in DC-DC converters," in *Conference Proceedings - IEEE Applied Power Electronics Conference and Exposition - APEC*, 2009, pp. 2043–2049.

[16] D. Mishra *et al.*, *Nanomagnetic Structures for Inductive Coupling and Shielding for Wireless Charging Applications*. .

[17] W. J. Lambert, M. J. Hill, K. Radhakrishnan, L. Wojewoda, and A. E. Augustine, "Package embedded inductors for integrated voltage regulators," in *Proceedings - Electronic Components and Technology Conference*, 2014, pp. 528–534.

[18] Y. Jang, M. M. Jovanović, and Y. Panov, "Multi-phase buck converters with extended duty cycle," in *Conference Proceedings - IEEE Applied Power Electronics Conference and Exposition - APEC*, 2006, vol. 2006, pp. 38–44.

[19] R. Alben, J. J. Becker, and M. C. Chi, "Random anisotropy in amorphous ferromagnets," *J. Appl. Phys.*, vol. 49, p. 1660, 1978.

[20] M. A. Swihart, “Inductor Cores – Material and Shape Choices.”

[21] TDK Electronics, “Ferrites: Low losses at high frequencies ,” 2017.

[22] DigiKey, “Material Advances Enable New Generation of Power Inductors ,” 2017.

[23] D. Azuma, N. Ito, and M. Ohta, “Recent progress in Fe-based amorphous and nanocrystalline soft magnetic materials,” *Journal of Magnetism and Magnetic Materials*, vol. 501. Elsevier B.V., 01-May-2020.

[24] F. Mazaleyrat, “Microstructure and magnetic properties of soft magnetic powder cores of amorphous and nanocrystalline alloys,” *J. Magn. Magn. Mater.*

[25] R. Tummala, H. Garmestani, R. Gerhradt, E. Shipton GTRI, and P. Markondeya Raj, “MODELING, DESIGN, FABRICATION AND DEMONSTRATION OF MULTILAYERED FERROMAGNETIC-POLYMER DIELECTRIC COMPOSITES FOR ULTRA-THIN HIGH-DENSITY POWER-INDUCTORS,” Georgia Institute of Technology, Aug. 2015.

[26] Y. Su, F. C. Lee, D. S. Ha, M. S. Hsiao, Q. Li, and K. P. Lu, “High Frequency, High Current 3D Integrated Point-of-Load Module,” 2014.

[27] T. Sun *et al.*, “Substrate embedded thin-film inductors with magnetic cores for Integrated Voltage Regulators,” 2016.

[28] R. Meere, T. O’Donnell, N. Wang, N. Achotte, S. Kulkarni, and S. C. O’Mathuna, “Size and performance tradeoffs in micro-inductors for high frequency DC-DC conversion,” in *IEEE Transactions on Magnetics*, 2009, vol. 45, no. 10, pp. 4234–4237.

[29] N. Wang, T. O’Donnell, S. Roy, M. Brunet, P. McCloskey, and S. C. O’Mathuna, “High-frequency micro-machined power inductors,” *J. Magn. Magn. Mater.*, vol. 290-291 PART 2, pp. 1347–1350, Apr. 2005.

[30] N. Wang, T. O’Donnell, S. Roy, P. McCloskey, and C. O’Mathuna, “Micro-inductors integrated on silicon for power supply on chip,” *J. Magn. Magn. Mater.*, vol. 316, no. 2 SPEC. ISS., pp. e233–e237, Sep. 2007.

[31] D. Yao, C. G. Levey, R. Tian, and C. R. Sullivan, “Microfabricated V-groove power inductors using multilayer Co-Zr-O thin films for very-high-frequency DC-DC converters,” *IEEE Trans. Power Electron.*, vol. 28, no. 9, pp. 4384–4394, 2013.

[32] P. R. Morrow, C. M. Park, H. W. Koertzen, and J. T. DiBene, “Design and fabrication of on-chip coupled inductors integrated with magnetic material for voltage regulators,” *IEEE Trans. Magn.*, vol. 47, no. 6 PART 2, pp. 1678–1686, Jun. 2011.

[33] K. Koh, D. S. Gardner, C. Yang, K. P. O’Brien, N. Tayebi, and L. Lin, “High frequency microwave on-chip inductors using increased ferromagnetic resonance frequency of magnetic films,” in *Proceedings of the IEEE International Conference on Micro Electro Mechanical Systems (MEMS)*, 2015, vol. 2015-February, no. February, pp. 208–211.

[34] S. Bierlich, T. Reimann, H. Bartsch, and J. Töpfer, “Co/Ti-substituted M-type hexagonal ferrites for high-frequency multilayer inductors,” *J. Magn. Magn. Mater.*, vol. 384, pp. 1–5, Jun. 2015.

[35] N. Sturcken *et al.*, “Magnetic thin-film inductors for monolithic integration with CMOS,” in *Technical Digest - International Electron Devices Meeting, IEDM*, 2015, vol. 2016-February, pp. 11.4.1-11.4.4.

[36] A. K., J. M., and A. A.Hadj, “Analysis techniques of polymeric encapsulant materials for photovoltaic modules: situation and perspectives ,” *Energy Procedia*, vol. 93, pp. 203–210, 2016.

[37] L. Taiyo Yuden Co., “MCFK1608T1R0M | Inductors.” [Online]. Available: https://ds.yuden.co.jp/TYCOMPAS/ut/detail?u=M&pn=MCFK1608T1R0M. [Accessed: 12-Mar-2020].

[38] L. Taiyo Yuden Co., “MCFK1608TR47M | Inductors.” [Online]. Available: https://ds.yuden.co.jp/TYCOMPAS/ut/detail?u=M&pn=MCFK1608TR47M. [Accessed: 12-Mar-2020].

[39] L. Taiyo Yuden Co., “MCFK1608TR24M | Inductors.” [Online]. Available: https://ds.yuden.co.jp/TYCOMPAS/ut/detail?u=M&pn=MCFK1608TR24M. [Accessed: 12-Mar-2020].

[40] L. Taiyo Yuden Co., “MCFE1608TR24MG | Inductors.” [Online]. Available: https://ds.yuden.co.jp/TYCOMPAS/ut/detail?u=M&pn=MCFE1608TR24MG. [Accessed: 12-Mar-2020].

[41] L. Taiyo Yuden Co., “MCFE1608TR47MG | Inductors.” [Online]. Available: https://ds.yuden.co.jp/TYCOMPAS/ut/detail?u=M&pn=MCFE1608TR47MG. [Accessed: 12-Mar-2020].

[42] Coilcraft, “Coilcraft XFL2005 Series Shielded Power Inductors.” [Online]. Available: https://www.coilcraft.com/xfl2005.cfm. [Accessed: 12-Mar-2020].

[43] Coilcraft, “Coilcraft XFL2006 Series Shielded Power Inductors.” [Online]. Available: https://www.coilcraft.com/xfl2006.cfm. [Accessed: 12-Mar-2020].

[44] Kemet and Digikey, “L0603B1R0MDWFT KEMET | Inductors, Coils, Chokes.” [Online]. Available: https://www.digikey.com/product-detail/en/kemet/L0603B1R0MDWFT/399-17787-1-ND/8601450. [Accessed: 12-Mar-2020].

[45] Kemet, “Surface Mount Ferrite Products,” 2014.

[46] TDK, “TFM160808ALC-R47MTAA TDK | Mouser.” [Online]. Available: https://www.mouser.com/ProductDetail/TDK/TFM160808ALC-R47MTAA/?qs=3SnDZBG9J%252b6tokb499UWsQ%3D%3D&gclid=Cj0KCQjwu6fzBRC6ARIsAJUwa2QNidiImXutB-rMcFJsMyYYTyVZ-dt1rewSdPw42nYtPDyXNv2sgzYaAhV5EALw_wcB. [Accessed: 12-Mar-2020].

[47] D.M. Zogbi, “Thin Film Passive Components World Markets, Technologies & Opportunities: 2016-2021,” *Paumanok Publ. Inc.*, 2016.

[48] A. T. Hindmarch, D. A. Arena, K. J. Dempsey, M. Henini, and C. H. Marrows, “Influence of deposition field on the magnetic anisotropy in epitaxial Co70Fe30 films on GaAs(001),” *Phys. Rev. B - Condens. Matter Mater. Phys.*, vol. 81, no. 10, p. 100407, Mar. 2010.

[49] C. Sullivan, J. Qiu, D. Harburg, and C. Levey, “Batch fabrication of radial anisotropy toroidal inductors,” *Int. Symp. 3D Power Electron. Integr. Manuf.*, pp. 1–15, 2016.

[50] M. Saidani and M. A. M. Gijs, “Cubic millimeter power inductor fabricated in batch-type wafer technology,” *J. Microelectromechanical Syst.*, vol. 12, no. 2, pp. 172–178, Apr. 2003.

[51] S. Kelly, C. Collins, M. Duffy, F. M. F. Rhen, and S. Roy, “Core materials for high frequency VRM inductors,” in *PESC Record - IEEE Annual Power Electronics Specialists Conference*, 2007, pp. 1767–1772.

[52] M. Ludwig, M. Duffy, T. O’Donnell, P. McCloskey, and S. C. Ó Mathùna, “PCB integrated inductors for low power DC/DC converter,” *IEEE Trans. Power Electron.*, vol. 18, no. 4, pp. 937–945, Jul. 2003.

[53] E. Waffenschmidt, “Performance limits of ultra-thin printed circuit board inductors,” in *PESC Record - IEEE Annual Power Electronics Specialists Conference*, 2006.

[54] K. Ishikawa, M. Ishizuka, and S. Kikuchi, “Performance characteristics of a new type of linear parametric motor with double driving surfaces,” *IEEE Trans. Magn.*, vol. 34, no. 4 PART 1, pp. 2051–2053, 1998.

[55] D. S. Gardner *et al.*, “Integrated on-chip inductors using magnetic material (invited),” *J. Appl. Phys.*, vol. 103, no. 7, p. 07E927, Apr. 2008.

[56] J. Y. Park, L. K. Lagorce, and M. G. Allen, “Ferrite-based integrated planar inductors and transformers fabricated at low temperature,” *IEEE Trans. Magn.*, vol. 33, no. 5 PART 1, pp. 3322–3324, 1997.

[57] D. Gardner, G. Schrom, F. Paillet, B. Jamieson, T. Karnik, and S. Borkar, “Review of On-Chip Inductor Structures With Magnetic Films,” *IEEE Trans. Magn.*, vol. 45, no. 10, pp. 4760–4766, 2009.

[58] J. Y. Park, S. H. Han, and M. G. Allen, “Batch-fabricated microinductors with electroplated magnetically anisotropie and laminated alloy cores,” *IEEE Trans. Magn.*, vol. 35, no. 5 PART 3, pp. 4291–4300, 1999.

[59] K. W. Moon, S. H. Hong, H. J. Kim, and J. Kim, “A fabrication of DC-DC converter using LTCC NiZnCu ferrite thick films,” in *INTERMAG ASIA 2005: Digests of the IEEE International Magnetics Conference*, 2005, p. 555.

[60] R. R. Tummala, P. M. Raj, D. Qin, E. Vogel, and H. Garmestani, "MODELING, DESIGN, FABRICATION AND CHARACTERIZATION OF MINIATURIZED, HIGH-CURRENT HANDLING AND HIGH-EFFICIENCY INDUCTORS," Georgia Institute of Technology, Dec. 2018.

[61] S. Mueller, K. Z. Ahmed, A. Singh, A. K. Davis, S. Mukhopadyay, and M. Swaminathan, "Design of High Efficiency Integrated Voltage Regulators with Embedded Magnetic Core Inductors," in *Electronic Components and Technology Conference*, 2016.

[62] C. Fei, M. H. Ahmed, F. C. Lee, and Q. Li, "Dynamic bus voltage control for light load efficiency improvement of two-stage voltage regulator," in *ECCE 2016 - IEEE Energy Conversion Congress and Exposition, Proceedings*, 2016.

[63] X. Zhao, C. S. Yeh, L. Zhang, J. S. Lai, and T. Labella, "A 2-MHz Wide-Input Hybrid Resonant Converter with Ultracompact Planar Coupled Inductor for Low-Power Integrated On-Chip Applications," in *IEEE Transactions on Industry Applications*, 2018, vol. 54, no. 1, pp. 376–387.

[64] "DrGaN PLUS Development Board EPC9201/3 Quick Start Guide Optimized Half-Bridge Circuit for eGaN ® FETs EPC9201 Top side EPC9203 Top side Mounting side," 2019.

[65] M. L. F. Bellaredj, S. Mueller, A. K. Davis, P. Kohl, M. Swaminathan, and Y. Mano, "Fabrication, Characterization and Comparison of FR4-Compatible Composite Magnetic Materials for High Efficiency Integrated Voltage Regulators with Embedded Magnetic Core Micro-Inductors," in *Proceedings - Electronic Components and Technology Conference*, 2017, pp. 2008–2014.

[66] H. Hoffmann, "Demagnetizing Field ," in *Hysteresis in Magnetism*, 1998.

[67] E. P. Wohlfarth, K. H. J. Buschow, and E. Brück, *Ferromagnetic materials : a handbook on the properties of magnetically ordered substances*. Amsterdam ; North-Holland Pub. Co., 1980.

[68] M. Lakshmanan, "The fascinating world of the Landau-Lifshitz-Gilbert equation: An overview," *Philosophical Transactions of the Royal Society A: Mathematical, Physical and Engineering Sciences*, vol. 369, no. 1939. Royal Society, pp. 1280–1300, 28-Mar-2011.

[69] R. Ramprasad, P. Zurcher, M. Petras, M. Miller, and P. Renaud, "Magnetic properties of metallic ferromagnetic nanoparticle composites," *J. Appl. Phys.*, vol. 96, no. 1, pp. 519–529, Jul. 2004.

[70] C. Kittel, "On the theory of ferromagnetic resonance absorption," *Phys. Rev.*, vol. 73, no. 2, pp. 155–161, Jan. 1948.

[71] I. T. Iakubov *et al.*, "A laminate of ferromagnetic films with high effective permeability at high frequencies," *AIP Adv.*, vol. 4, no. 10, p. 107143, Oct. 2014.

[72] B. Lu *et al.*, "Microwave absorption properties of the core/shell-type iron and nickel nanoparticles," *J. Magn. Magn. Mater.*, vol. 320, no. 6, pp. 1106–1111, Mar. 2008.

[73] P. Markondeya Raj, H. Sharma, S. Samtani, D. Mishra, V. Nair, and R. Tummala, "Magnetic losses in metal nanoparticle-insulator nanocomposites," *J. Mater. Sci. Mater. Electron.*, vol. 24, no. 9, pp. 3448–3455, Sep. 2013.

[74] TDK, "Magnetic Sheets for RFID," 2016.

[75] S. Ohnuma, H. Fujimori, T. Masumoto, X. Y. Xiong, D. H. Ping, and K. Hono, "FeCo-Zr-O nanogranular soft-magnetic thin films with a high magnetic flux density," *Appl. Phys. Lett.*, vol. 82, no. 6, pp. 946–948, Feb. 2003.

[76] Kemet, "Magnetic Sheet for RFID Sheet ," 2016.

[77] Richtek Technology, "Current Ripple Factor of a Buck Converter ."

[78] Z. Zhang, "Coupled-inductor magnetics in power electronics," 1986.

[79] V. Bulovic, R. Ram, S. Leeb, J. Lang, and Y. Gu, "Electromagnetic Energy: From Motors to Lasers," *MIT Open Courseware*, 2011.

[80] R. Ridley, "Proximity loss in magnetics windings," 2005.

[81] T. Eichhorn, "Estimate Inductor Losses Easily in Power Supply Designs ," *Power Electronics* , 2005.

[82] Wurth Elektronik, “WE-PDF SMT Power Inductor.” [Online]. Available: https://www.we-online.com/catalog/en/WE-PDF/. [Accessed: 13-Mar-2020].

[83] P. Mccloskey, “Integrated Magnetics for PwrSiP and PwrSoc,” 2015.

[84] A. T. Hindmarch, D. A. Arena, K. J. Dempsey, M. Henini, and C. H. Marrows, “Influence of deposition field on the magnetic anisotropy in epitaxial Co70Fe30 films on GaAs(001),” *Phys. Rev. B - Condens. Matter Mater. Phys.*, vol. 81, no. 10, Mar. 2010.

[85] C. Alvarez, M. Bellaredj, and M. Swaminathan, “Open and Closed Loop Inductors for High-Efficiency System-on-Package Integrated Voltage Regulators,” in *Electronics Components and Technology Conference*, 2019, pp. 1672–1679.

[86] C. Alvarez and S. Suresh, “Expandable Interleaved Toroidal Inductor Cell with Vias-in-Slot Thru Magnetic Sheet, Invention Disclosure,” GTRC ID 8341, 2019.

[87] M. Sunohara, A. Shiraishi, Y. Taguchi, K. Murayama, M. Higashi, and M. Shimizu, “Development of silicon module with TSVs and global wiring (L/S=0.8/0.8μm),” in *Proceedings - Electronic Components and Technology Conference*, 2009, pp. 25–31.

[88] M. Ma *et al.*, “The Development and the Integration of the 5 μm to 1 μm Half Pitches Wafer Level Cu Redistribution Layers,” in *Proceedings - Electronic Components and Technology Conference*, 2016, vol. 2016-August, pp. 1509–1514.

[89] Y. H. Chen, S. L. Cheng, D. C. Hu, and T. J. Tseng, “Ultra-thin line embedded substrate manufacturing for 2.1D/2.5D SiP application,” in *ICEP-IAAC 2015 - 2015 International Conference on Electronic Packaging and iMAPS All Asia Conference*, 2015, pp. 166–169.

[90] A. Renbi, A. Risseh, R. Qvarnström, and J. Delsing, “Impact of etch factor on characteristic impedance, crosstalk and board density,” 2012.